NASA
Technical
Paper
2000

AVRADCOM
Technical
Report
82-B-2

May 1982

Two-Dimensional Aerodynamic Characteristics of Three Rotorcraft Airfoils at Mach Numbers From 0.35 to 0.90

Gene J. Bingham
and Kevin W. Noonan

NASA

NASA Technical Paper 2000

AVRADCOM Technical Report 82-B-2

1982

Two-Dimensional Aerodynamic Characteristics of Three Rotorcraft Airfoils at Mach Numbers From 0.35 to 0.90

Gene J. Bingham
and Kevin W. Noonan
Structures Laboratory
AVRADCOM Research and Technology Laboratories
Langley Research Center
Hampton, Virginia

National Aeronautics
and Space Administration

Scientific and Technical Information Branch

SUMMARY

Three airfoils designed for helicopter rotor application have been investigated to determine the two-dimensional aerodynamic characteristics at Mach numbers from 0.34 to 0.88 and respective Reynolds numbers from about 4.4×10^6 to 9.5×10^6. The airfoils have thickness-to-chord ratios of 0.08, 0.10, and 0.12 with maximum thickness at 40 percent chord and maximum camber at about 35 percent chord. The maximum camber of the 10-percent-thick airfoil is 1.55 times that of the 8-percent-thick section, and the maximum camber of the 12-percent-thick section is 2 times that of the 8-percent-thick section. Trailing-edge reflex was applied to minimize pitching moment.

The maximum normal-force coefficient of the RC(3)-12 airfoil is from 0.1 to 0.2 higher, depending on Mach number M, than that of the NACA 0012 airfoil tested in the same facility. The maximum normal-force coefficient of the RC(3)-10 is about equal to that of the NACA 0012 at Mach numbers to 0.40 and is higher than that of the NACA 0012 at Mach numbers above 0.40. The maximum normal-force coefficient of the RC(3)-08 is about 0.19 lower than that of the NACA 0012 at $M = 0.35$ and about 0.05 lower at $M = 0.54$.

At Mach numbers from 0.34 to 0.58, the pitching-moment coefficient about the aerodynamic center for the three airfoils discussed herein varied from 0 to -0.01. The coefficient reached a value of about -0.02 at $M \approx 0.69$ for the RC(3)-12, $M \approx 0.80$ for the RC(3)-10, and $M \approx 0.86$ for the RC(3)-08.

The drag-divergence Mach number of the RC(3)-08 airfoil at normal-force coefficients below 0.1 was indicated to be greater than the maximum test Mach number of 0.88. At zero lift, the drag-divergence Mach numbers of the RC(3)-12 and the RC(3)-10 are about 0.77 and 0.82, respectively. The drag-divergence Mach numbers are generally higher than those of comparable airfoils designed for helicopter rotors, but the maximum normal-force coefficients are about 0.1 lower.

INTRODUCTION

As part of an effort by the NASA and the U.S. Army to provide airfoils with improved efficiency for helicopter rotors, an airfoil design approach was analytically and experimentally evaluated. The results are presented in references 1 and 2. Based on these results, another airfoil section (ref. 3) was designed in an attempt to increase the maximum normal-force coefficient at Mach numbers near 0.4 to 0.5 while maintaining the same drag-divergence characteristics indicated in reference 2. The results of reference 3 show that the basic design objectives were reached but an unexpected increase in drag coefficient with increasing Mach number (or drag creep) occurred at normal-force coefficients near zero. Analysis of the data indicated that the drag creep resulted from the lower-surface leading-edge supersonic flow associated with the combination of leading-edge radius and leading-edge camber. In order to reduce the drag creep while retaining the other favorable characteristics, a new set of three airfoils was designed, each of which had a new camber distribution. The new airfoils had thickness-to-chord ratios of 0.08, 0.10, and 0.12 to cover a range of thicknesses that could be used at different stations along the radius of a typical helicopter rotor.

Models of these three airfoils were tested in the Langley 6- by 28-Inch Transonic Tunnel (ref. 4) at Mach numbers from about 0.34 to 0.88. The respective Reynolds numbers varied from about 4.4×10^6 to 9.5×10^6 for the lowest to highest Mach number, respectively. The models were tested with natural boundary-layer transition. Normal-force and pitching-moment coefficients were determined from measurements of airfoil surface static pressures, and drag coefficients were determined from measurements of wake total and static pressures. The drag-divergence characteristics and maximum normal-force coefficients of these three airfoils are compared with those for other airfoils with similar thickness-to-chord ratios in reference 5. The comparisons of reference 5 are presented herein also. As mentioned later in the section "Airfoil Description," the airfoil designation applied in reference 5 has been changed to the new NASA designation.

SYMBOLS

The units used for the physical quantities in this paper are given in both the International System of Units (SI) and U.S. Customary Units. The measurements and calculations were made in U.S. Customary Units.

c airfoil chord, cm (in.)

c_d section profile-drag coefficient, $\sum_{\text{Wake}} c'_d \frac{\Delta h}{c}$

c'_d point-drag coefficient,

$$2\left(\frac{p}{p_\infty}\right)^{6/7}\left[\frac{\left(p_t/p\right)^{2/7}-1}{\left(p_{t,\infty}/p_\infty\right)^{2/7}-1}\right]^{1/2}\left\{\left(\frac{p_t}{p_{t,\infty}}\right)^{1/7}-\left[\frac{\left(p_t/p_\infty\right)^{2/7}-1}{\left(p_{t,\infty}/p_\infty\right)^{2/7}-1}\right]^{1/2}\right\}$$

c_m section pitching-moment coefficient about quarter-chord,

$$\sum_{\text{U.S.}}\left[c_p\left(0.25-\frac{x}{c}\right)\left(\frac{\Delta x}{c}\right)+c_p\left(\frac{z}{c}\right)\left(\frac{\Delta z}{c}\right)\right]+\sum_{\text{L.S.}}\left[c_p\left(0.25-\frac{x}{c}\right)\left(\frac{\Delta x}{c}\right)+c_p\left(\frac{z}{c}\right)\left(\frac{\Delta z}{c}\right)\right]$$

$c_{m,o}$ section pitching-moment coefficient about aerodynamic center

c_n section normal-force coefficient, $\sum_{\text{U.S.}} c_p\left(\frac{\Delta x}{c}\right)+\sum_{\text{L.S.}} c_p\left(\frac{\Delta x}{c}\right)$

c_p static-pressure coefficient, $\frac{p_l-p_\infty}{q_\infty}$

h absolute magnitude of height of wake-survey probe tubes from given reference plane, cm (in.)

M Mach number

M_{dd} Mach number for drag divergence, $\frac{dc_d}{dM}=0.1$

p	static pressure, Pa (psi)
q	dynamic pressure, $\frac{1}{2}\rho v^2$, Pa (psi)
R	Reynolds number based on airfoil chord and free-stream conditions
t	airfoil thickness, cm (in.)
v	velocity, m/sec (ft/sec)
x	airfoil abscissa, cm (in.)
z	airfoil ordinate, cm (in.)
z_c	ordinate of airfoil mean line, cm (in.)
α	angle of attack, angle between airfoil chord line and airstream direction, deg
α_c	angle of attack corrected for lift-interference effects, deg
Δ	change in parameter
ρ	density, kg/m^3 (slugs/ft^3)

Subscripts:

ι	local
max	maximum
min	minimum
t	total
∞	free stream
sonic	Mach number equal to 1

Abbreviations:

L.S.	lower surface
U.S.	upper surface

APPARATUS AND METHODS

Airfoil Designation

The airfoils are designated in the form RC(3)-XX. The RC(3) indicates rotorcraft (third series); the two digits designate the airfoil thickness in percent chord. Thus, the airfoil section previously designated in reference 5 as the RC12(B)3 becomes the RC(3)-12, the RC10(B)3 becomes the RC(3)-10, and the RC08(B)3 becomes the RC(3)-08.

Airfoils

The airfoil profiles, thickness distributions, and mean lines (midpoint between upper and lower surfaces) are presented in figures 1 and 2, and the design coordinates are presented in tables I, II, and III. The thickness-to-chord ratios are 0.08, 0.10, and 0.12. The maximum thickness of each section is located at 40 percent chord, and the sections are directly scaled in thickness distribution, i.e., the 12-percent thickness distribution is 1.5 times the 8-percent thickness distribution. The maximum camber is located at about 35 percent chord on each airfoil. The maximum camber of the 10-percent-thick section is 1.55 times that of the 8-percent-thick section, and the maximum camber of the 12-percent-thick section is 2 times that of the 8-percent-thick section. Trailing-edge reflex was applied to minimize pitching moment. On a helicopter rotor blade, pitching moments are reflected into pitch-link (control-rod) loads and therefore must be kept low.

Each model was machined from a stainless-steel block and had a surface finish of 0.813 μm (0.000032 in.) (root mean square). Each had a chord of 15.24 cm (6.00 in.) and a span of 15.27 cm (6.01 in.) with a leading-edge orifice and with 22 orifices (tables IV, V, and VI) located on each surface in chordwise rows; the rows were positioned at 12.5 percent of the span on either side of the midspan. Slots were milled in the airfoil surface, and tubes were placed in the slots and covered with epoxy to restore the airfoil profile. The orifices were then drilled from the metal sides of the model to the embedded tubes, so that there were no surface irregularities near the orifice row. The orifices had diameters of 0.0508 cm (0.020 in.) and were drilled perpendicular to the local surface contour.

Wind Tunnel

Tunnel description.- The Langley 6- by 28-Inch Transonic Tunnel (ref. 4) is a blowdown wind tunnel with a slotted floor and ceiling and is generally operated at stagnation pressures from about 207 Pa (30 psia) to 620 Pa (90 psia) and at Mach numbers from 0.35 to 0.90. The selection of the 0.05-open slot geometry is described in reference 6. At a stagnation pressure of 620 Pa, the maximum Reynolds number, based on a 15.24-cm (6.00-in.) chord, varies from about 7.2×10^6 at a Mach number of 0.35 to about 14.2×10^6 at a Mach number of 0.90. Mach number is controlled by hydraulically actuated choker doors located downstream of the test section. The airfoil model spans the 15.27-cm (6.01-in.) width of the tunnel (fig. 3) and is rigidly attached by mounting tangs to two circular end plates which are driven by a hydraulic actuator to position the airfoil at the desired geometric angle of attack. A test run usually consists of an angle-of-attack sweep at a constant Mach number and Reynolds number.

Two-dimensionality of flow.- The results of an earlier investigation of rotorcraft airfoils in the Langley 6- by 28-Inch Transonic Tunnel (ref. 7) have shown that the indicated maximum normal-force coefficient is reduced by tunnel sidewall boundary-layer influences. This is characteristic of two-dimensional wind tunnels without proper sidewall boundary-layer control.

A comparison of the NACA 0012 data measured in this facility with unpublished data from two other facilities has been useful in indicating the magnitude of the maximum normal-force coefficient. The facilities are the Langley Low-Turbulence Pressure Tunnel and the United Technologies Research Center 8-foot tunnel. At similar Reynolds numbers and at a Mach number of 0.36, the maximum normal-force coefficients measured are about 0.15 higher than those from the Langley 6- by 28-Inch

Transonic Tunnel. The difference between the data from the Langley 6- by 28-Inch Transonic Tunnel and the United Technologies data decreases to near 0.05 to 0.10 at a Mach number of about 0.53. The same trends could reasonably be expected for other airfoil sections although the numerical increments may be different.

An investigation conducted in the Office National d'Etudes et de Recherches Aerospatiale (ONERA)R1 Ch wind tunnel (ref. 8) has shown that the tunnel sidewall boundary layer can affect the normal-force coefficients at all angles of attack. In the investigation of reference 8, the sidewall boundary-layer thickness was varied by applying sidewall suction upstream of the model while the Mach number and Reynolds number were held constant. Generally, an increase in sidewall boundary-layer thickness resulted in a decrease in the normal-force coefficient at a given angle of attack.

Although some progress has been made toward an understanding of the influences of tunnel sidewall boundary layer on airfoil test results, the state-of-the-art does not permit a general correction of two-dimensional wind-tunnel data to account for these influences. Because of this, test results in this report are compared (as appropriate) with those for the NACA 0012 airfoil tested in the same wind tunnel (ref. 7) at comparable Reynolds numbers.

Apparatus

Wake-survey probe.- A traversing wake-survey probe is cantilevered from one tunnel sidewall to measure the profile drag of the airfoils. The probe sweep rate, which was selected after experimental determination of acceptable lag time in the pressure measurements, was about 2.54 cm/sec (1.00 in/sec).

The probe (fig. 3) was located 1.67c (based on the 15.24-cm (6.00-in.) chord model) downstream of the airfoil trailing edge and had a maximum vertical travel of about ±27.9 cm (±11.0 in.) from the tunnel center line. Data are acquired with four total-pressure tubes, which are made of stainless-steel tubing with a 1.53-mm (0.060-in.) outside diameter and a 1.02-mm (0.040-in.) inside diameter and which are spaced 0.953 cm (0.375 in.) apart laterally as shown in figure 4.

Instrumentation.- All measurements were obtained with a high-speed computer-controlled digital data acquisition system and were recorded by a high-speed tape recording unit (ref. 4). All free-stream conditions were determined from stagnation and static pressures. All airfoil surface pressures and all wake pressures were measured with precision capacitive potentiometer pressure transducers. The electrical outputs from each of these transducers were connected to individual autoranging signal conditioners which have seven available ranges. The output signals from the four signal conditioners measuring the wake pressures were filtered with 20-Hz low-pass filters before input to the data acquisition system; the range of frequencies to be passed was experimentally determined during a previous investigation. The geometric angle of attack was determined from the output of a digital shaft encoder attached to a pinion engaging a rack on one model support end plate.

Tests and Methods

The tests were conducted at Mach numbers from 0.34 to 0.88 and at Reynolds numbers from 4.4×10^6 to 9.5×10^6 at the lowest and highest test Mach numbers, respec-

tively. Geometric angles of attack ranged from -4.0° to 14.0° at the lower test Mach numbers; this range was decreased at the higher test Mach numbers.

Section normal-force and pitching-moment coefficients were calculated from the airfoil surface pressures by a trapezoidal integration of the pressure coefficients. The pressure coefficient at the most rearward orifice on each surface was applied from that station to the airfoil trailing edge in the integration. Each of the pressure coefficients represents the average of five measurements obtained in a 1.0-second interval.

A form of the equation described in reference 9 was used to calculate the point-drag coefficients from the measured wake pressures, and a trapezoidal integration of the point-drag coefficients was used to calculate the drag coefficient. The static pressures used in the wake-drag calculation were measured with tunnel sidewall orifices located at the same longitudinal tunnel station as the tips of the tubes on the wake-survey probe. All the drag coefficients presented in this paper represent the mean of the measurements made with four total-pressure tubes on the wake-survey probe in one sweep through a wake.

The corrections for lift interference, which have been applied to the angles of attack, were obtained from references 6 and 10. The basic equations for the correction (see ref. 10) are

$$\alpha_c = \alpha + \Delta\alpha$$

where

$$\Delta\alpha = \frac{-c_n}{8}\left(\frac{c}{36.195}\right)\left(\frac{1}{k+1}\right)\left(\frac{180}{\pi}\right)$$

$$k = \frac{a}{h}K$$

In the expression for k, a is the slot spacing and h is the semiheight of the tunnel. The slotted-wall boundary-condition coefficient k for the present tunnel configuration is $0.4211K$. A value of 3.5 was selected for the slotted-wall performance coefficient K, based on the data and discussion presented in reference 6. This substitution results in a correction given by the equation

$$\Delta\alpha = -c_n c(0.0800)$$

where $\Delta\alpha$ is the angle-of-attack correction in degrees, c is the airfoil chord in centimeters, c_n is the section normal-force coefficient, and the constant (0.0800) is in degrees per centimeter.

PRESENTATION OF RESULTS

The results of the investigation have been reduced to coefficient form and are presented as follows:

DISCUSSION OF RESULTS

Normal-Force Coefficient

The maximum normal-force coefficients of the RC(3)-08, RC(3)-10, and RC(3)-12 airfoils are indicated by the normal-force coefficient curves of figure 5(a) and are summarized in figure 6. The results of figure 6 are presented as a function of Mach number along with data for the NACA 0012 (ref. 7) measured in the same wind tunnel at comparable Reynolds numbers. As indicated in the discussion of the two-dimensionality of the flow, the maximum normal-force coefficients are believed to be conservative (or low) but incrementally correct. Both figures 5(a) and 6 show that at Mach numbers below about 0.63, $c_{n,max}$ increases with increases in test airfoil thickness. This trend results from increases in both leading-edge radius and camber. An analysis of the pressure distributions (figs. 14, 15, and 16) at midrange angles of attack shows that the leading-edge minimum pressure coefficients become less negative and the midchord minimum pressures become more negative due to the combined increases in thicknesses and camber. This change in pressure distribution (which results in decreases in local Mach number in the leading-edge region and decreases in upper-surface pressure gradient) permits higher normal-force coefficients before stall with increasing thickness.

RC(3)-12.- The RC(3)-12 airfoil provided a maximum normal-force coefficient about 0.10 higher than that of the NACA 0012 airfoil (fig. 6) at a Mach number of about 0.35 (1.22 compared to 1.12). At a Mach number of 0.54 (the highest Mach number at which $c_{n,max}$ was defined for the NACA 0012 airfoil by ref. 7), the indicated difference is about 0.2 (1.10 compared to 0.90). The difference results from the camber of the RC(3)-12 airfoil. Locating the maximum thickness for the RC(3)-12 at 40 percent chord may have a slightly adverse influence on $c_{n,max}$ compared to that for a more forward location (ref. 11) but would be expected to have a favorable influence on the drag divergence Mach number (ref. 1).

RC(3)-10.- The maximum normal-force coefficients for the RC(3)-10 and the NACA 0012 airfoils (fig. 6) are about equal at Mach numbers between about 0.35 and 0.50, with indicated values for the RC(3)-10 varying from about 1.10 to 0.94. The camber of the RC(3)-10 airfoil compensates for the difference in thickness and leading-edge radius by resulting in a higher loading between about 0.25c and 0.75c than that for the NACA 0012 airfoil (figs. 15(a) and 15(b) and ref. 7). Supercritical flow is indicated in the leading-edge region (fig. 15) for $c_{n,max}$ at all test Mach numbers. Generally, this caused a decrease in $c_{n,max}$ with increase in Mach number; however, at Mach numbers above 0.54, supercritical flow resulted in a favorable influence, so that $c_{n,max}$ is slightly higher than at a Mach number of 0.54.

RC(3)-08.- The combined reduction in thickness and camber caused the RC(3)-08 airfoil to have an indicated $c_{n,max}$ of about 0.93 at a Mach number of 0.34 compared with about 1.10 for the RC(3)-10. An analysis of the static-pressure distributions of figure 14 suggests that at $c_{n,max}$, local supercritical flow occurs at a stream Mach number of about 0.38. (See $\alpha_c = 7.1°$.) That is, the pressure coefficient measured at 0.0705c (fig. 14(b)) is slightly supercritical at $\alpha_c = 7.1°$, which is below the angle corresponding to $c_{n,max}$ (fig. 5). It seems likely that the local Mach number at this location is even higher at angles of attack greater than 7.1°. Therefore, the gradual decrease in $c_{n,max}$ with increasing Mach number to about 0.54 apparently results from a corresponding increase in the influences of supercritical flow. At Mach numbers of 0.63 to 0.69 (fig. 6), the supercritical flow has a favorable influence on $c_{n,max}$.

An analysis of the static-pressure distributions of the RC(3)-10 and the RC(3)-12 airfoils indicates that stall results from trailing-edge boundary-layer separation which exists at $c_{n,max}$ at all Mach numbers of this investigation. The trailing-edge separation is indicated by the more negative upper-surface pressure coefficients at the trailing edge of the airfoil as $c_{n,max}$ is reached. Although not as easily discerned, the stall of the RC(3)-08 is believed to be of the trailing-edge type also, but with a more rapid forward movement of the upper surface separation point with increasing angle of attack above the value for $c_{n,max}$. For example, at $\alpha_c = 9.1°$ (which corresponds to $c_{n,max}$), the pressure coefficient at 0.95c (fig. 14(a)) is slightly more negative than it is for $\alpha_c = 7.1°$, and the same trend can be observed at 0.0705c. This is characteristic of trailing-edge stall. The shapes of the curves of figure 5(a) for the RC(3)-08 airfoil are similar to those of the RC(3)-10 and RC(3)-12 airfoils, and the curves do not show the abrupt discontinuity characteristic of airfoils that stall from the leading edge when the angle of attack for $c_{n,max}$ is exceeded (ref. 12).

Pitching-Moment Coefficient

The pitching-moment coefficients about the aerodynamic center of the RC(3)-08, RC(3)-10, and RC(3)-12 airfoils (fig. 5(b)) are summarized in figure 7 as a function of Mach number. At Mach numbers from 0.34 to 0.58, the pitching-moment coefficients for the three airfoils vary from about 0 to -0.01; the larger value is indicated for the RC(3)-12 airfoil, which is more highly cambered. An analysis of the static-pressure distributions for the three airfoils (figs. 14, 15, and 16) indicates that supercritical flow develops in the lower-surface leading-edge region as the Mach number is increased above about 0.63. The distributions are thus altered to cause the pitching-moment coefficients to become more negative as the Mach number is increased.

It is interesting to note that $c_m = |0.02|$, the value of pitching-moment coefficient that is considered to be acceptable by some authors (for example, ref. 13), was satisfied at Mach numbers up to about 0.69 for the RC(3)-12, up to about 0.80 for the RC(3)-10, and up to about 0.86 for the RC(3)-08. If these three airfoils were applied to a single helicopter rotor, the 12-percent-thick section would be used in the inboard regions and would operate at the lower Mach numbers. If a lower pitching-moment coefficient was desired for the design, the trailing-edge reflex should be increased.

Drag Coefficient

Minimum drag.- The minimum drag of the RC(3)-08 and RC(3)-10 airfoils (fig. 5(c)) is constant at about 0.0060 (for Mach numbers to 0.69) and is less than the value 0.0065 of the NACA 0012 airfoil investigated in the same facility (ref. 7) at comparable Reynolds numbers. A difference in transition location apparently accounts for this difference in drag coefficient. An analysis of the static-pressure coefficients (figs. 14 and 15 and ref. 7) indicates that at $c_{d,min}$, the minimum pressure on the upper surface of the RC(3) airfoils is forward of that of the NACA 0012 airfoil, but on the lower surface it is more aft of that of the NACA 0012. Since boundary-layer transition would be expected to occur near the minimum pressure location (ref. 11), a difference in transition is implied. The lower-surface influences must be predominant in this case to account for the difference in drag coefficient.

The minimum drag of the RC(3)-12 airfoil is about 0.0070 to 0.0075 (for Mach numbers to 0.63 (fig. 5(c)) or about 0.0005 to 0.0010 higher than that of the NACA 0012 airfoil (ref. 7). An analysis of the static-pressure distributions of figure 16 and reference 7 indicates that the increased camber of the RC(3)-12 airfoil causes a forward movement of the minimum pressure (and the transition location) on both the upper and lower surfaces and thus an increase in skin friction drag.

Normal force-to-drag ratio.- The maximum ratios of normal force to drag of the RC(3)-08, RC(3)-10, and RC(3)-12 airfoils as determined from the data of figure 5(c) are compared with that for the NACA 0012 airfoil (ref. 7) in figure 8. As expected, the ratio is higher for the RC(3)-12 section than for the NACA 0012 at the lower Mach numbers because of the higher maximum normal-force coefficients (fig. 5(a)) previously discussed and the corresponding lower drag coefficients. At the higher Mach numbers, the RC(3)-08 section provides a higher ratio than the RC(3)-12 and RC(3)-10 because of the lower drag at lower normal-force coefficients (fig. 5(c)). These results display the potential aerodynamic advantages of applying thicker, more highly cambered airfoils in the inboard regions of a helicopter rotor, where the local section Mach numbers are lower, and of applying the thinner, less highly cambered sections to the outboard regions, which experience higher local section Mach numbers.

Drag divergence.- The drag coefficients of figure 5(c) were cross-plotted as a function of Mach number at constant normal-force coefficients (fig. 9) to determine drag-divergence Mach number (fig. 10). Drag divergence is defined here as the free-stream Mach number at which $dc_d/dM = 0.1$. The drag-divergence Mach number of the RC(3)-08 airfoil at normal-force coefficients below about 0.1 was indicated to be some value greater than the maximum test Mach number of 0.88. Therefore, the curve of figure 10 is presented at normal-force coefficients equal to or greater than 0.1.

At $c_n = -0.2$, all three airfoils display an increase in drag coefficient (or drag creep) at Mach numbers less than that for drag divergence (fig. 9). For the

RC(3)-10 and RC(3)-12 airfoils, the onset of drag creep appears at Mach numbers between about 0.53 and 0.58. Analysis of the static-pressure distributions (figs. 15 and 16) suggests the onset of supercritical flow within this Mach number range at the angles of attack (between about -2.0° and -4.0°) which bracket $c_n = -0.2$. The supercritical flow is entirely forward of the lower-surface crest (which is near 0.1c at $c_n = -0.2$) and thus would not be expected to adversely influence the pressure drag of the airfoil. Therefore, the increase in drag coefficient at Mach numbers between 0.53 and 0.58 must result from an adverse influence of the supercritical flow on the lower-surface boundary layer to result in increased skin-friction drag. For the RC(3)-08 airfoil, lower-surface leading-edge-region supercritical flow probably occurs at $M = 0.58$ for $c_n = -0.2$ (fig. 14(f), $\alpha_c = -1.9$). However, drag creep does not occur at this normal-force coefficient until the Mach number exceeds 0.73. The influence of supercritical flow is delayed to a higher Mach number for this airfoil. The reason for the delay in drag creep to $M > 0.73$ is not readily apparent.

As c_n is increased from -0.2 to -0.1, drag creep is not indicated for either the RC(3)-10 or RC(3)-12 airfoils below a Mach number of about 0.66 (fig. 9). Analysis of the pressure distributions (figs. 15 and 16) indicates supercritical flow is present in the lower-surface leading-edge region. Apparently, the supercritical flow is primarily in the high-curvature region of the leading edge and has little influence on the boundary-layer thickness and skin-friction drag. For the RC(3)-08 airfoil at $c_n = -0.1$, drag creep begins at a Mach number of about 0.78. The onset of supercritical flow is not confirmed by the pressure distributions at $c_n = -0.1$ because data points were not obtained at Mach numbers from 0.63 to 0.69. The operation of the RC(3)-12 airfoil at negative normal-force coefficients can be avoided by proper distribution of these three airfoils along the rotor-blade radius. The RC(3)-10 or the RC(3)-08 might be applied at the rotor tip.

At the higher normal-force coefficients presented for each airfoil (fig. 10), the slope of the c_n versus M_{dd} curves decreases. Analysis of the pressure distributions (figs. 14, 15, and 16) indicates that the boundary layer is attached at the rearmost orifice location (0.95c). This is indicated by the continuous negative slope of the respective C_p versus x/c curves. Analysis also indicates that for each case the supercritical flow extends behind the airfoil crest. Therefore, the increased drag (resulting in the decrease in the c_n versus M_{dd} slope) probably results primarily from an increase in pressure drag instead of from an increase in skin friction drag.

Airfoil Comparisons

The drag-divergence Mach number and maximum normal-force characteristics of the RC(3)-12, RC(3)-10, and RC(3)-08 airfoils have been compared with those of other rotorcraft airfoils with similar thickness-to-chord ratios. (See ref. 5.) These comparisons are presented in figures 11, 12, and 13 and are based on data from the Langley 6- by 28-Inch Transonic Tunnel. Therefore, the results are subject to the same considerations discussed in the "Wind Tunnel" section of this paper. Except for the VR-7, the sections which are compared with RC(3)-12, RC(3)-10, and RC(3)-08 airfoils did not apply trailing-edge tabs or trailing-edge reflex to the mean line to provide near-zero pitching moment about the aerodynamic center.

A comparison of the RC(3)-12 airfoil with the classic NACA 0012 and the Boeing Vertol VR-7 with a -4.6° trailing-edge tab (to provide near-zero pitching moment) is presented in figure 11. The NACA 0012 provides the higher drag-divergence Mach num-

bers at near-zero normal-force coefficient, primarily because of the absence of camber. The lack of camber also results in both a lower drag-divergence Mach number at normal-force coefficient above about 0.3 and lower maximum normal-force coefficients. The drag-divergence Mach number of the RC(3)-12 is generally higher than that of the VR-7, but the maximum normal-force coefficient is about 0.1 lower.

A comparison of airfoil sections with thickness-to-chord ratios of about 10 percent is presented in figure 12. Included in the comparison is the Wortmann FX-098 (9.8 percent thick) designed for Bell Helicopter and the SC 1095 (9.5 percent thick) designed by Sikorsky Aircraft. As shown by figure 12, the largest gain in drag-divergence Mach number was obtained for the RC(3)-10 airfoil (larger than for the RC(3)-12 or RC(3)-08); the increase is greatest at normal-force coefficients above about 0.2. As before, the maximum normal-force coefficient of the RC(3)-10 is about 0.1 lower than that of the other two configurations (FX-098 and SC 1095).

The sections at or near 8 percent thick are compared in figure 13 and include the Wortmann FX-080 (8.0-percent-thick) and FX-083 (8.3-percent-thick) airfoils designed for Bell Helicopter and the NLR No. 1 (8.6-percent-thick) airfoil designed for Bell Helicopter and NASA. Again, the drag-divergence characteristics of the RC(3)-08 are favorable, but the maximum normal-force coefficient is up to 0.1 lower than that of other airfoils shown.

CONCLUSIONS

Three airfoils designed for helicopter rotor application have been investigated in the Langley 6- by 28-Inch Transonic Tunnel to determine the two-dimensional aerodynamic characteristics at Mach numbers from 0.34 to 0.88 and respective Reynolds numbers from about 4.4×10^6 to 9.5×10^6. The airfoils have thickness-to-chord ratios of 0.08, 0.10, and 0.12 with maximum thickness at 40 percent chord and maximum camber at about 35 percent chord. The maximum camber of the 10-percent-thick airfoil is 1.55 times that of the 8-percent-thick section, and the maximum camber of the 12-percent-thick section is 2 times that of the 8-percent-thick section. Trailing-edge reflex was applied to minimize pitching moment. An analysis of the test data has resulted in the following conclusions:

1. The maximum normal-force coefficient of the 12-percent-thick airfoil section is about 0.1 higher than that of an NACA 0012 airfoil at a Mach number of about 0.35 and about 0.2 higher at a Mach number of 0.54.

2. The maximum normal-force coefficient of the 10-percent-thick airfoil section is about equal to that of an NACA 0012 airfoil at Mach numbers to 0.40 and is higher at Mach numbers above 0.40.

3. The maximum normal-force coefficient of the 8-percent-thick airfoil section is about 0.19 lower than that of an NACA 0012 airfoil at a Mach number of 0.35 and about 0.05 lower at a Mach number of 0.54.

4. At Mach numbers from 0.34 to 0.58, the pitching-moment coefficient about the aerodynamic center for the three airfoils varies from 0 to -0.01. The coefficient reaches a value of -0.02 at a Mach number of about 0.69 for the 12-percent-thick section, at a Mach number of 0.80 for the 10-percent-thick section, and at a Mach number of 0.86 for the 8-percent-thick section.

5. The drag-divergence Mach number of the 8-percent-thick section at normal-force coefficients below 0.1 was indicated to be greater than the maximum test Mach number of 0.88. At zero lift, the drag-divergence Mach numbers of the 12- and 10-percent-thick sections are about 0.77 and 0.82, respectively.

6. The drag-divergence Mach numbers are generally higher than those of comparable airfoils designed for helicopters, but the maximum normal-force coefficients are about 0.1 lower.

Langley Research Center
National Aeronautics and Space Administration
Hampton, VA 23665
February 25, 1982

REFERENCES

1. Bingham, Gene J.: An Analytical Evaluation of Airfoil Sections for Helicopter Rotor Applications. NASA TN D-7796, 1975.

2. Bingham, Gene J.; and Noonan, Kevin W.: Experimental Investigation of Three Helicopter Rotor Airfoils Designed Analytically. NASA TP-1396, AVRADCOM TR 79-11, 1979.

3. Bingham, Gene J.; Noonan, Kevin W.; and Sewall, William G.: Two-Dimensional Aerodynamic Characteristics of an Airfoil Designed for Rotorcraft Application. NASA TP-1965, AVRADCOM TR 81-B-6, 1981.

4. Ladson, Charles L.: Description and Calibration of the Langley 6- × 28-Inch Transonic Tunnel. NASA TN D-8070, 1975.

5. Bingham, Gene J.; Noonan, Kevin W.; and Jones, Henry E.: Results of an Investigation of Several New Rotorcraft Airfoils as Related to Airfoil Requirements. Advanced Technology Airfoil Research, Volume II, NASA CP-2046, 1979, pp. 109-119.

6. Barnwell, Richard W.: Design and Performance Evaluation of Slotted Walls for Two-Dimensional Wind Tunnels. NASA TM-78648, 1978.

7. Noonan, Kevin W.; and Bingham, Gene J.: Two-Dimensional Aerodynamic Characteristics of Several Rotorcraft Airfoils at Mach Numbers From 0.35 to 0.90. NASA TM X-73990, 1977.

8. Bernard-Guelle, René: Influence of Wind Tunnel Wall Boundary Layers on Two-Dimensional Transonic Tests. NASA TT F-17,255, 1976.

9. Baals, Donald D.; and Mourhess, Mary J.: Numerical Evaluation of the Wake-Survey Equations for Subsonic Flow Including the Effect of Energy Addition. NACA WR L-5, 1945. (Formerly NACA ARR L5H27.)

10. Davis, Don D., Jr.; and Moore, Dewey: Analytical Study of Blockage- and Lift-Interference Corrections for Slotted Tunnels Obtained by the Substitution of an Equivalent Homogeneous Boundary for the Discrete Slots. NACA RM L53E07b, 1953.

11. Abbott, Ira H.; Von Doenhoff, Albert E.; and Stivers, Louis S., Jr.: Summary of Airfoil Data. NACA Rep. 824, 1945. (Supersedes NACA WR L-560.)

12. McCullough, George B.; and Gault, Donald E.: Examples of Three Representative Types of Airfoil-Section Stall at Low Speed. NACA TN 2502, 1951.

13. Wortmann, F. X.; and Drees, Jan M.: Design of Airfoils for Rotors. CAL/AVLABS Symposium Proceedings: Aerodynamics of Rotary Wing and V/STOL Aircraft, Volume I - Rotor/Propeller Aerodynamics, Rotor Noise, June 1969.

TABLE I.- DESIGN COORDINATES FOR RC(3)-08 AIRFOIL

[Stations and ordinates given in percent airfoil chord]

Station	Upper surface	Lower surface
0.00	0.00	0.00
.31	.67	-.66
1.17	1.31	-1.10
2.53	1.90	-1.45
4.37	2.46	-1.73
6.51	2.95	-1.95
8.89	3.39	-2.13
11.47	3.77	-2.28
14.24	4.10	-2.40
17.19	4.38	-2.51
20.30	4.61	-2.61
23.56	4.79	-2.69
26.96	4.93	-2.79
30.48	5.02	-2.85
34.12	5.08	-2.88
37.84	5.09	-2.91
41.61	5.05	-2.93
45.40	4.99	-2.94
49.20	4.88	-2.93
52.98	4.73	-2.90
56.77	4.53	-2.86
60.55	4.30	-2.80
64.37	4.02	-2.71
68.24	3.70	-2.61
72.15	3.34	-2.47
76.06	2.94	-2.30
79.84	2.53	-2.10
83.46	2.11	-1.87
86.93	1.69	-1.60
90.28	1.27	-1.29
93.54	.86	-.94
96.78	.49	-.51
100.00	.13	-.05

TABLE II.- DESIGN COORDINATES FOR RC(3)-10 AIRFOIL

[Stations and ordinates given in percent airfoil chord]

Station	Upper surface	Lower surface
0.00	0.00	0.00
.31	.91	-.77
1.09	1.70	-1.23
2.40	2.46	-1.62
4.21	3.19	-1.95
6.35	3.85	-2.20
8.72	4.44	-2.40
11.31	4.94	-2.56
14.08	5.38	-2.70
17.02	5.75	-2.82
20.14	6.05	-2.92
23.40	6.29	-3.02
26.81	6.47	-3.11
30.34	6.60	-3.18
34.00	6.66	-3.25
37.73	6.67	-3.30
41.52	6.63	-3.34
45.34	6.53	-3.36
49.15	6.38	-3.36
52.95	6.17	-3.35
56.75	5.91	-3.31
60.55	5.59	-3.26
64.38	5.22	-3.18
68.28	4.79	-3.08
72.23	4.30	-2.94
76.19	3.76	-2.76
80.00	3.20	-2.54
83.62	2.64	-2.27
87.08	2.10	-1.96
90.41	1.56	-1.59
93.63	1.05	-1.17
96.83	.60	-.63
100.00	.18	-.02

TABLE III.- DESIGN COORDINATES FOR RC(3)-12 AIRFOIL

[Stations and ordinates given in percent airfoil chord]

Station	Upper surface	Lower surface
0.00	0.00	0.00
.37	1.00	-.90
1.25	1.94	-1.57
2.60	2.86	-2.08
4.38	3.76	-2.49
6.52	4.59	-2.78
8.92	5.33	-2.98
11.53	5.98	-3.13
14.33	6.53	-3.25
17.30	7.01	-3.35
20.44	7.40	-3.44
23.72	7.71	-3.52
27.13	7.95	-3.60
30.66	8.10	-3.68
34.29	8.19	-3.74
38.01	8.19	-3.80
41.77	8.13	-3.85
45.58	8.00	-3.88
49.39	7.79	-3.90
53.21	7.52	-3.90
57.03	7.17	-3.89
60.88	6.76	-3.85
64.75	6.27	-3.79
68.71	5.70	-3.69
72.72	5.07	-3.55
76.71	4.37	-3.36
80.53	3.67	-3.12
84.15	2.96	-2.82
87.44	2.31	-2.49
90.56	1.70	-2.08
93.62	1.14	-1.54
96.75	.62	-.89
100.00	.13	-.13

TABLE IV.- STATIC-PRESSURE ORIFICE LOCATIONS FOR RC(3)-08 AIRFOIL

[Locations given in percent airfoil chord]

Upper-surface station	Lower-surface station
1.17	1.17
2.60	2.43
4.92	4.99
7.46	7.48
10.00	10.00
15.03	15.02
20.04	20.01
25.02	24.98
30.06	30.00
35.05	34.98
39.99	40.02
45.00	45.04
50.05	50.00
55.02	55.01
60.05	60.01
65.01	65.04
70.02	70.03
75.01	75.01
79.97	80.01
84.96	85.08
89.98	90.03
94.99	95.04

TABLE V.- STATIC-PRESSURE ORIFICE LOCATIONS FOR RC(3)-10 AIRFOIL

[Locations given in percent airfoil chord]

Upper-surface station	Lower-surface station
1.29	1.21
2.42	2.45
4.91	4.98
7.44	7.55
9.96	10.02
15.00	15.07
19.99	20.03
24.97	25.04
29.98	30.06
35.00	35.05
39.92	40.02
44.95	45.07
49.97	49.99
54.99	54.97
59.99	60.00
64.97	64.97
69.99	69.98
74.99	75.00
80.00	79.97
83.34	85.02
89.95	90.00
94.98	95.05

TABLE VI.- STATIC-PRESSURE ORIFICE LOCATIONS FOR RC(3)-12 AIRFOIL

[Locations given in percent airfoil chord]

Upper-surface station	Lower-surface station
1.00	1.15
2.33	2.44
4.84	4.92
7.38	7.47
9.85	9.96
14.91	14.98
19.91	20.00
24.92	24.98
29.94	29.99
34.96	34.98
39.99	39.98
44.97	44.99
49.98	49.99
55.03	54.98
60.01	59.98
65.08	65.00
70.03	70.06
75.02	74.99
80.10	80.01
85.04	85.00
90.02	89.91
95.02	95.00

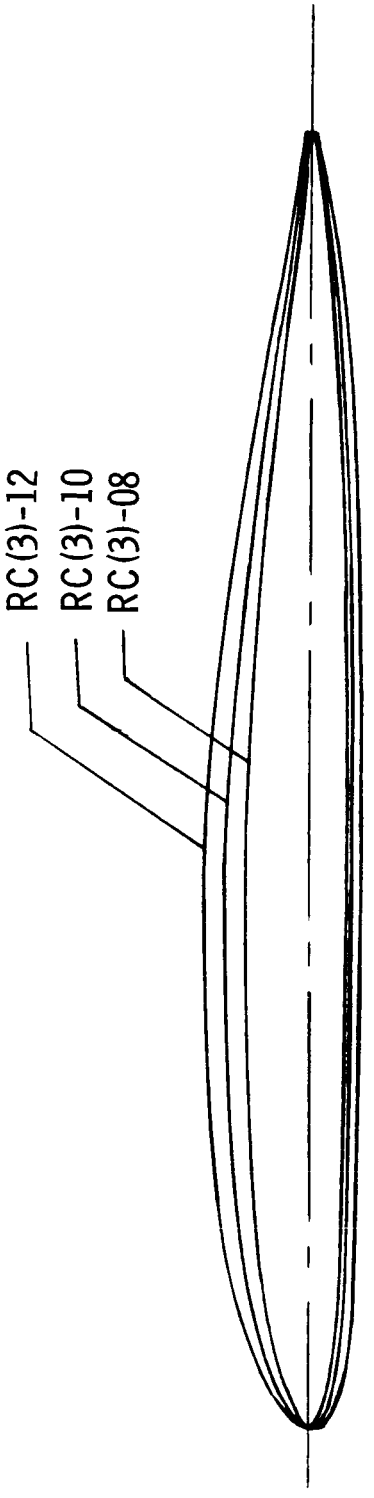

Figure 1.- Airfoil profiles.

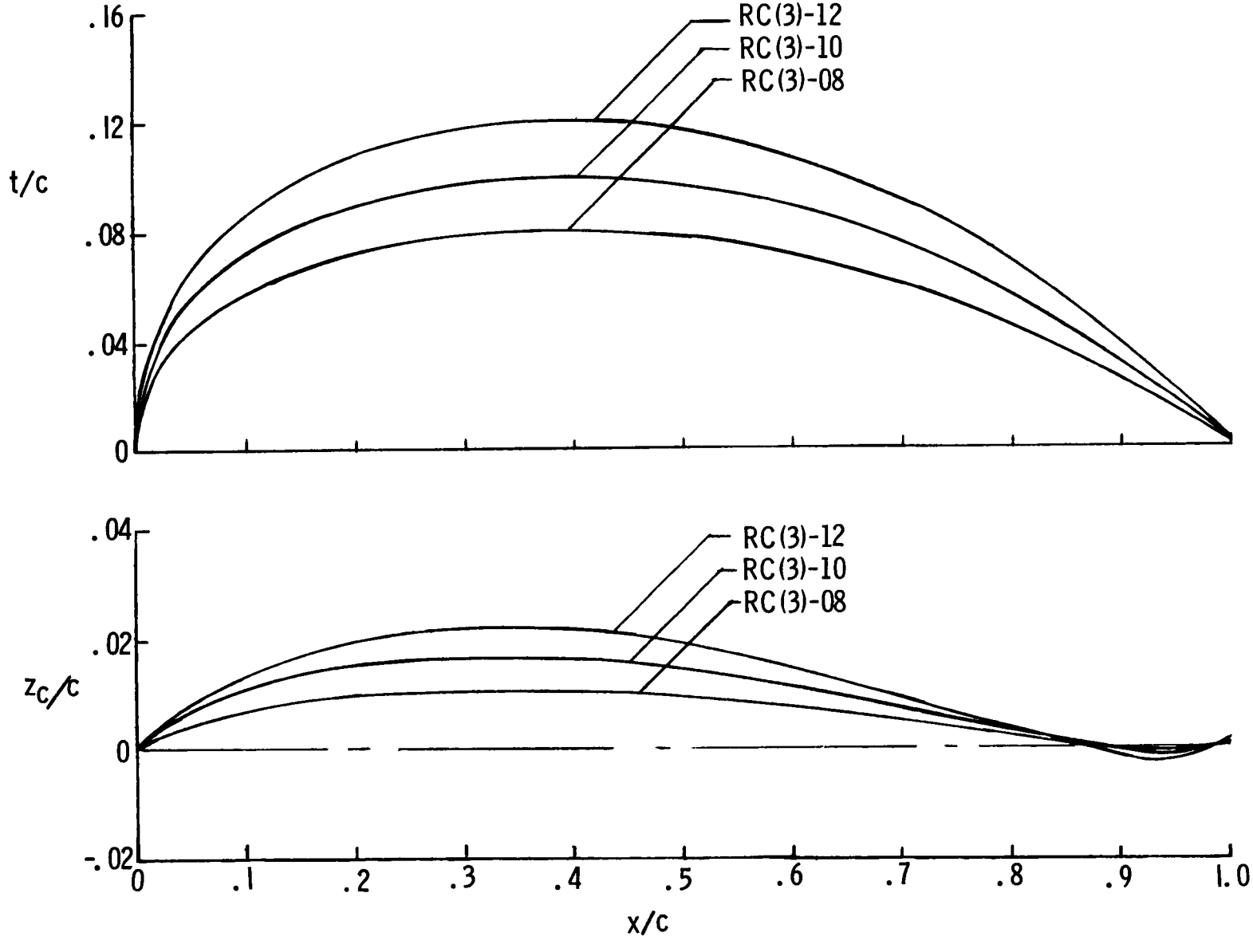

Figure 2.- Airfoil thickness distribution and mean line.

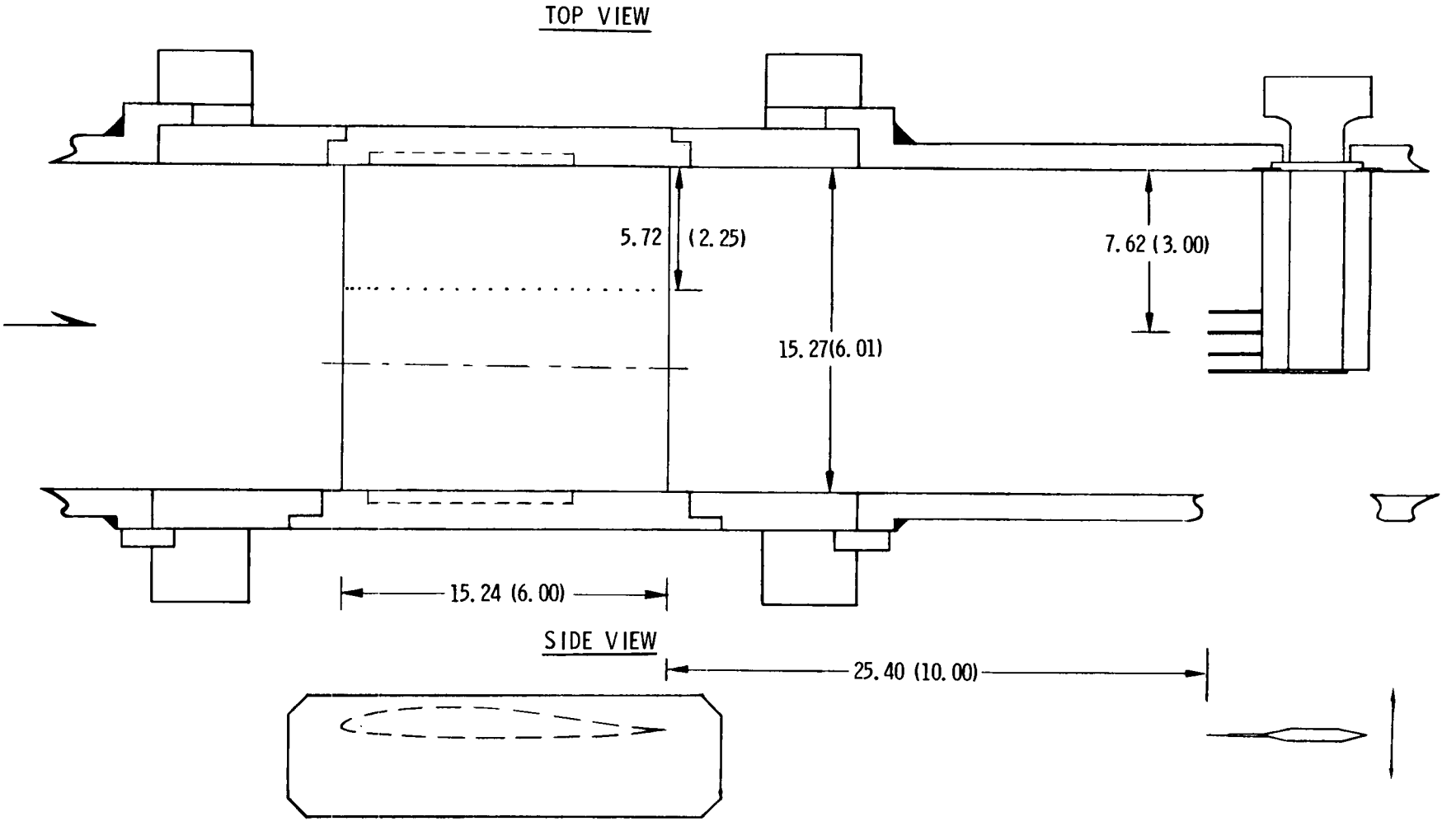

Figure 3.- Model and wake-survey probe installation in Langley 6- by 28-Inch Transonic Tunnel. All dimensions are in centimeters (inches).

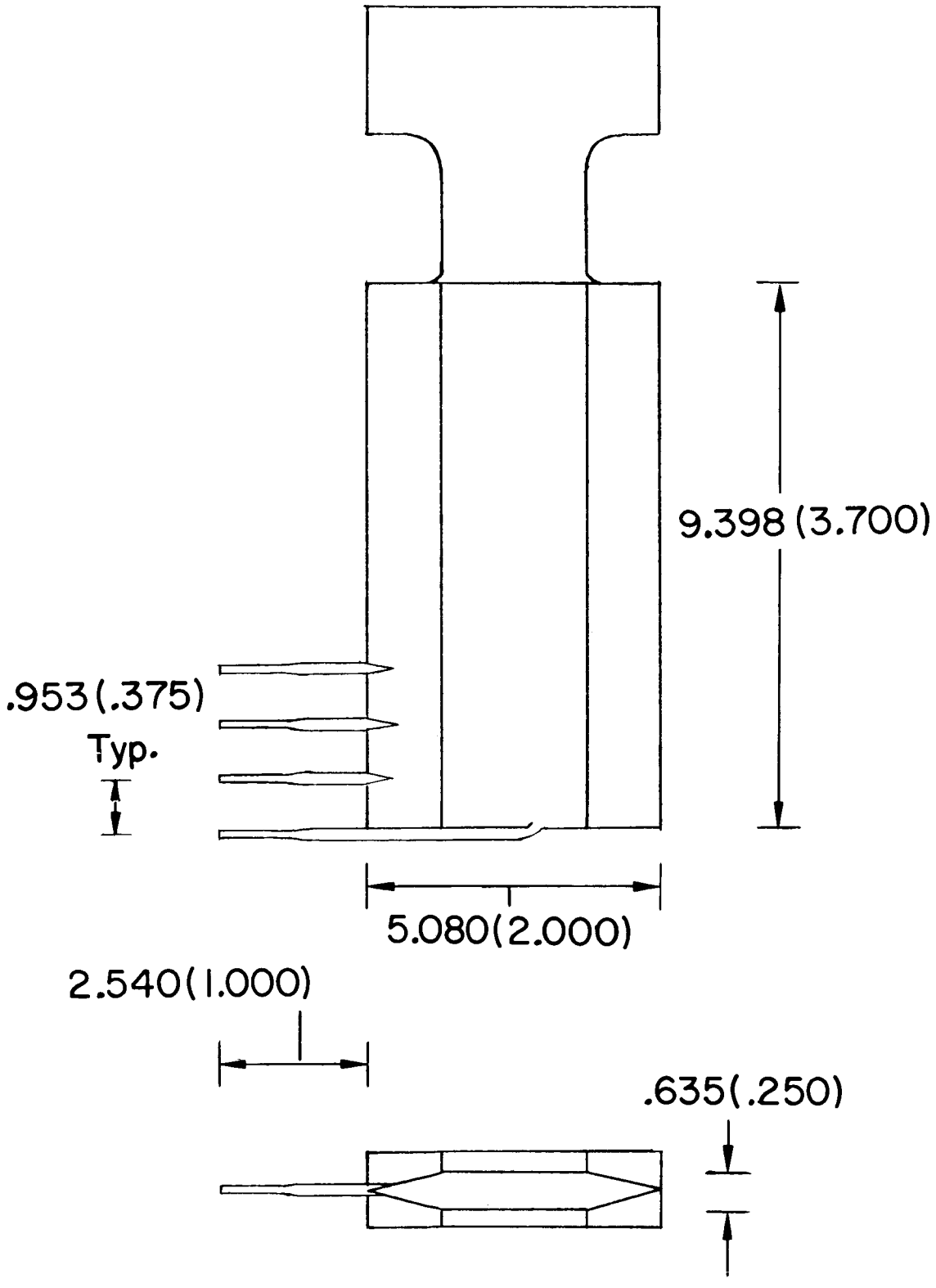

Figure 4.- Wake-survey probe used in Langley 6- by 28-Inch Transonic Tunnel. All dimensions are in centimeters (inches).

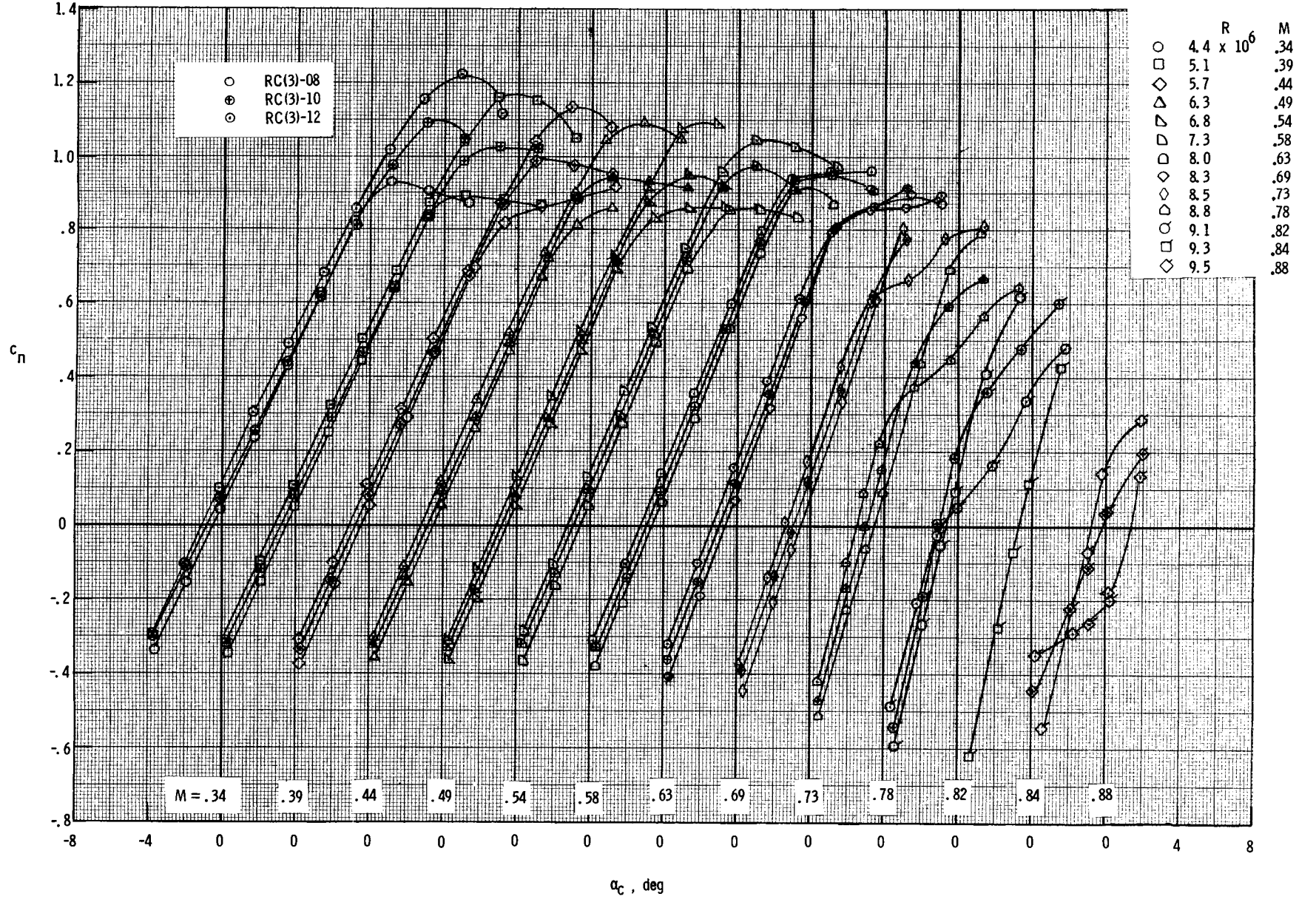

(a) Section normal-force coefficient.

Figure 5.- Aerodynamic characteristics of RC(3)-08, RC(3)-10, and RC(3)-12 airfoils measured in Langley 6- by 28-Inch Transonic Tunnel.

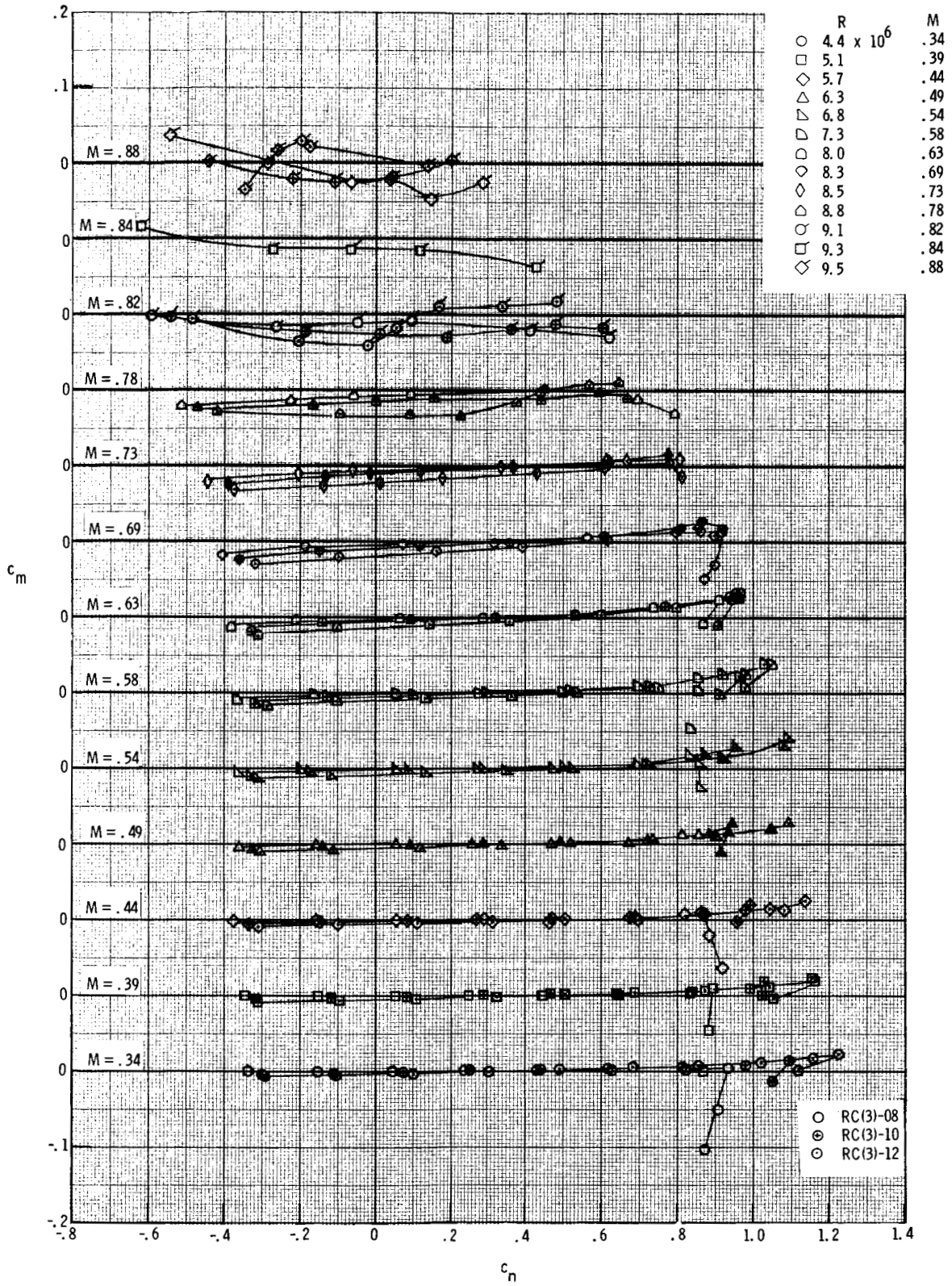

(b) Section pitching-moment coefficient.

Figure 5.- Continued.

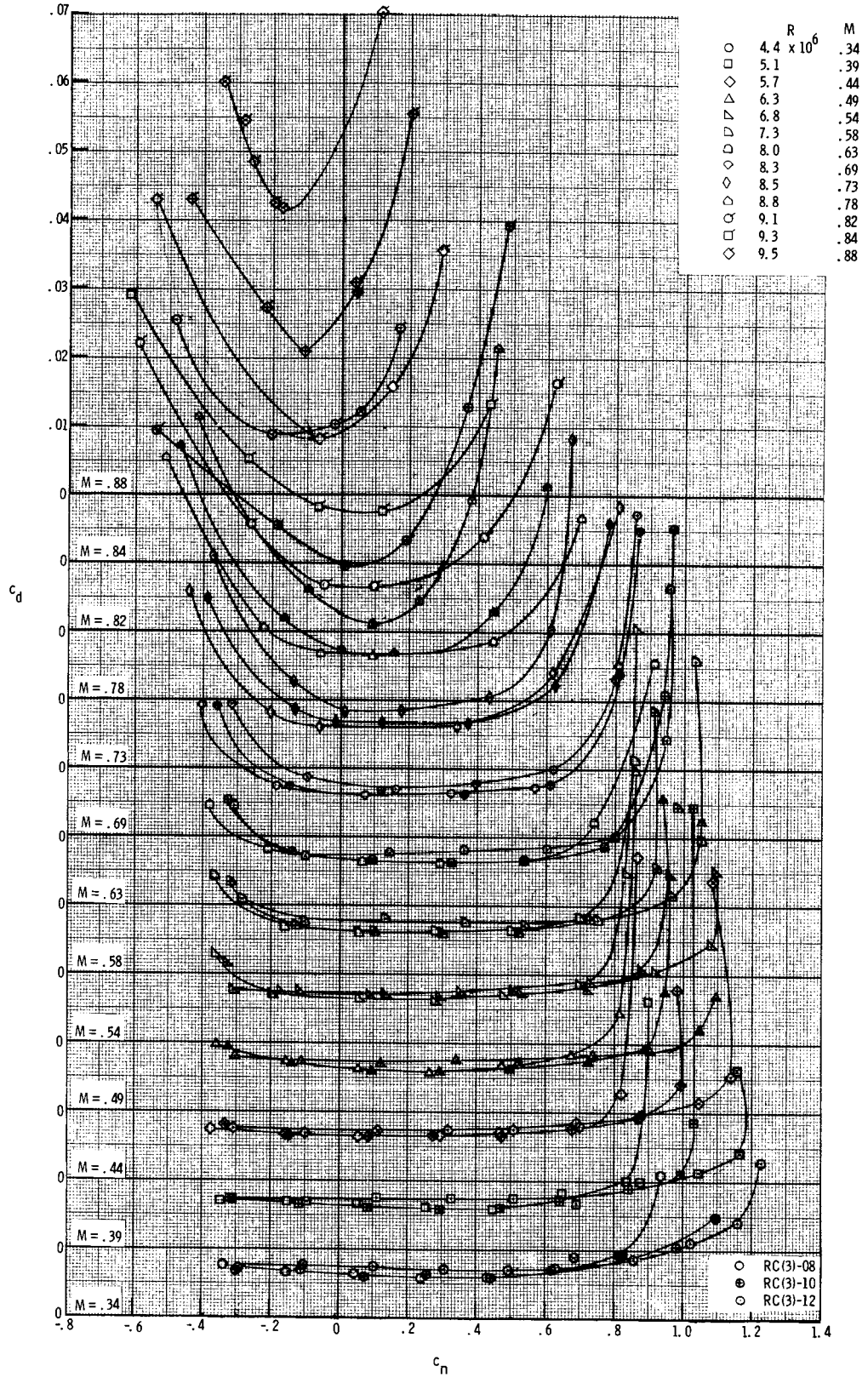

(c) Section drag coefficient.

Figure 5.- Concluded.

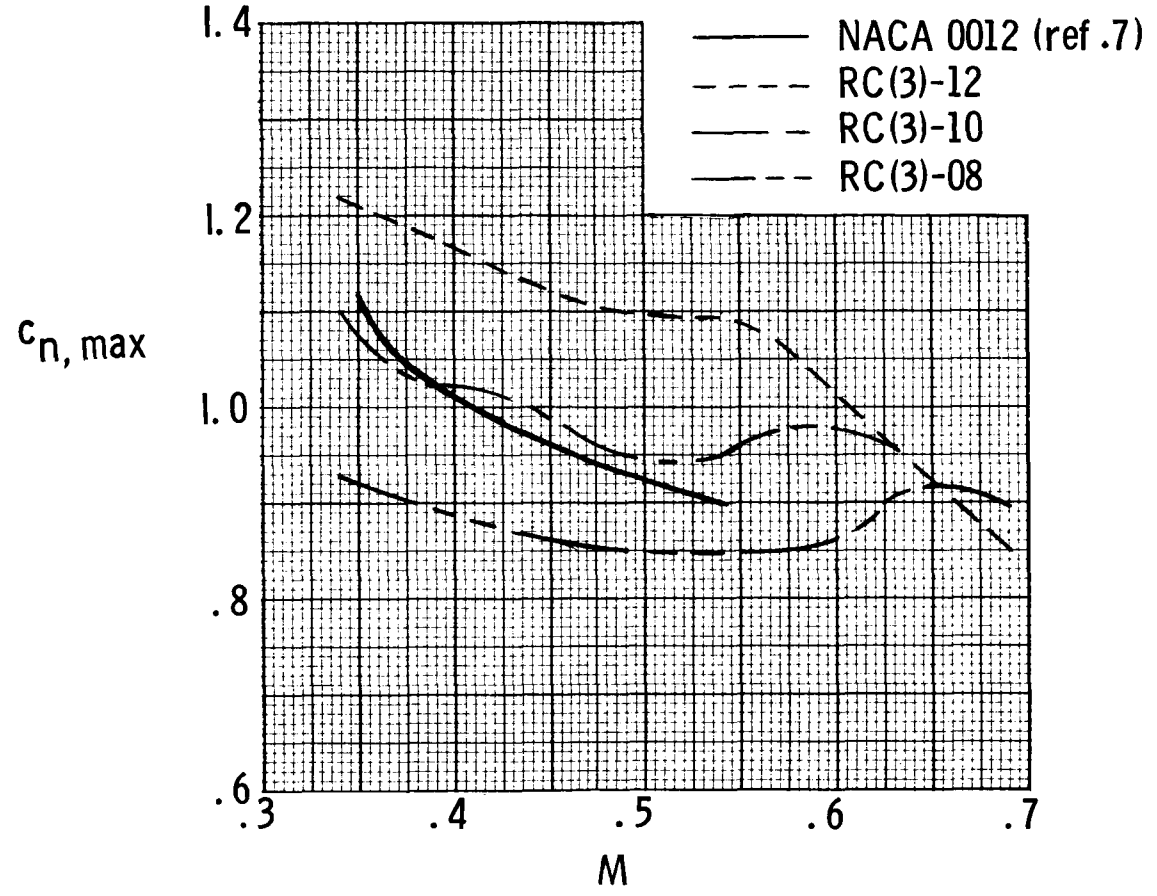

Figure 6.- Variation in maximum normal-force coefficient with Mach number.

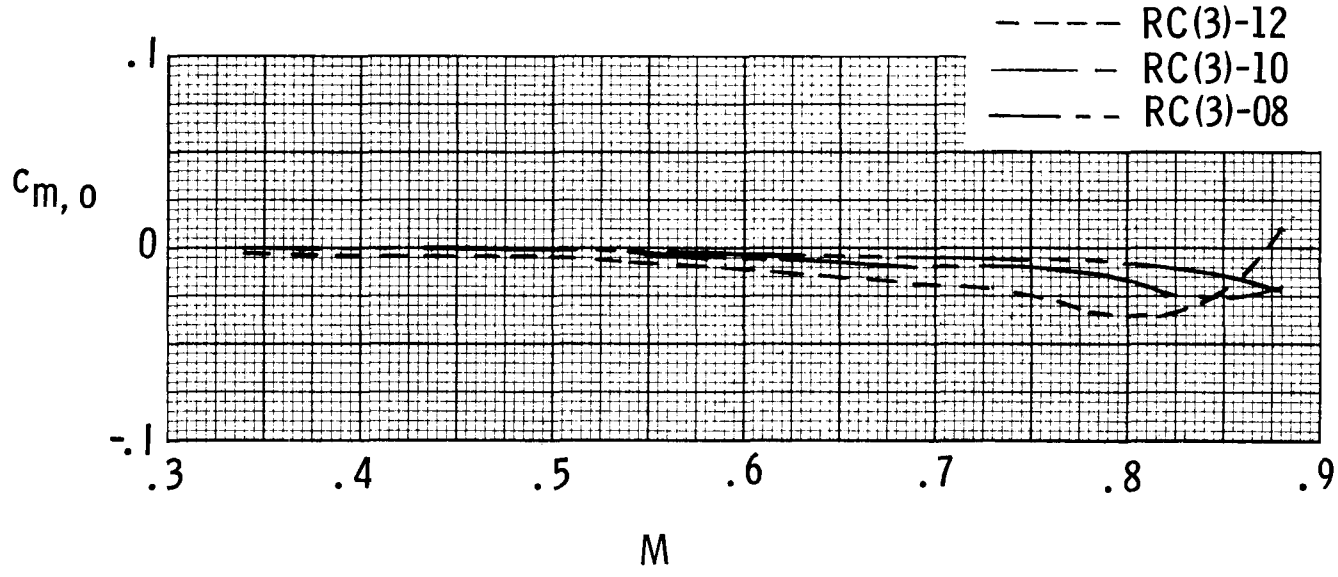

Figure 7.- Variation in pitching-moment coefficient about aerodynamic center with Mach number.

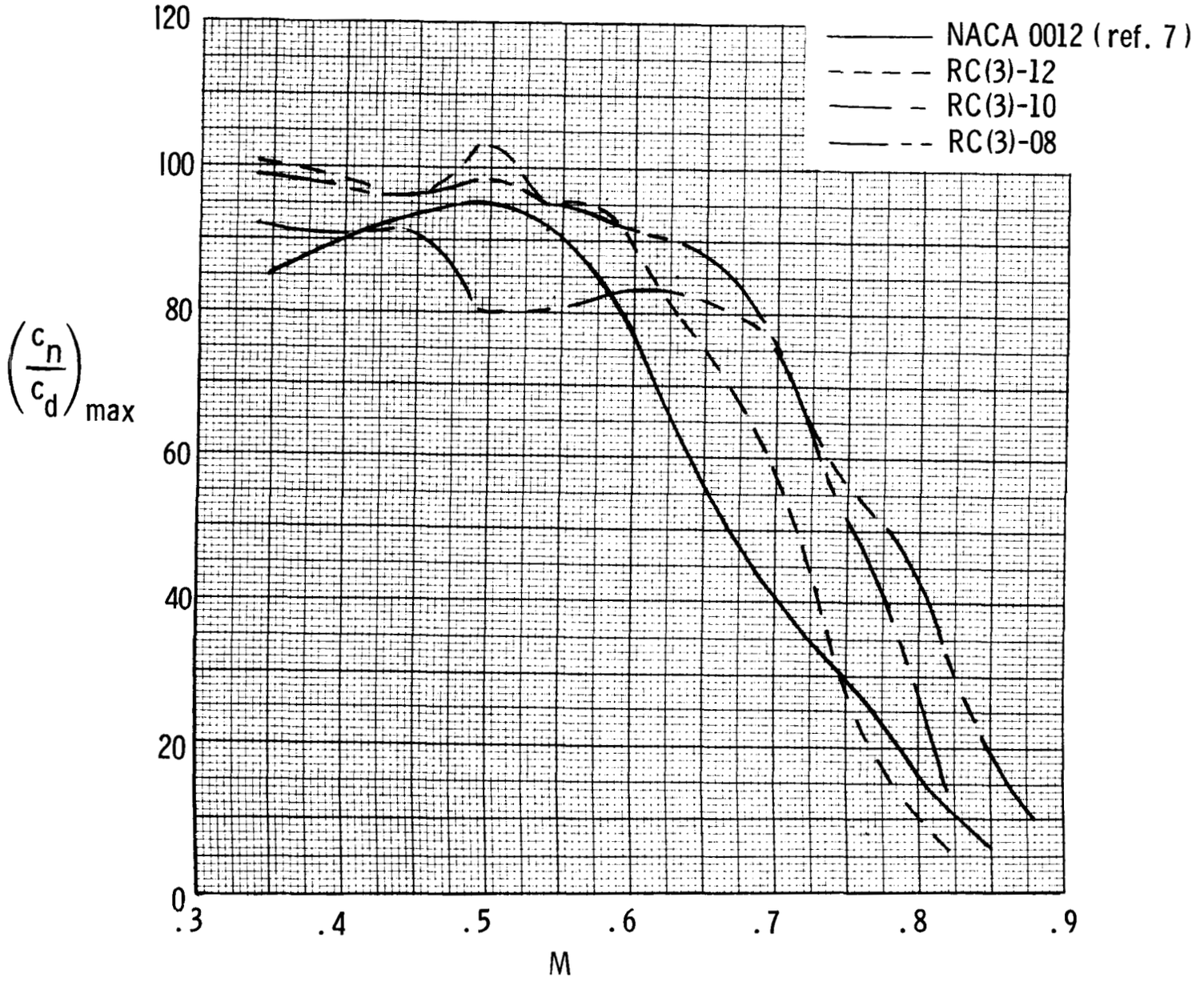

Figure 8.- Variation in maximum ratio of section normal-force coefficient to drag coefficient with Mach number.

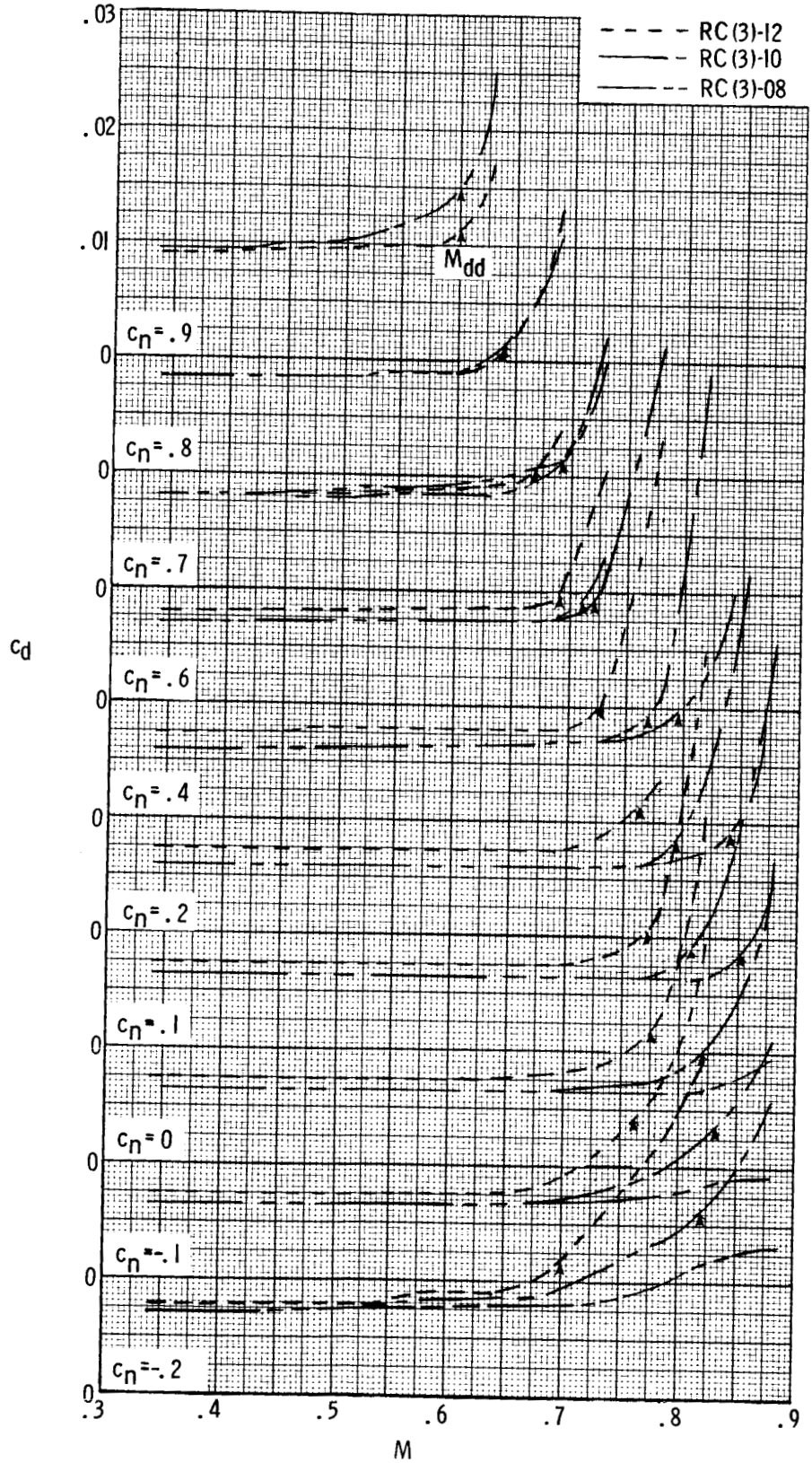

Figure 9.- Variation in section drag coefficient with Mach number.

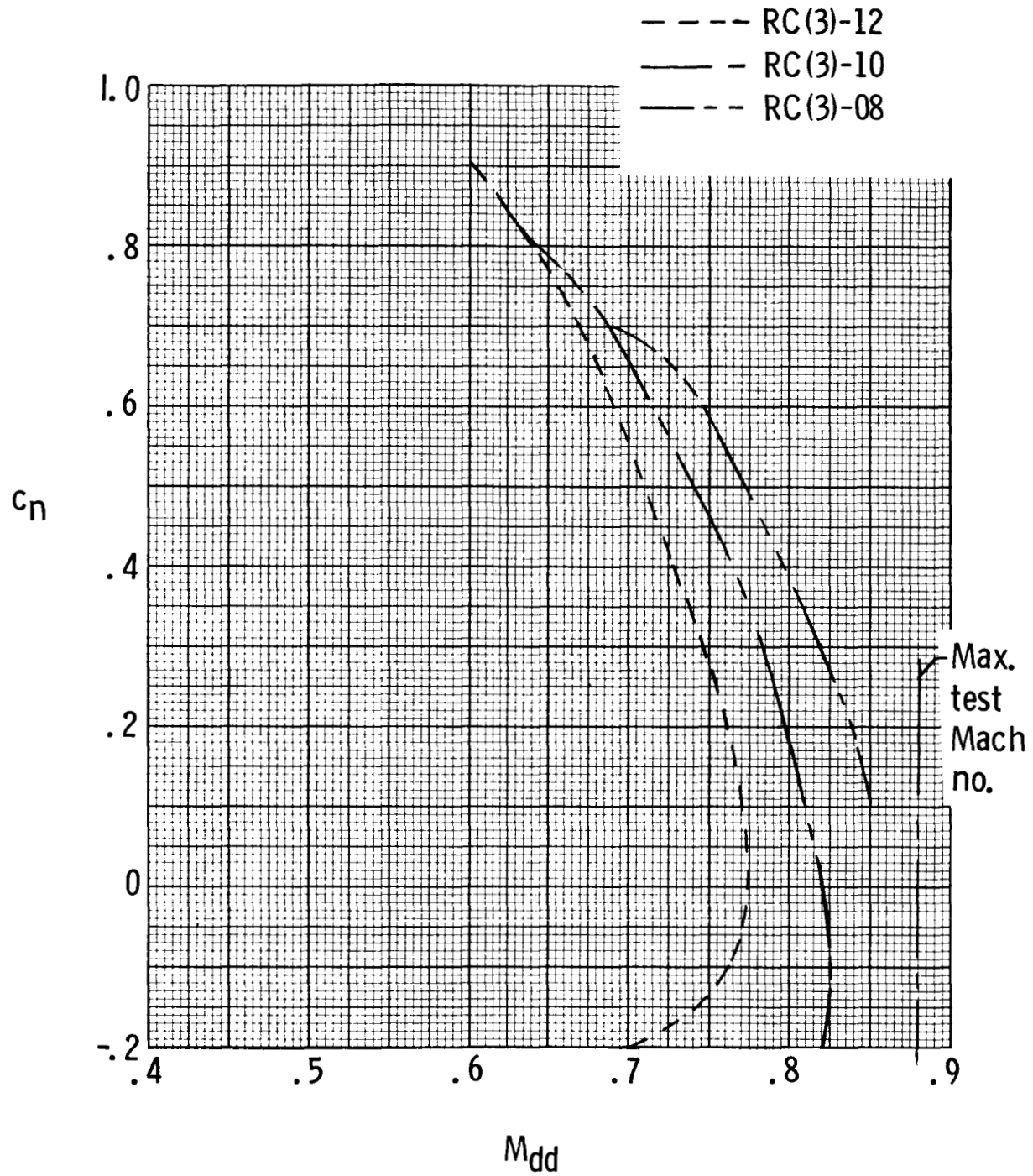

Figure 10.- Variation in section normal-force coefficient with drag-divergence Mach number.

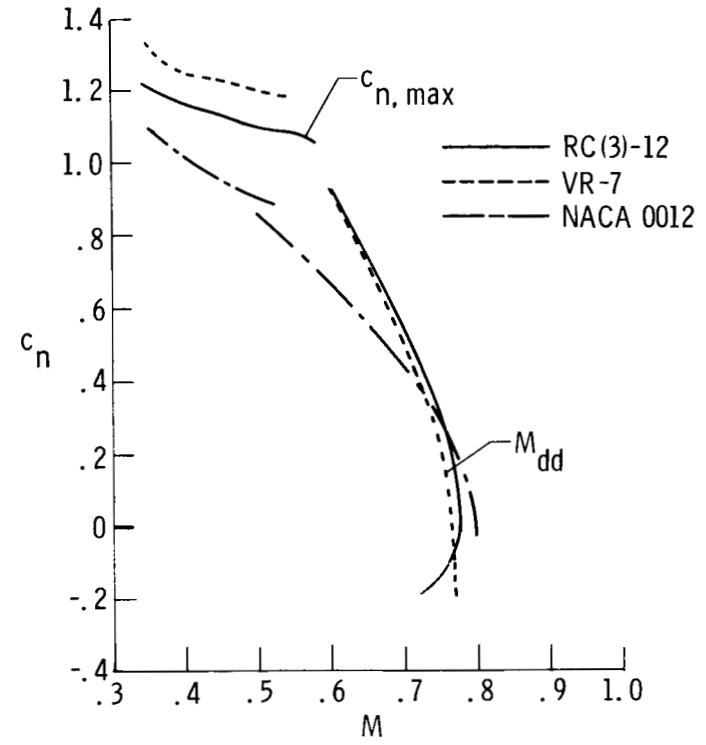

Figure 11.- Comparison of maximum normal-force coefficient and drag-divergence Mach number for 12-percent-thick airfoils (data from Langley 6- by 28-Inch Transonic Tunnel).

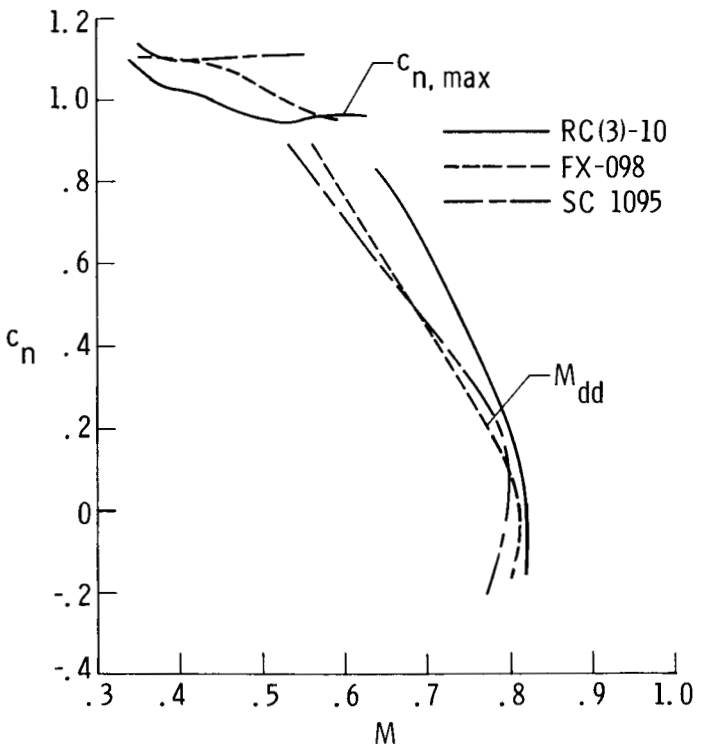

Figure 12.- Comparison of maximum normal-force coefficient and drag-divergence Mach number for near-10-percent-thick airfoils (data from Langley 6- by 28-Inch Transonic Tunnel).

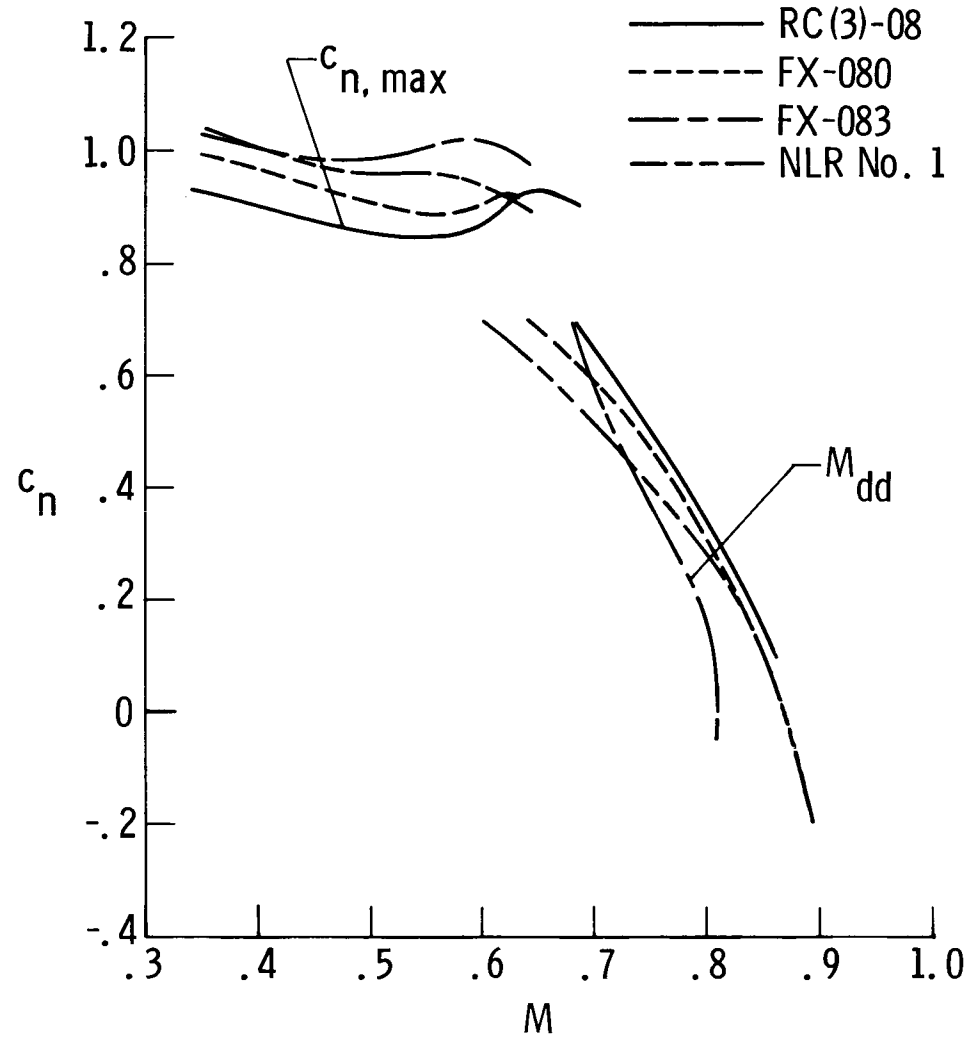

Figure 13.- Comparison of maximum normal-force coefficient and drag-divergence Mach number for near-8-percent-thick airfoils (data from Langley 6- by 28-Inch Transonic Tunnel).

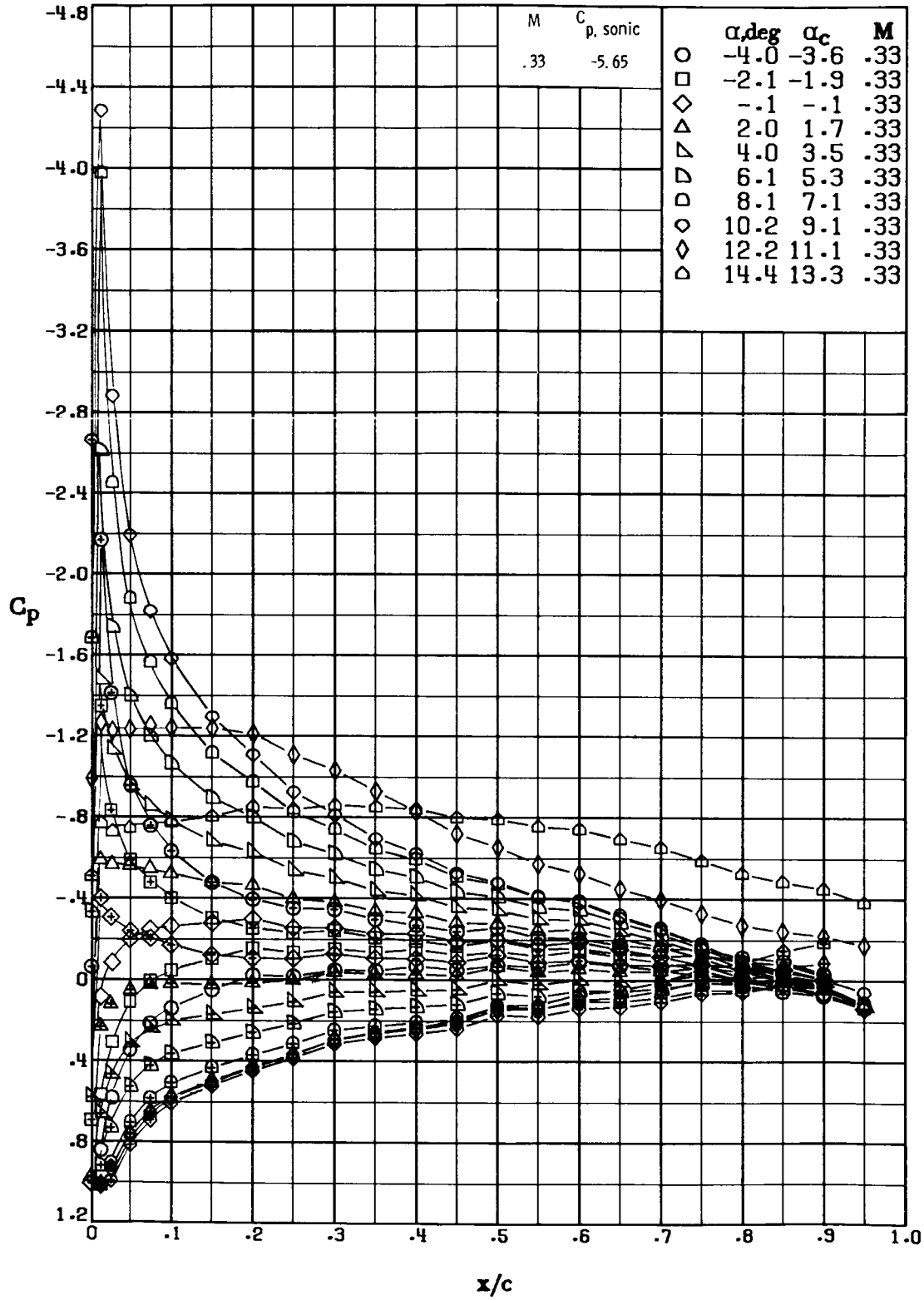

(a) M = 0.33; R ≈ 4.4 × 10^6.

Figure 14.- Pressure distribution over RC(3)-08 airfoil. Symbols with "+" inside indicate lower surface.

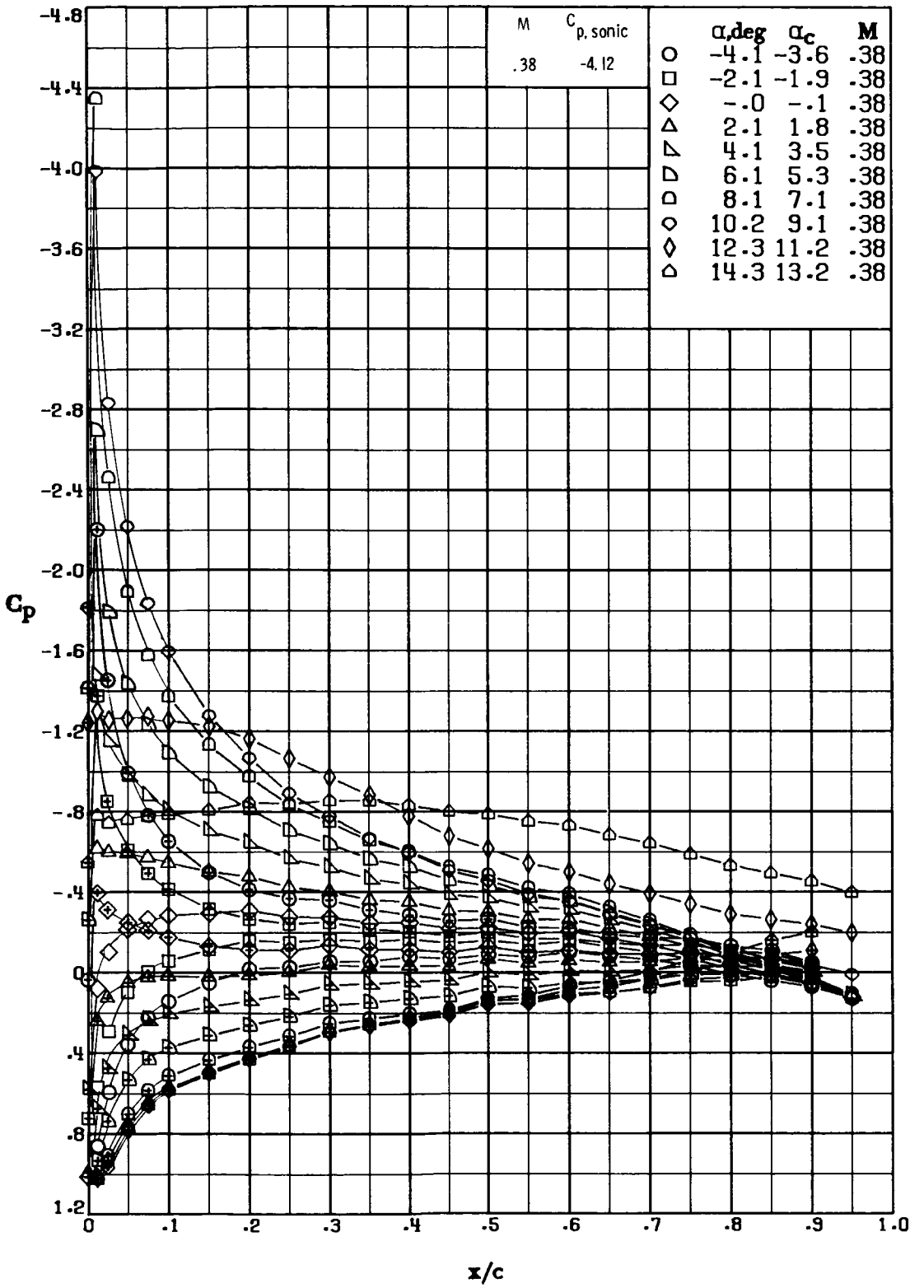

(b) M = 0.38; R ≈ 5.1×10^6.

Figure 14.- Continued.

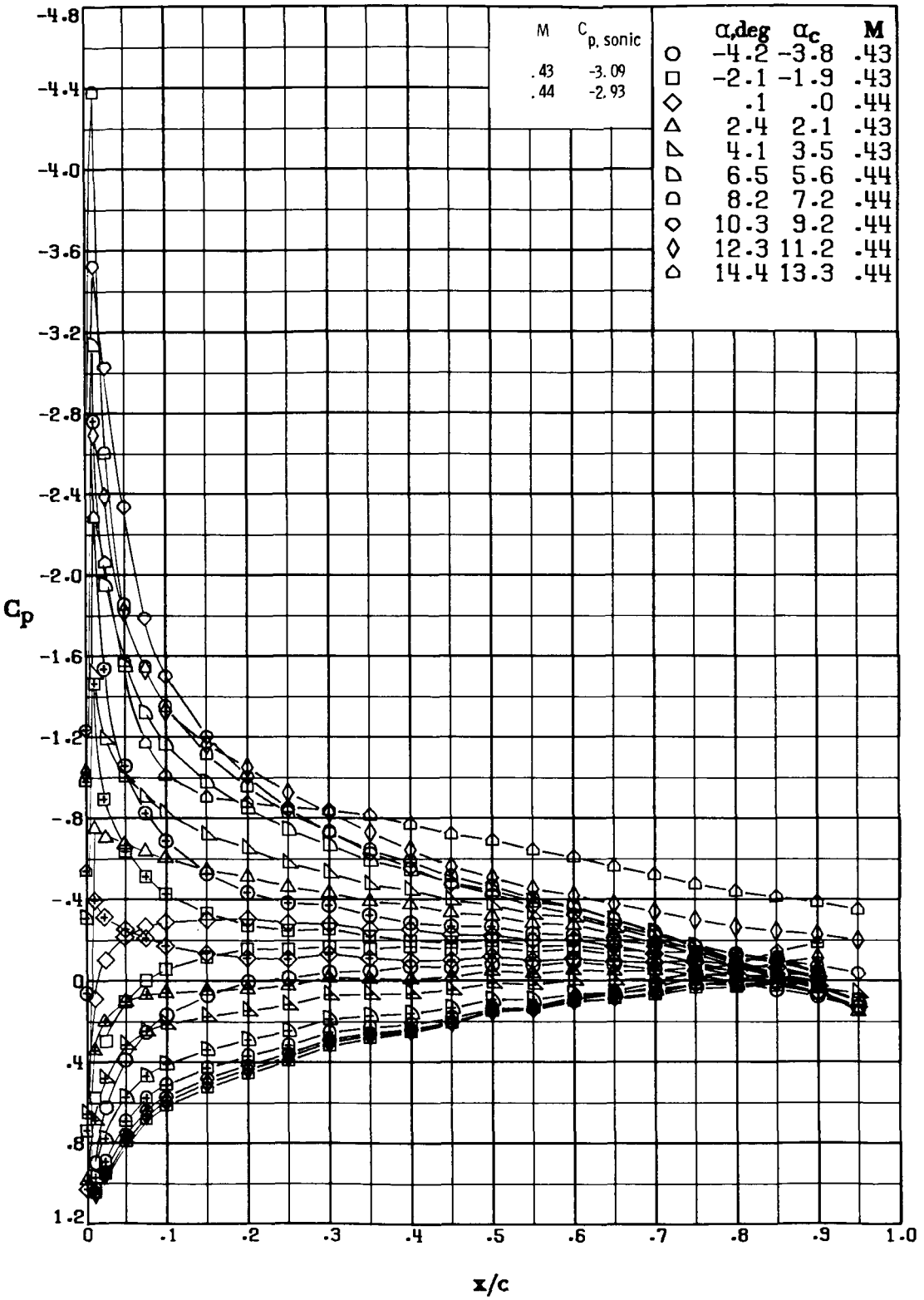

(c) $M \approx 0.44$; $R \approx 5.7 \times 10^6$.

Figure 14.- Continued.

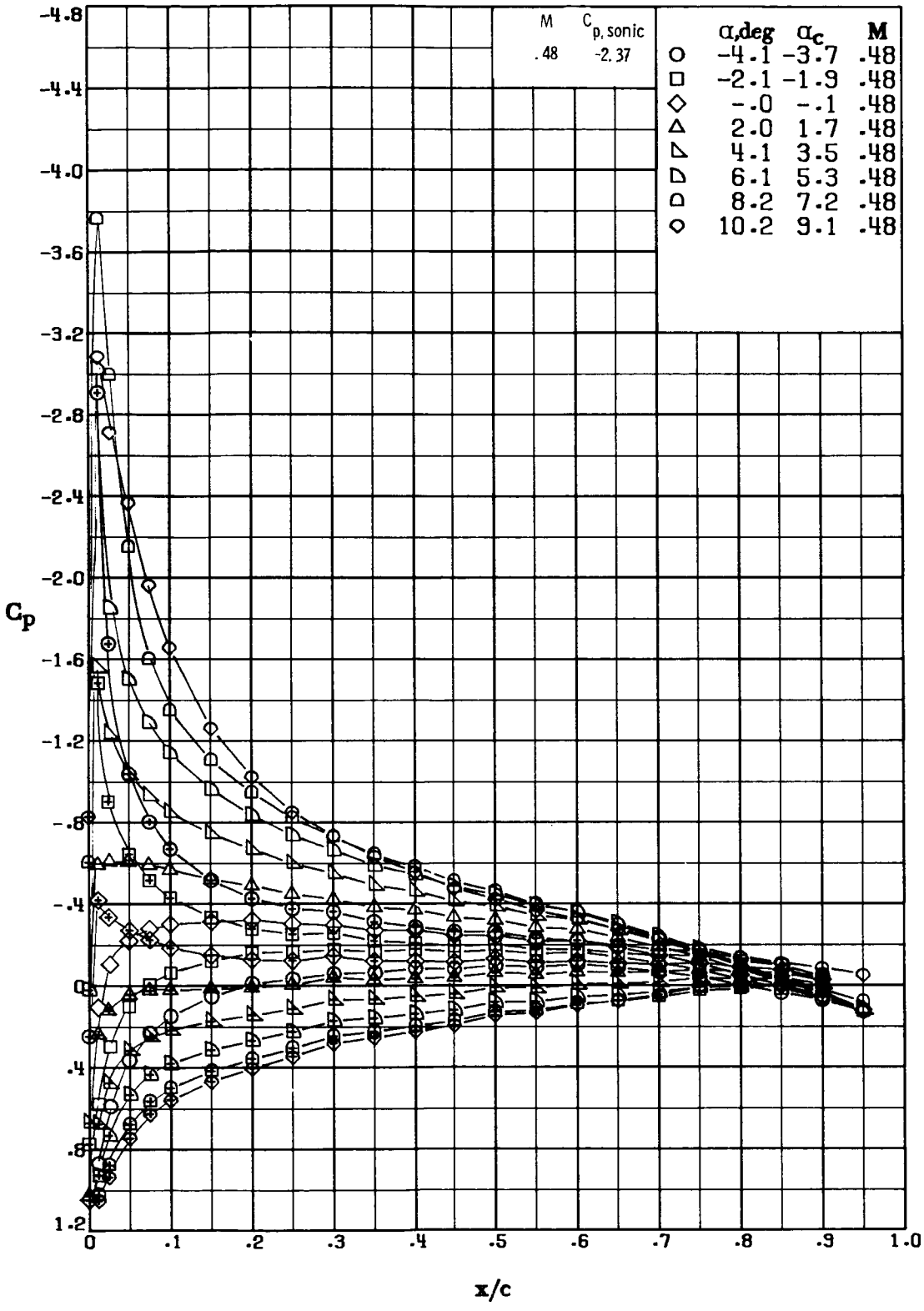

(d) M = 0.48; R ≈ 6.3×10^6.

Figure 14.- Continued.

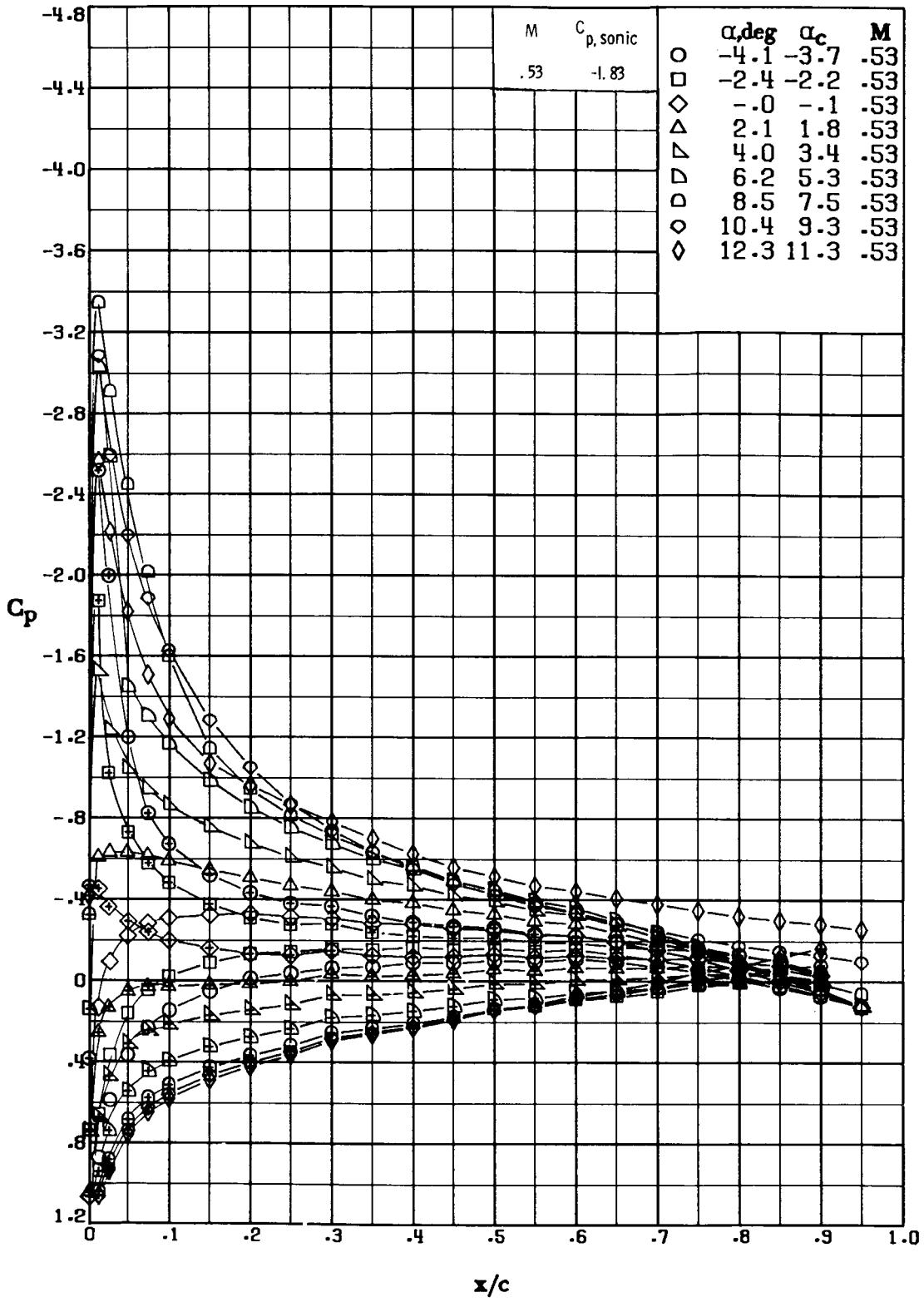

(e) M = 0.53; R ≈ 6.8×10^6.

Figure 14.- Continued.

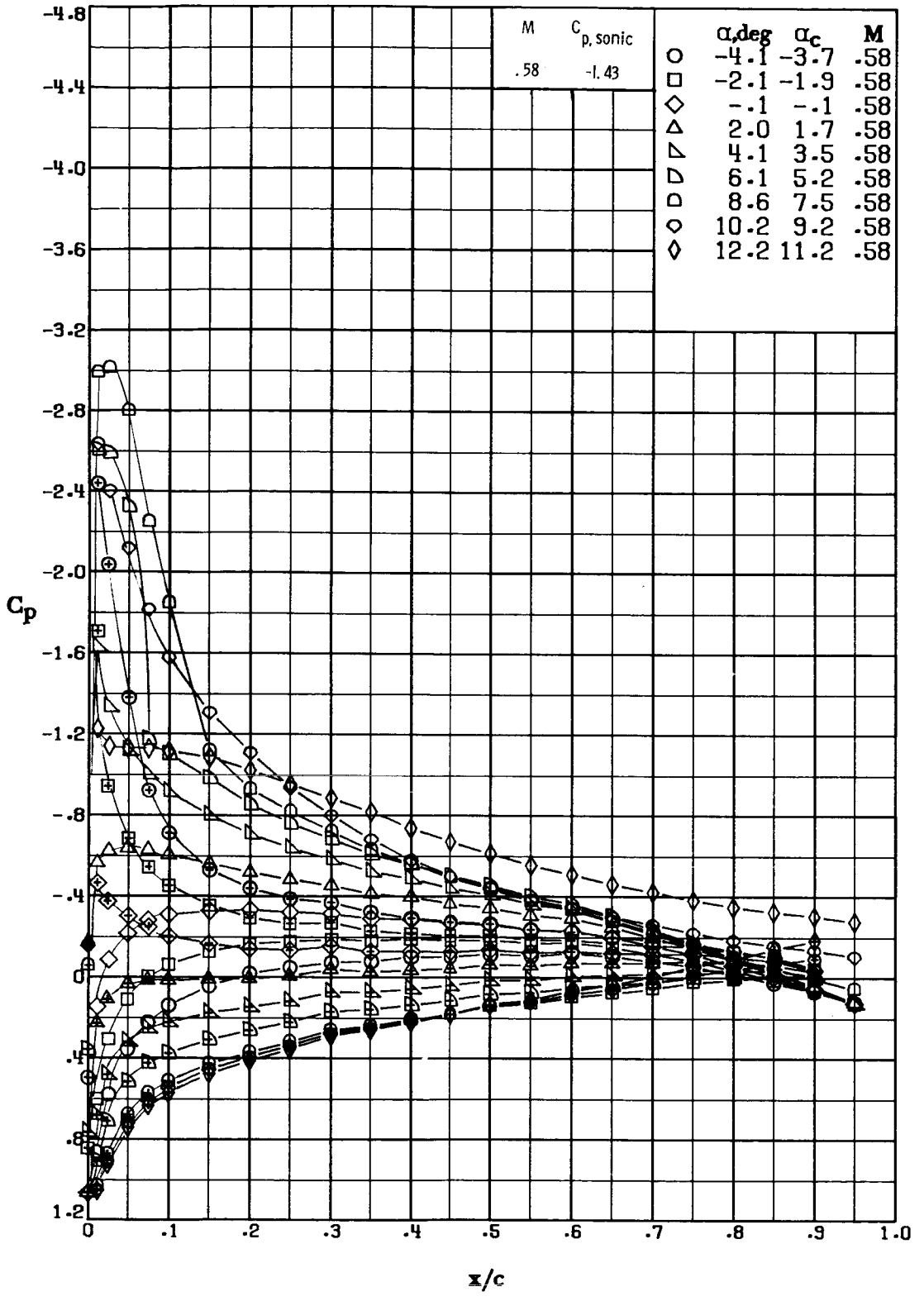

(f) M = 0.58; R ≈ 7.3×10^6.

Figure 14.- Continued.

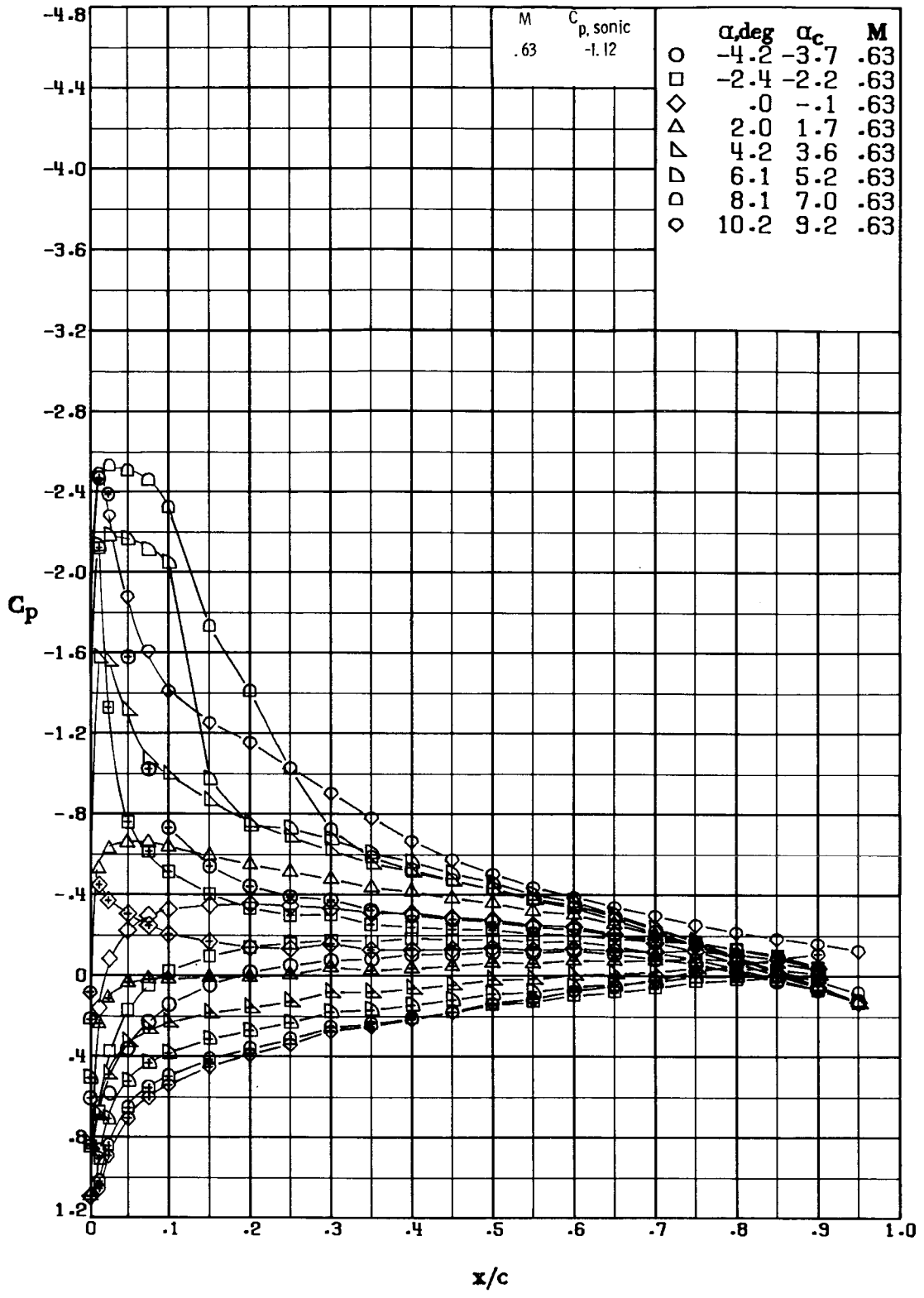

(g) M = 0.63; R ≈ 8.0 × 10^6.

Figure 14.- Continued.

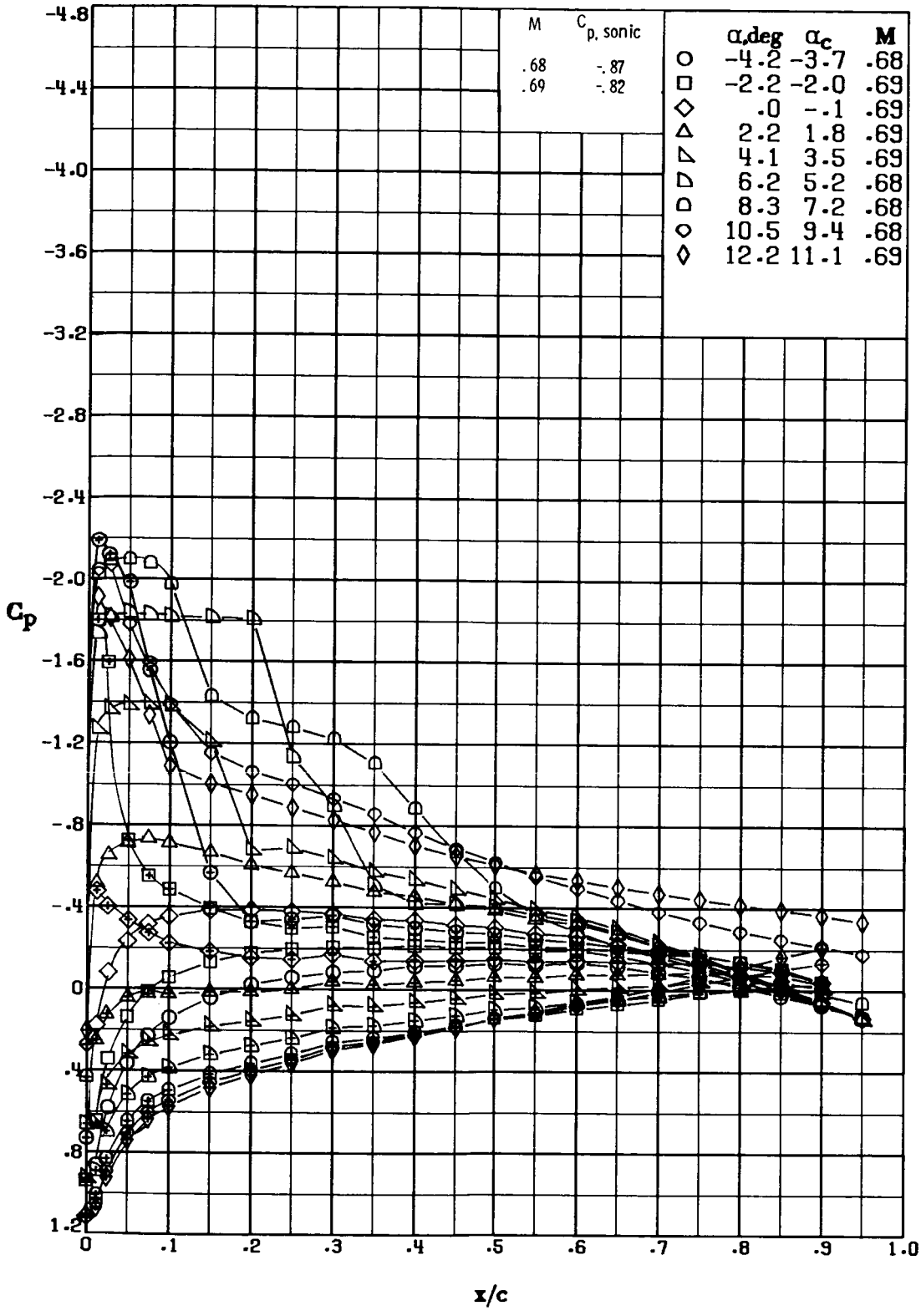

(h) $M \approx 0.69$; $R \approx 8.3 \times 10^6$.

Figure 14.- Continued.

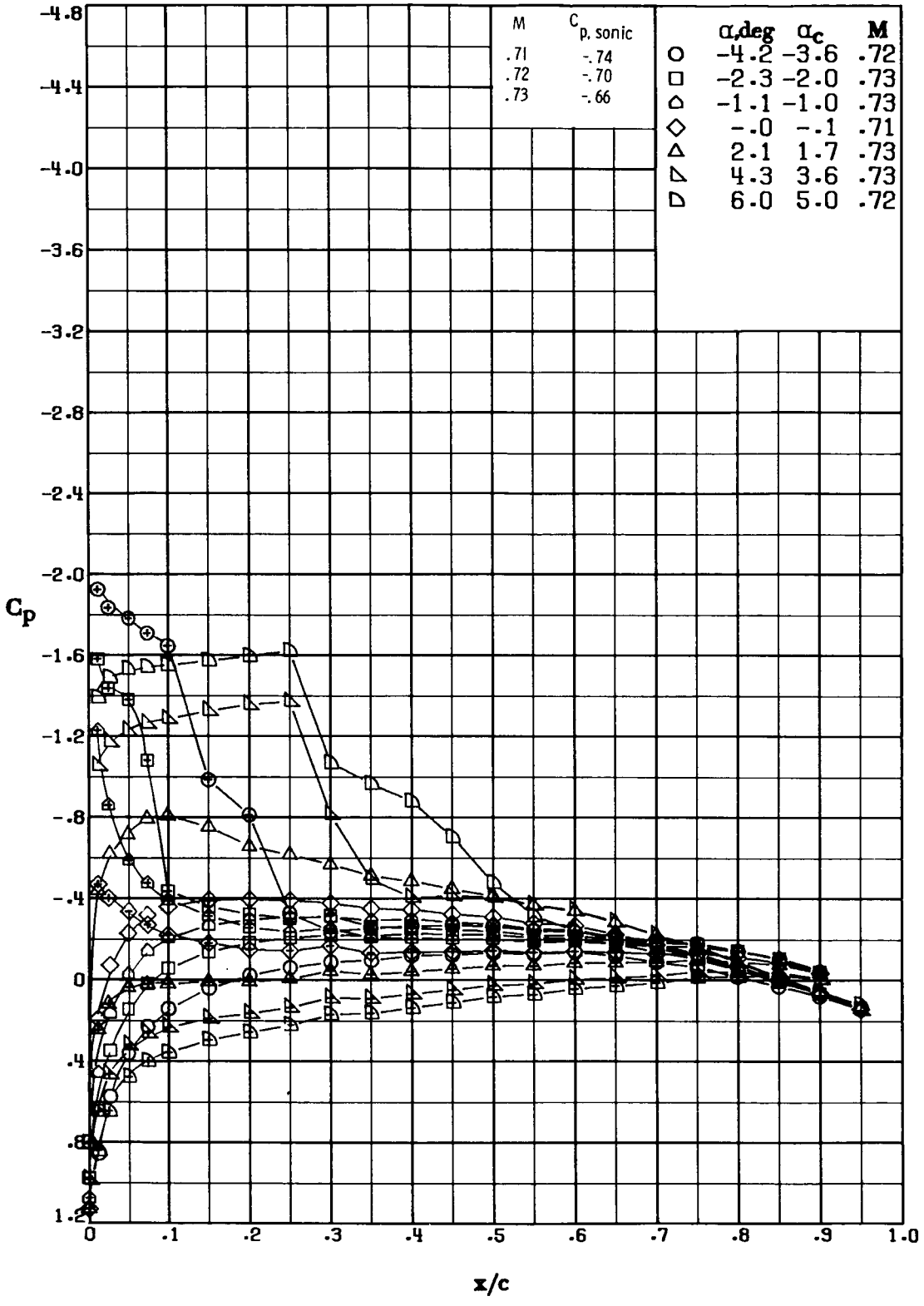

(i) $M \approx 0.72$; $R \approx 8.5 \times 10^6$.

Figure 14.- Continued.

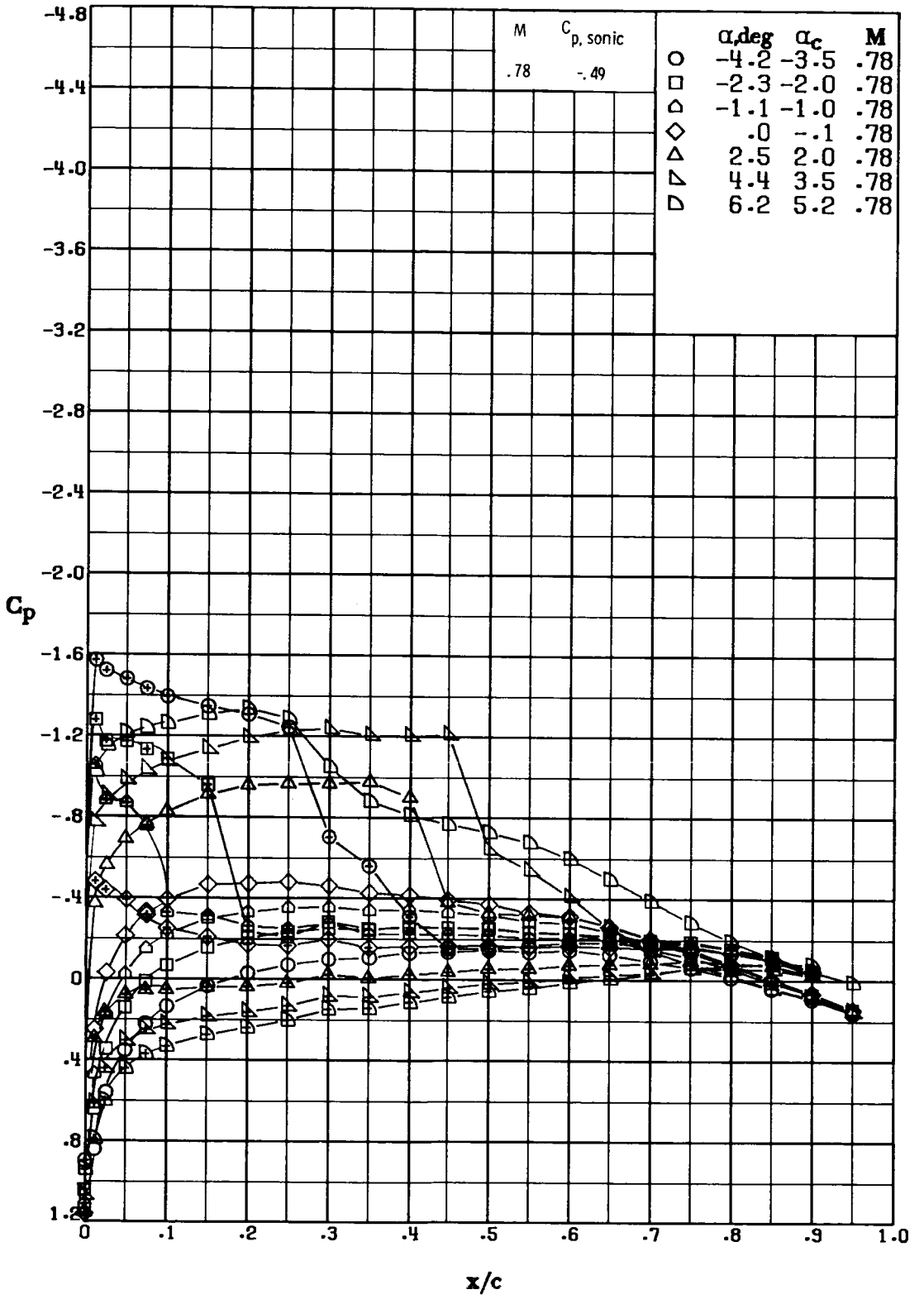

(j) M = 0.78; R ≈ 8.8 × 10^6.

Figure 14.- Continued.

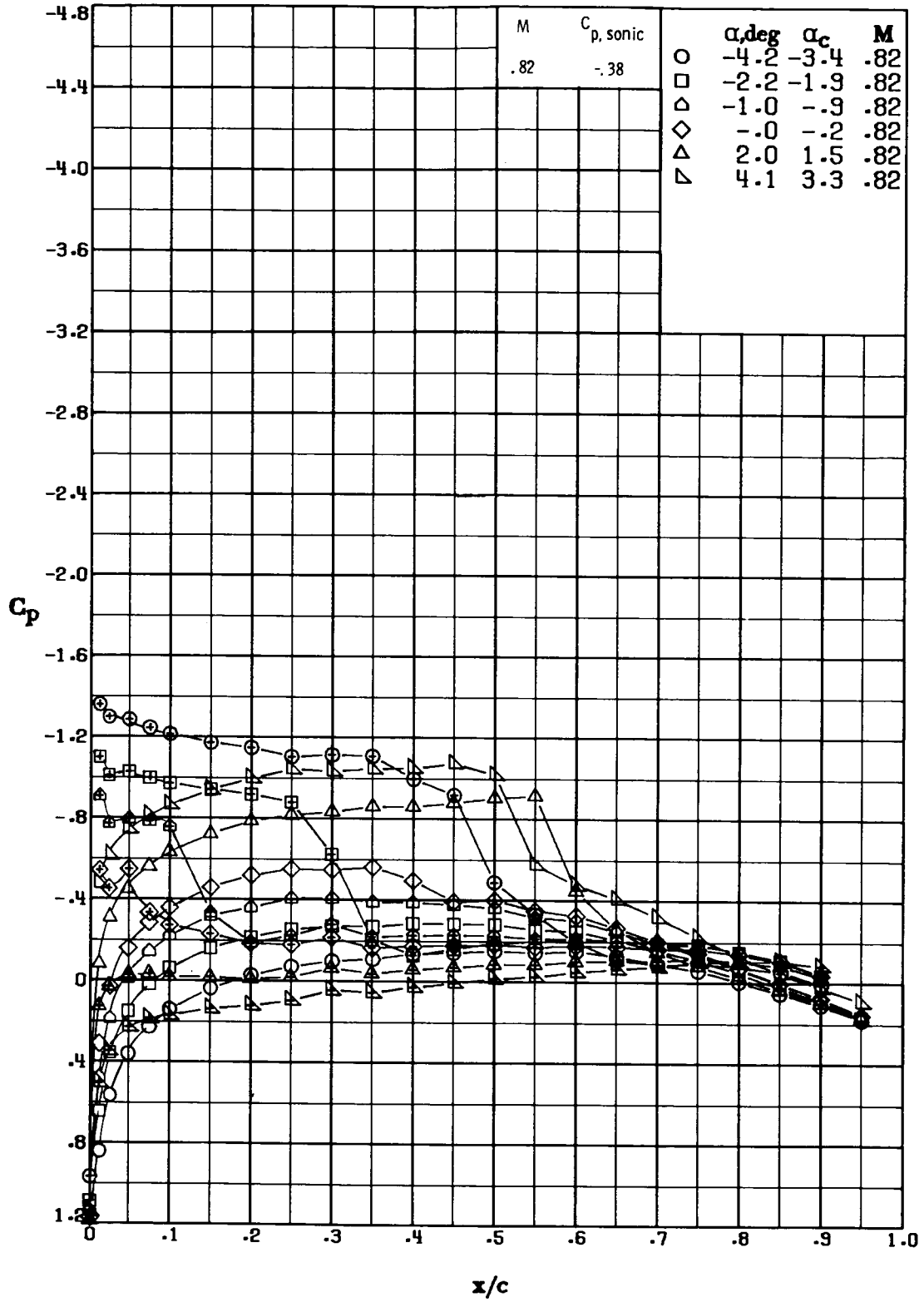

(k) M = 0.82; R ≈ 9.3 × 10^6.

Figure 14.- Continued.

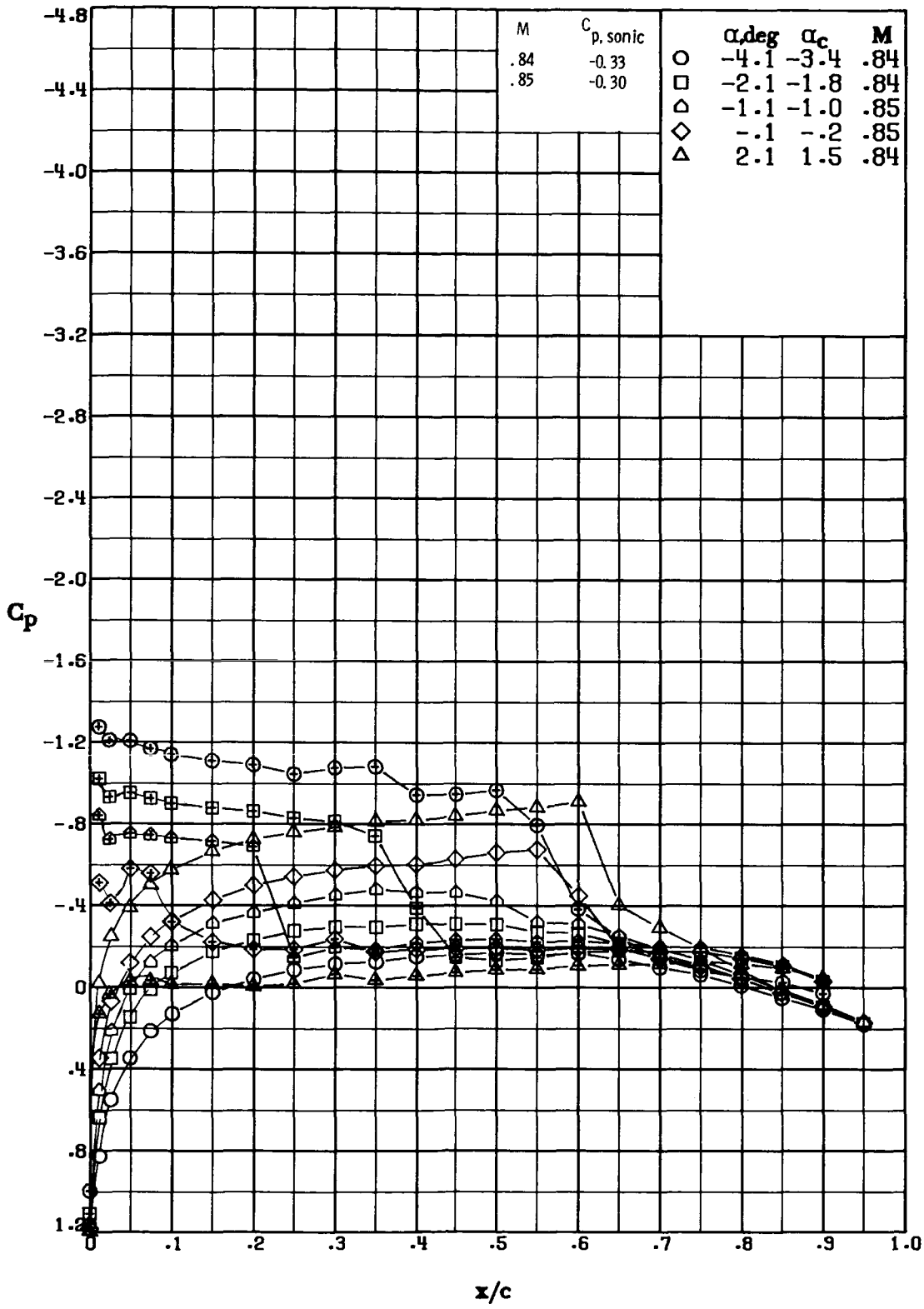

(l) M ≈ 0.84; R ≈ 9.1×10^6.

Figure 14.- Continued.

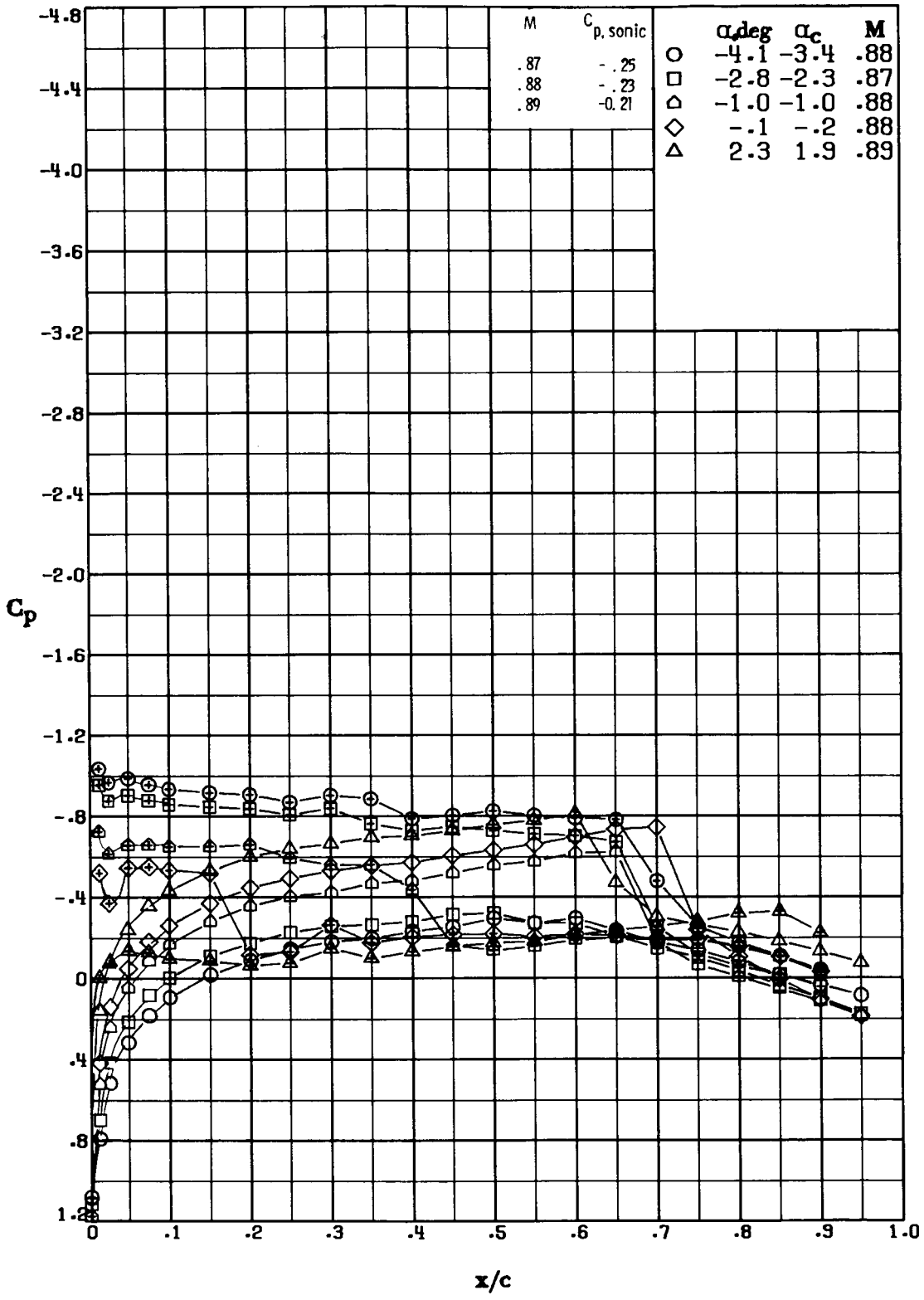

(m) $M \approx 0.88$; $R \approx 9.5 \times 10^6$.

Figure 14.- Concluded.

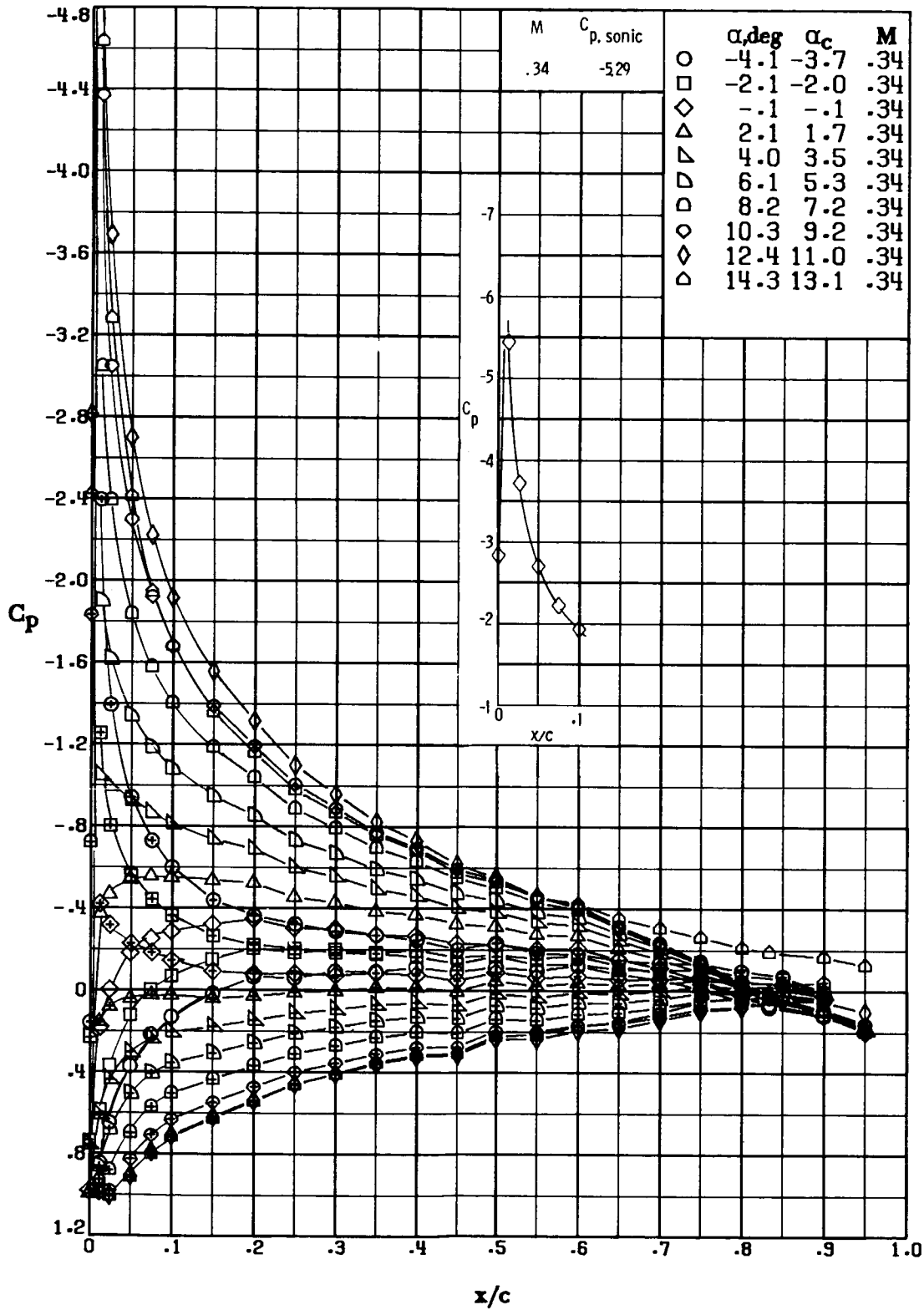

(a) M = 0.34; R ≈ 4.4×10^6.

Figure 15.- Pressure distribution over RC(3)-10 airfoil. Symbols with "+" inside indicate lower surface.

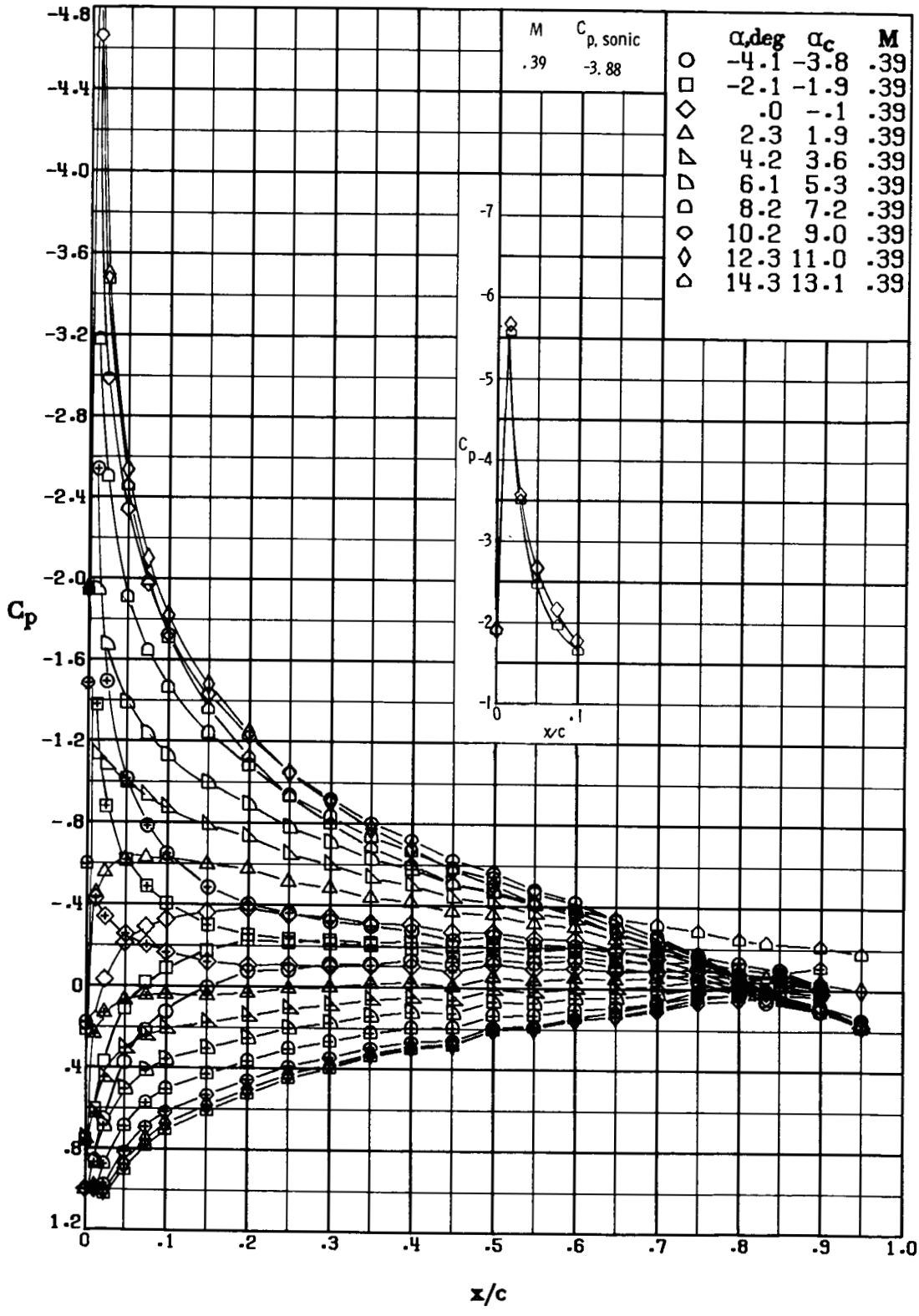

(b) M = 0.39; R ≈ 5.1 × 10^6.

Figure 15.- Continued.

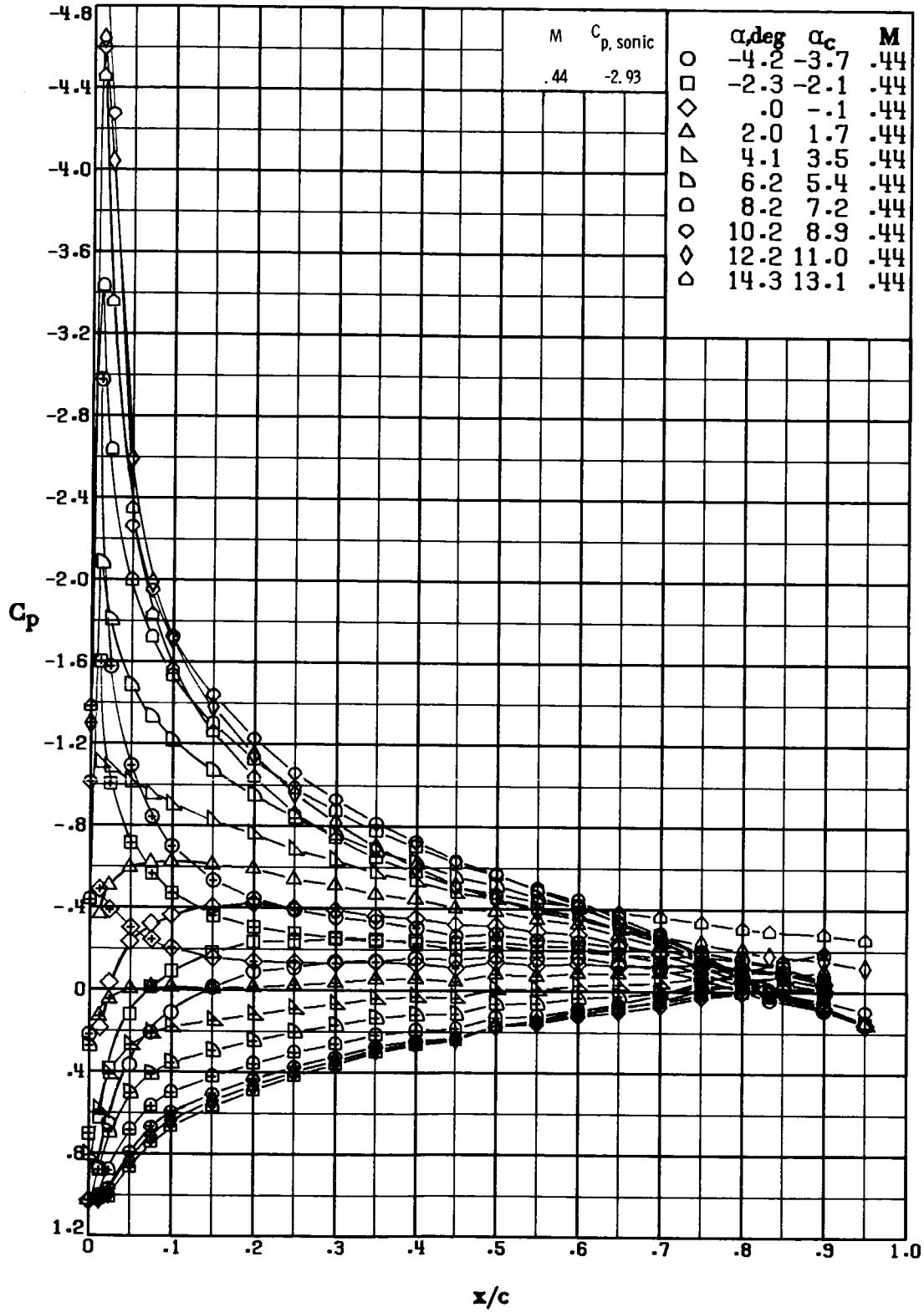

(c) M = 0.44; R ≈ 5.7×10^6.

Figure 15.- Continued.

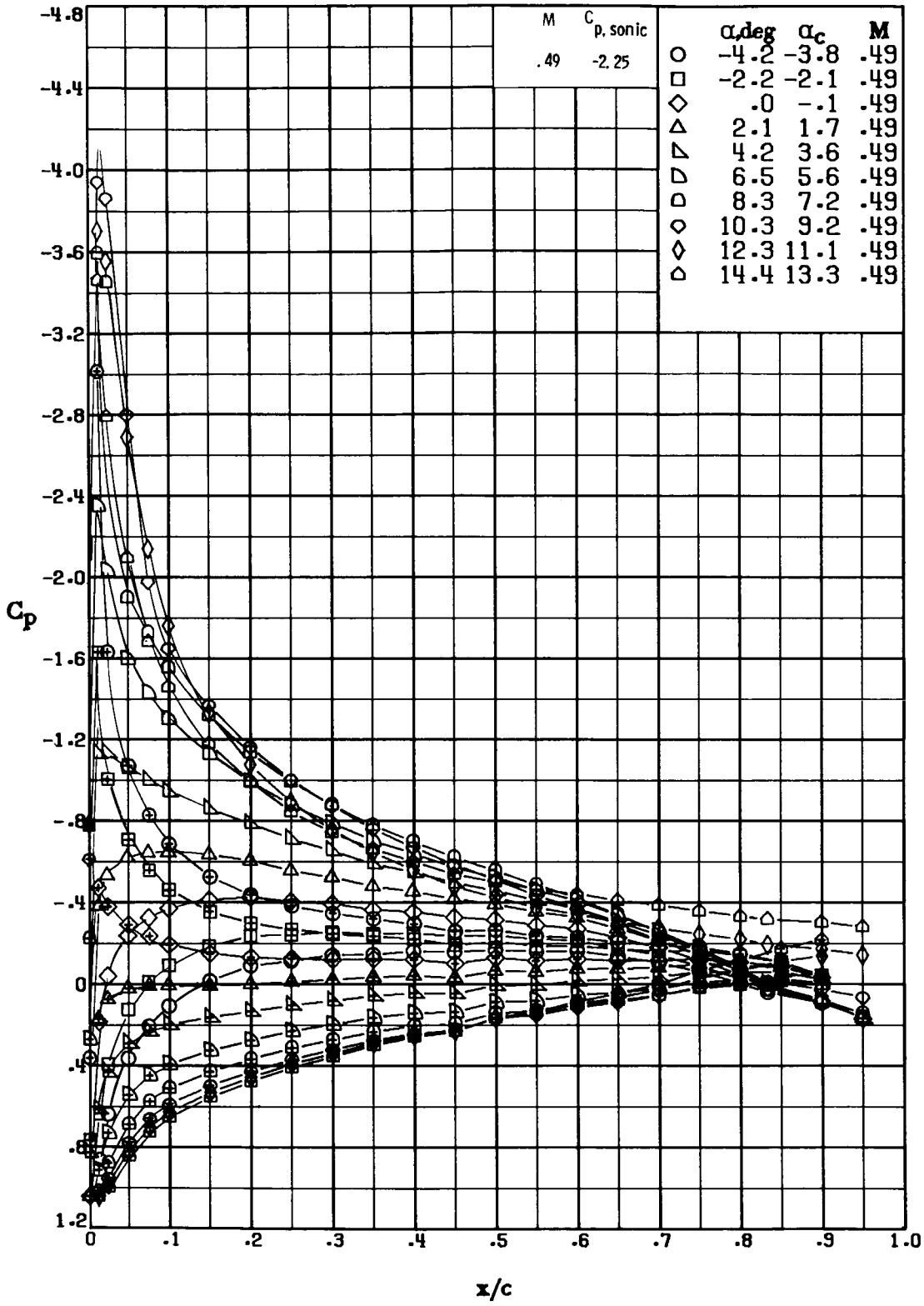

(d) M = 0.49; R ≈ 6.3 × 10^6.

Figure 15.- Continued.

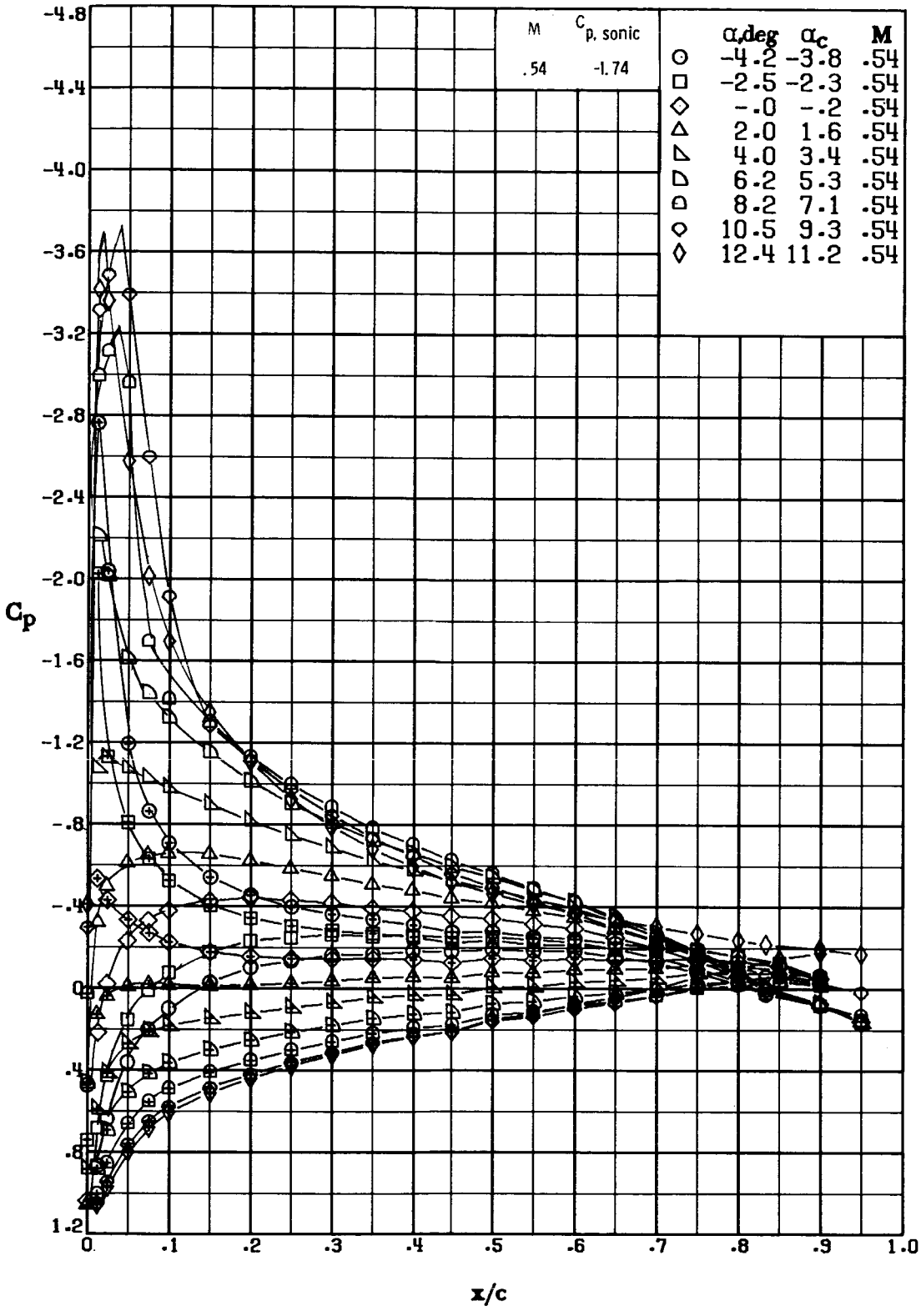

(e) M = 0.54; R ≈ 6.8×10^6.

Figure 15.- Continued.

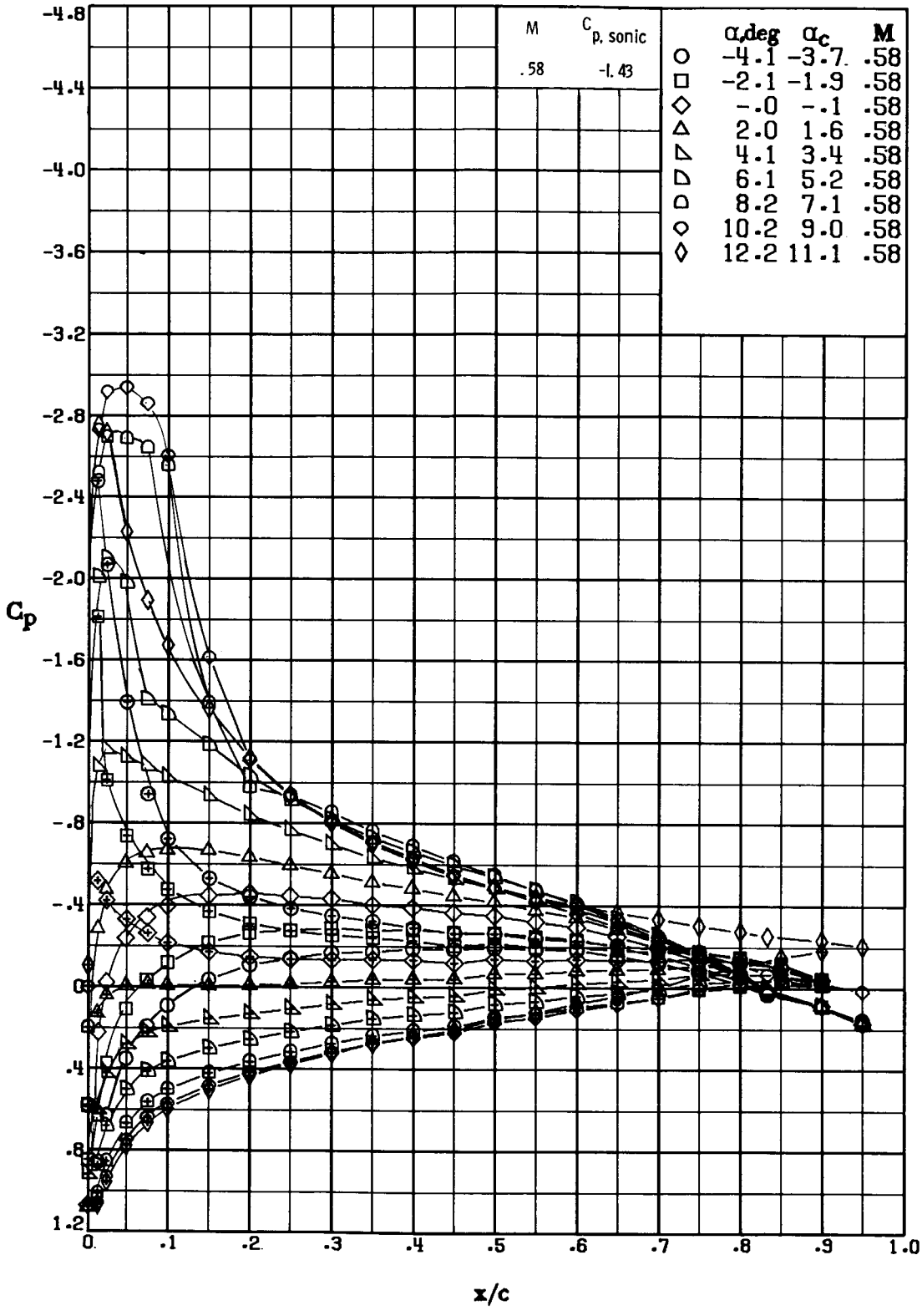

(f) M = 0.58; R ≈ 7.3 × 10^6.

Figure 15.- Continued.

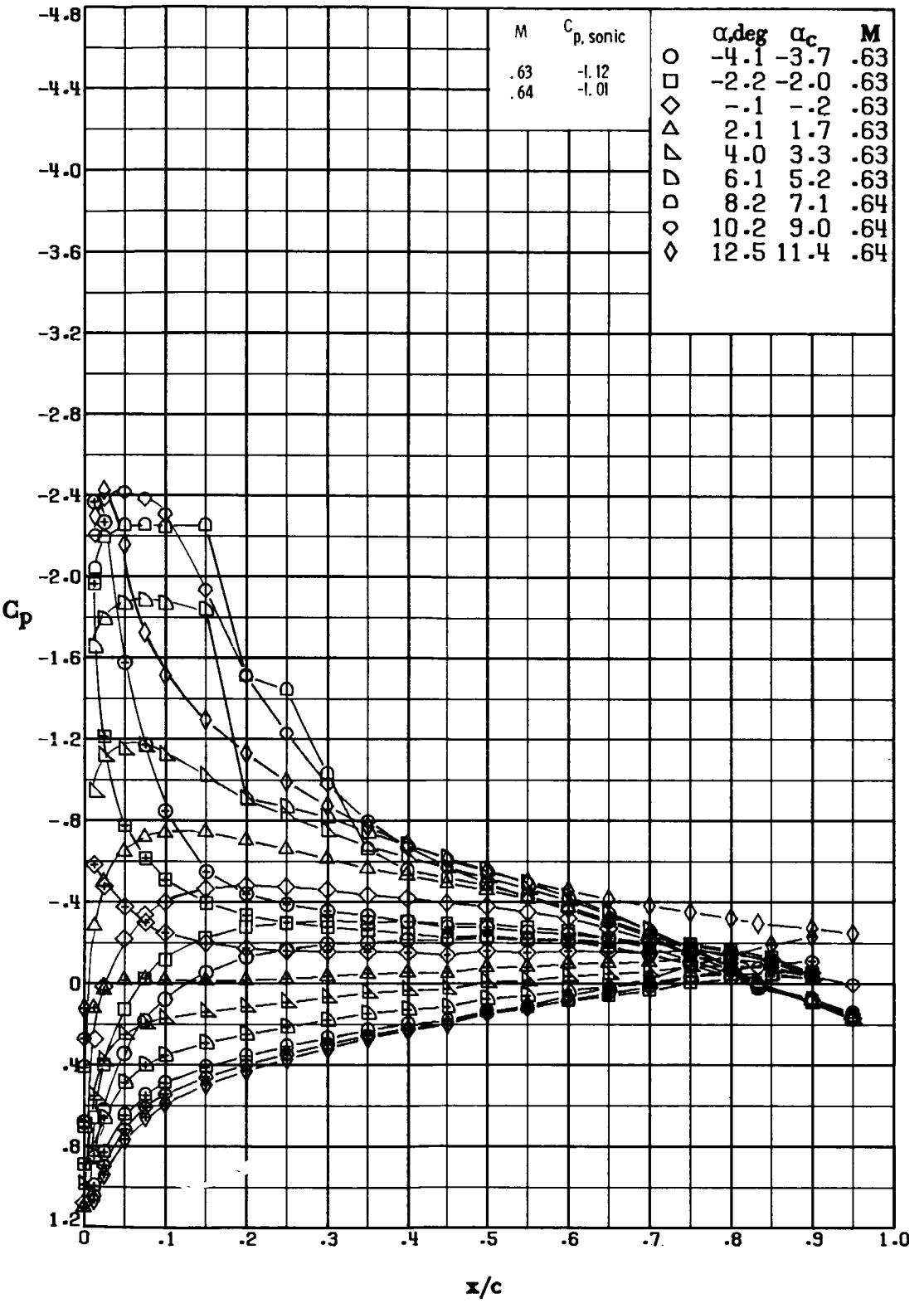

(g) $M \approx 0.63$; $R \approx 8.0 \times 10^6$.

Figure 15.- Continued.

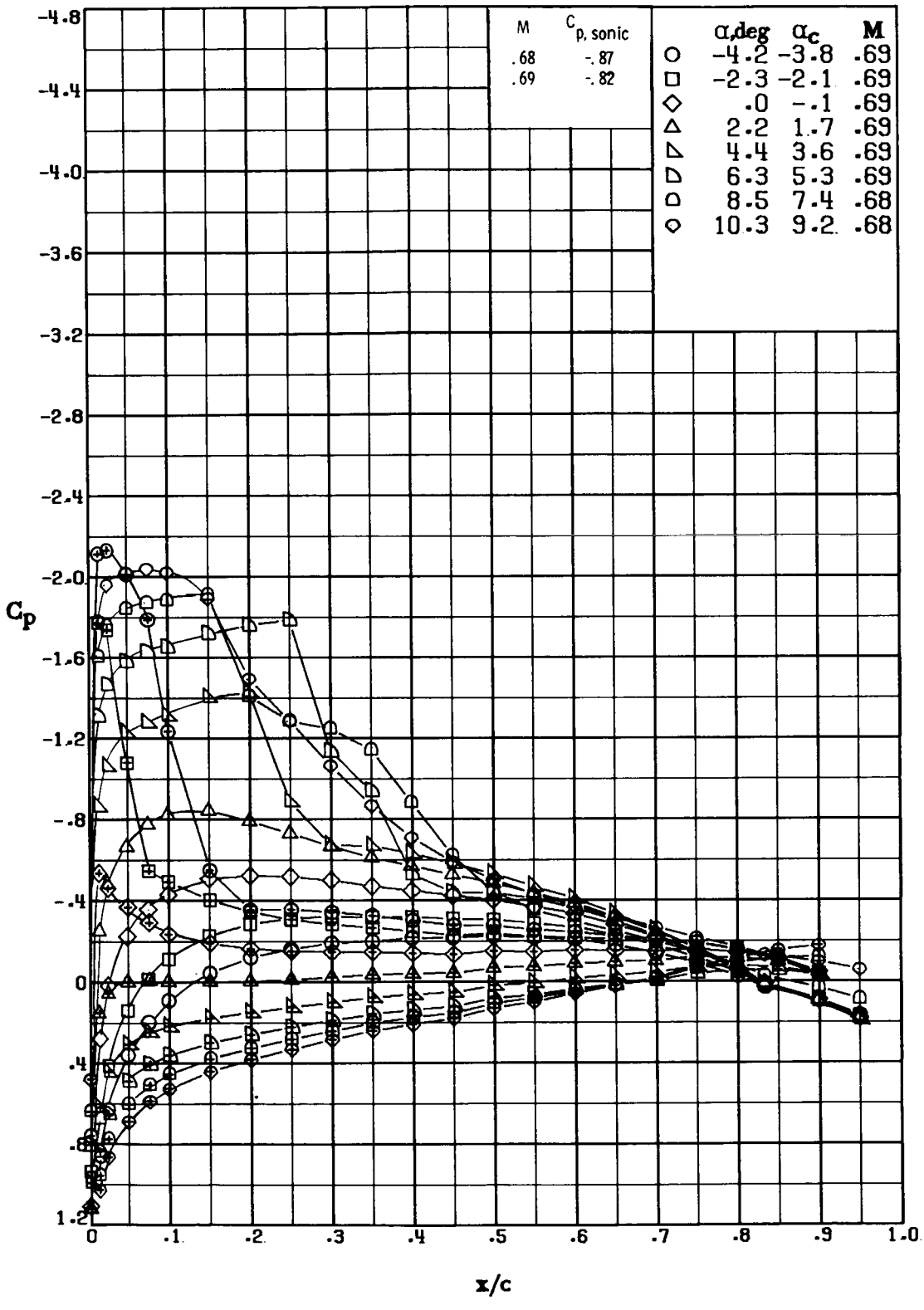

(h) $M \approx 0.69$; $R \approx 8.3 \times 10^6$.

Figure 15.- Continued.

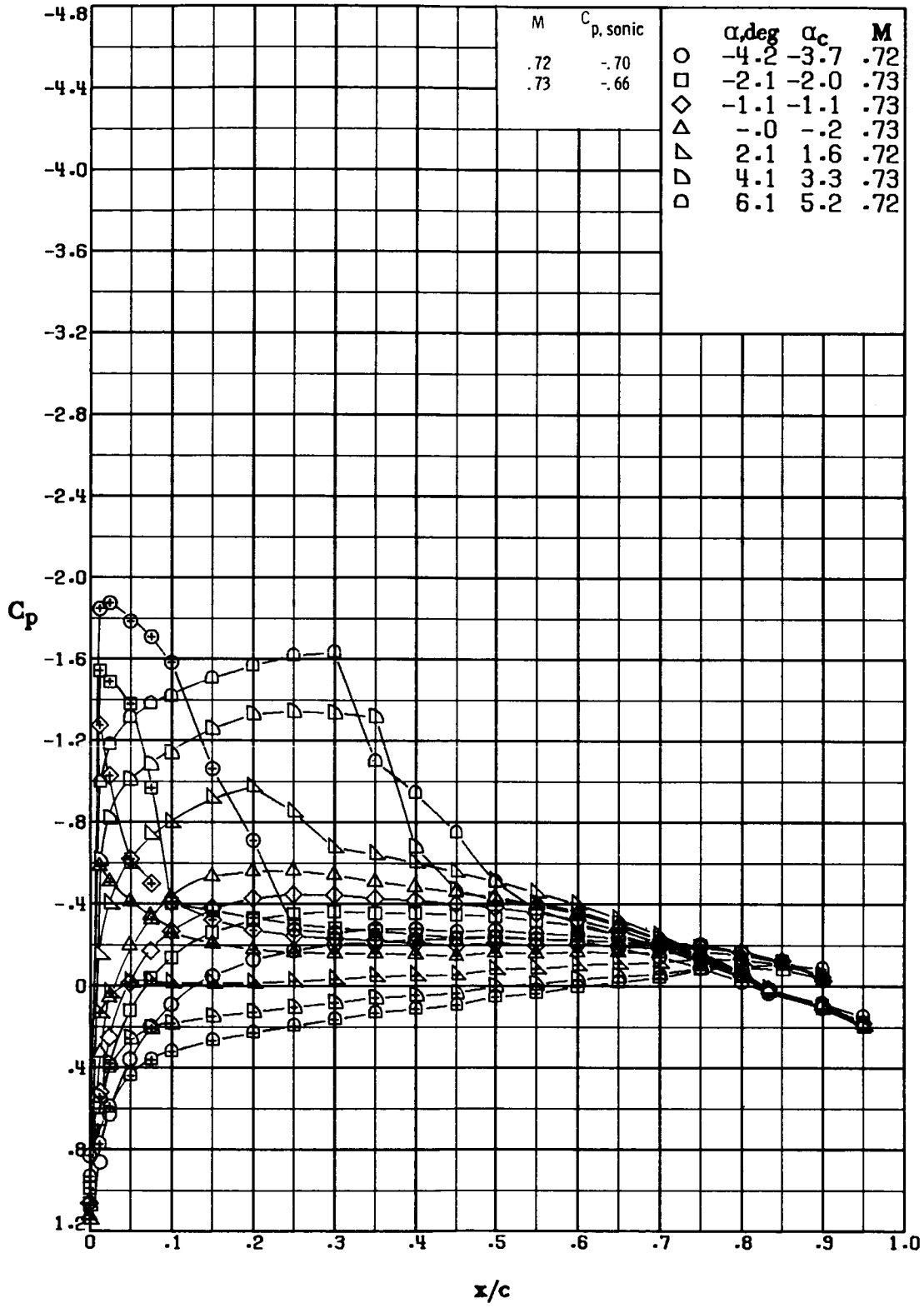

(i) M ≈ 0.73; R ≈ 8.5×10^6.

Figure 15.- Continued.

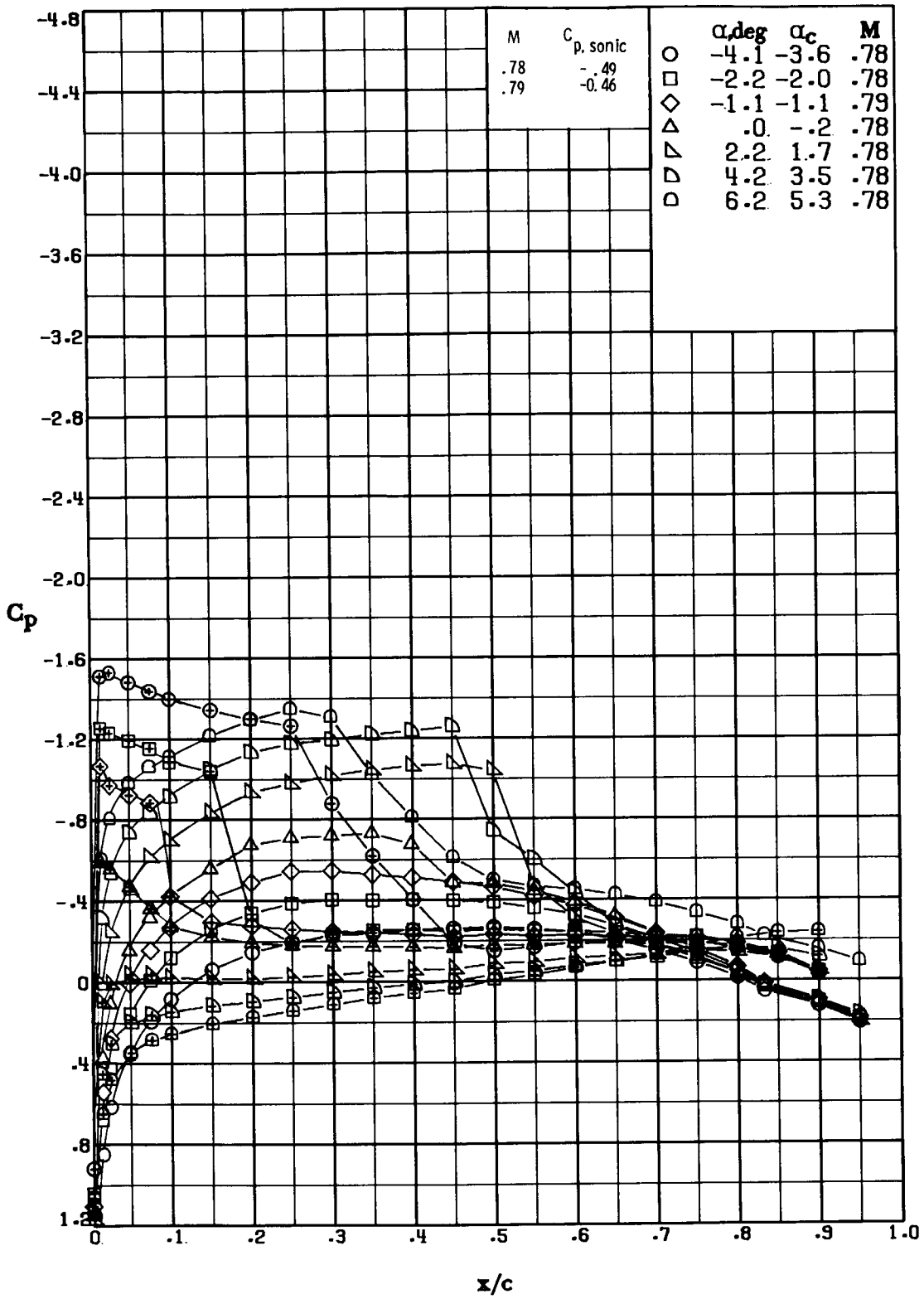

(j) $M \approx 0.78$; $R \approx 8.8 \times 10^6$.

Figure 15.- Continued.

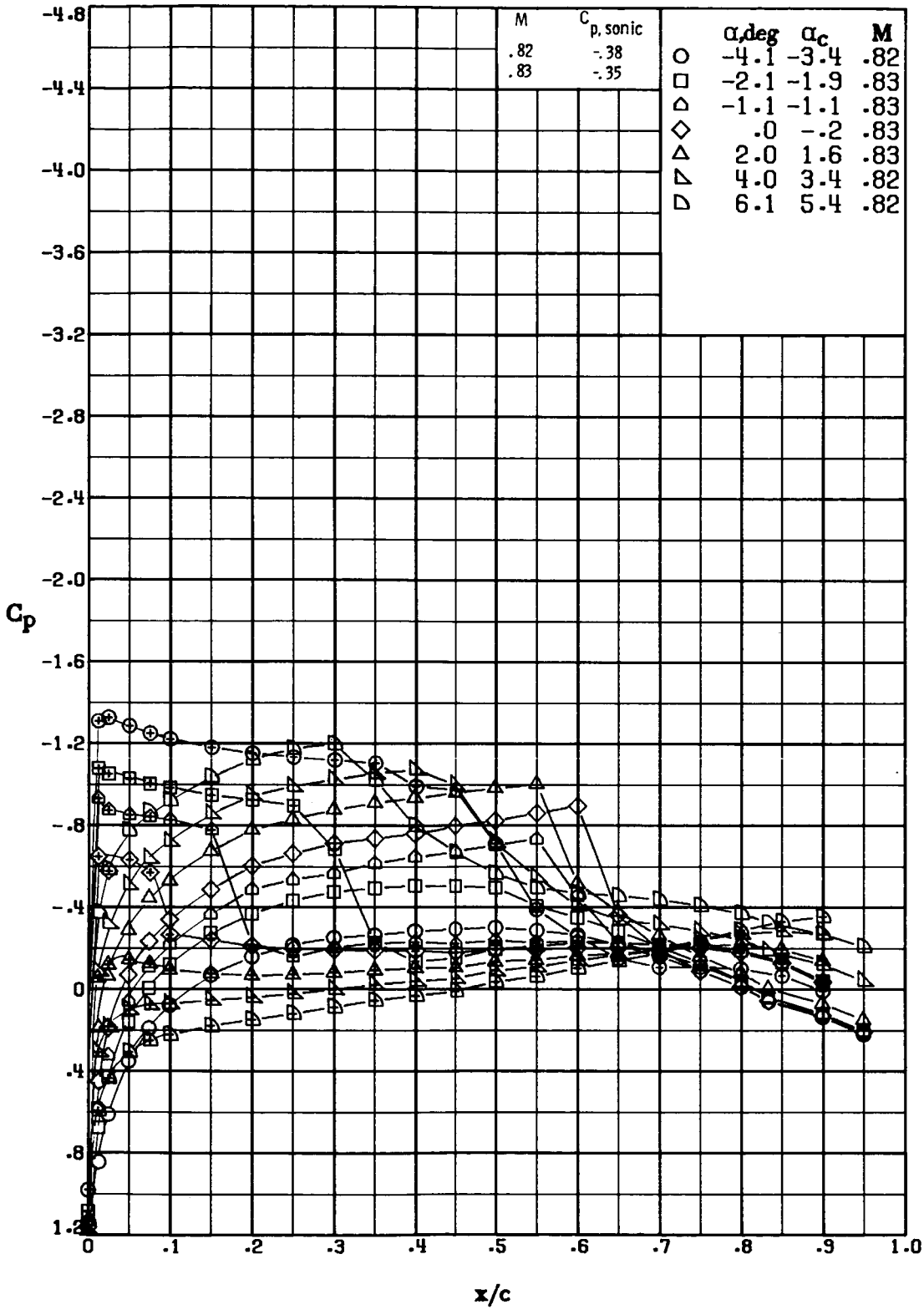

(k) $M \approx 0.83$; $R \approx 9.1 \times 10^6$.

Figure 15.- Continued.

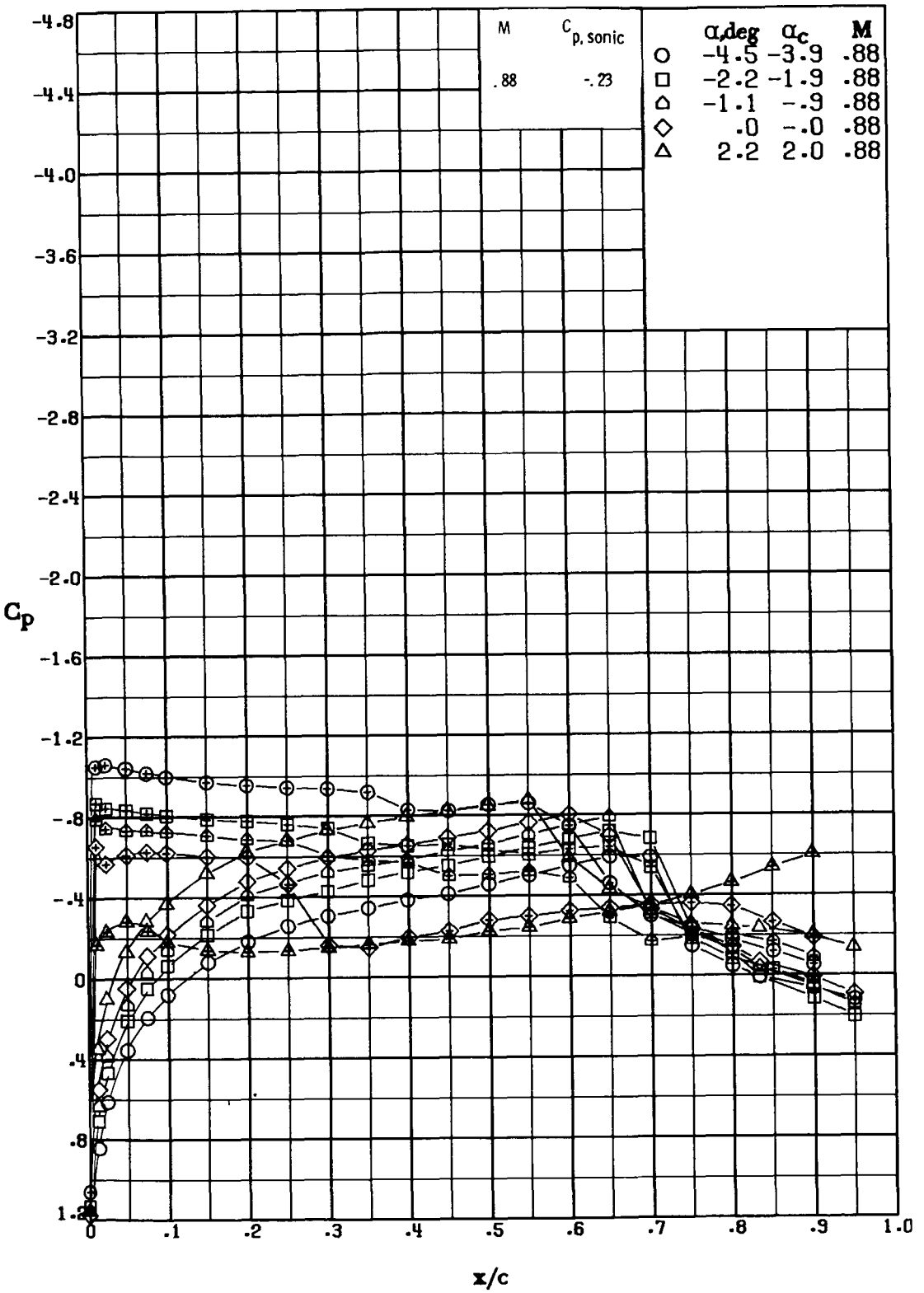

(l) M = 0.88; R ≈ 9.5 × 10^6.

Figure 15.- Concluded.

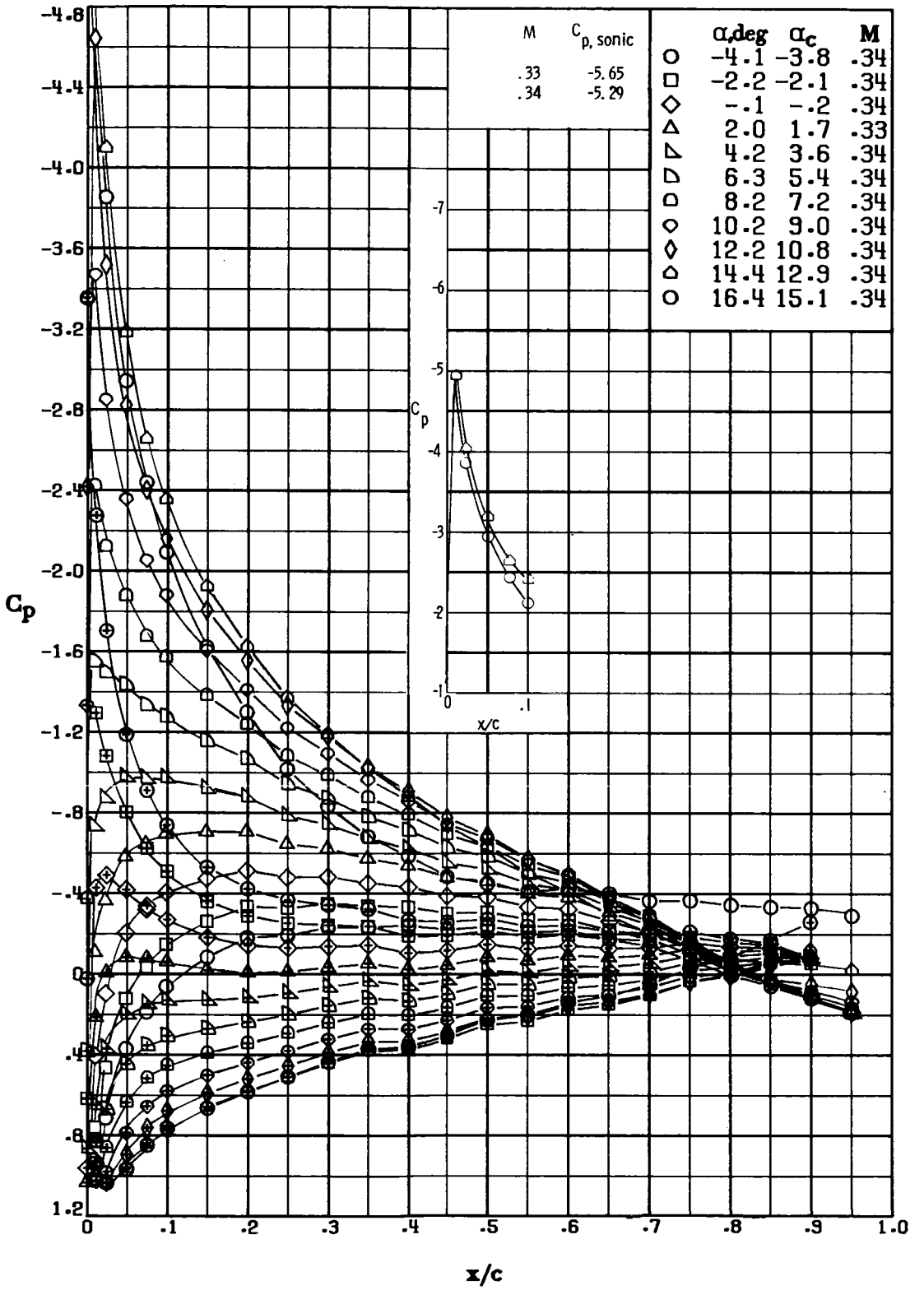

(a) $M \approx 0.34$; $R \approx 4.4 \times 10^6$.

Figure 16.- Pressure distribution over RC(3)-12 airfoil. Symbols with "+" inside indicate lower surface.

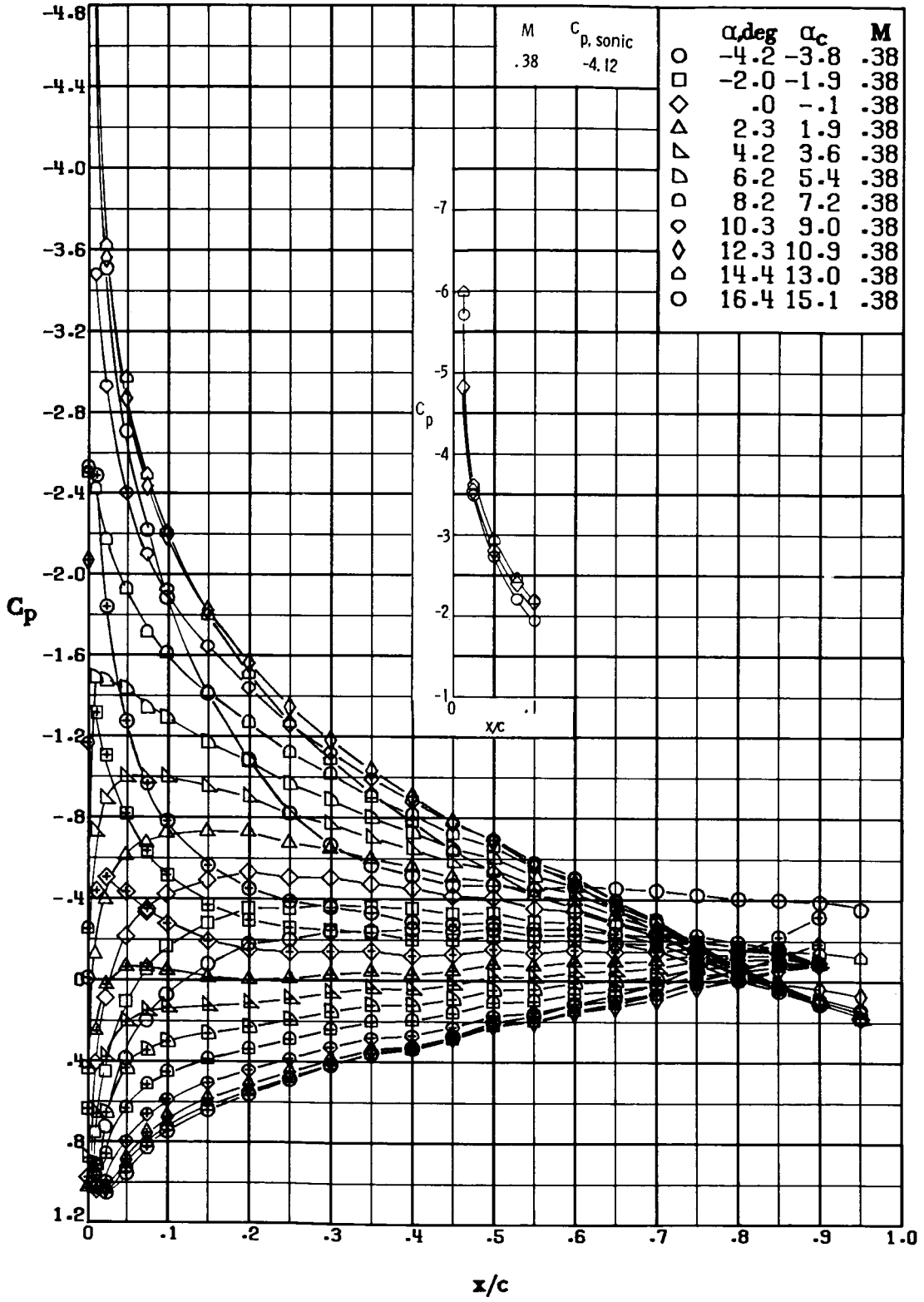

(b) M = 0.38; R ≈ 5.1 × 10^6.

Figure 16.- Continued.

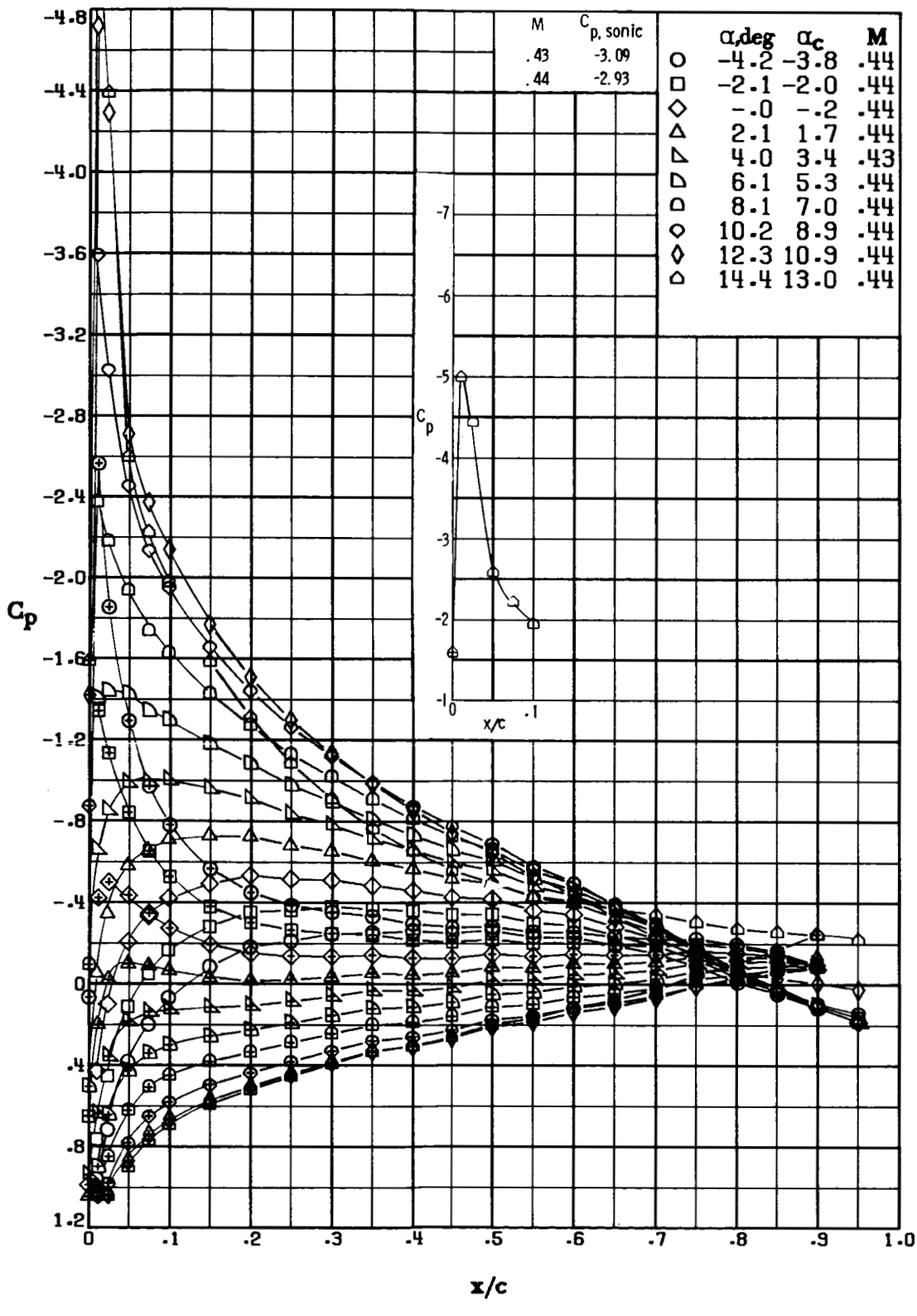

(c) M ≈ 0.44; R ≈ 5.7×10^6.

Figure 16.- Continued.

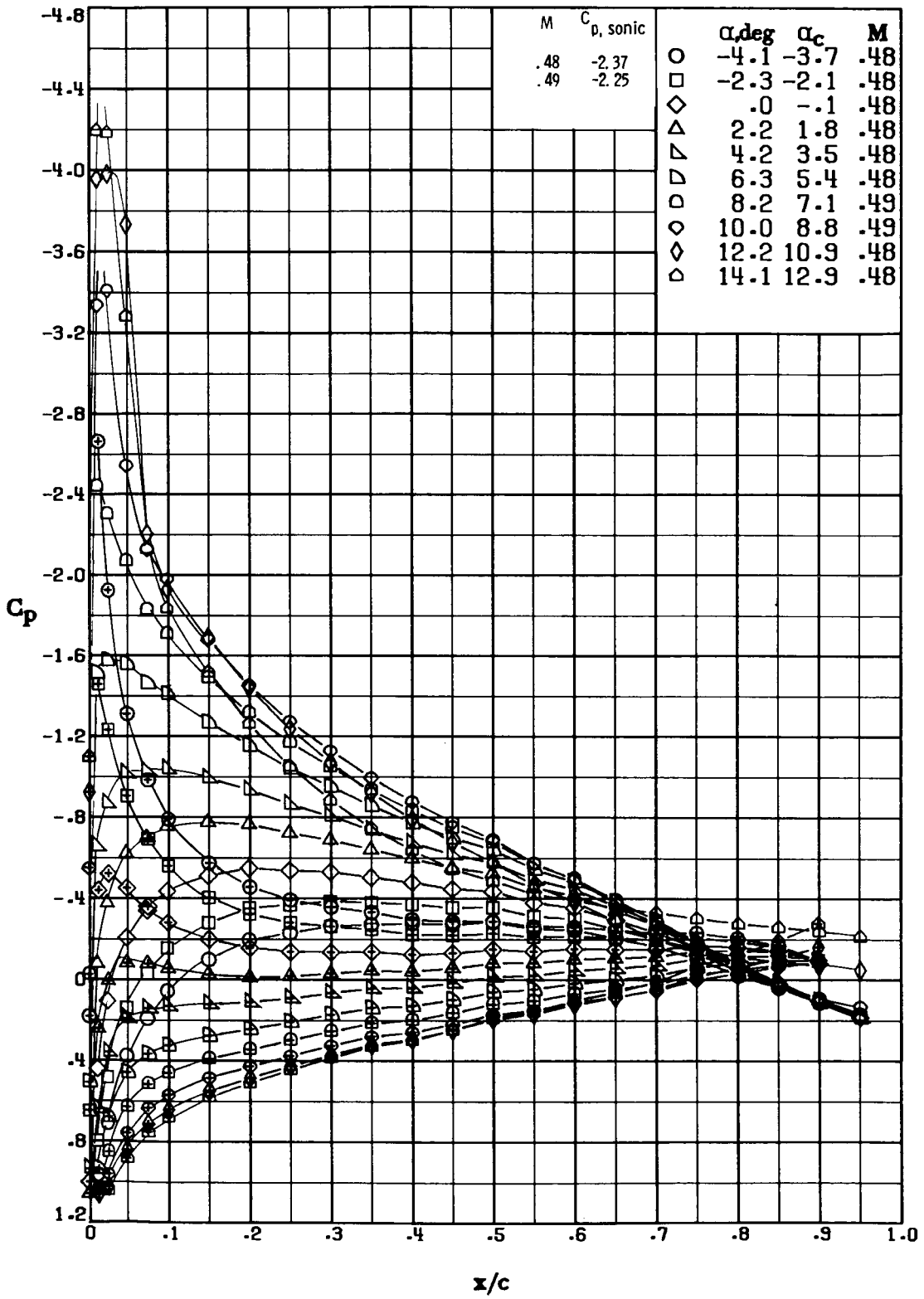

(d) $M \approx 0.48$; $R \approx 6.3 \times 10^6$.

Figure 16.- Continued.

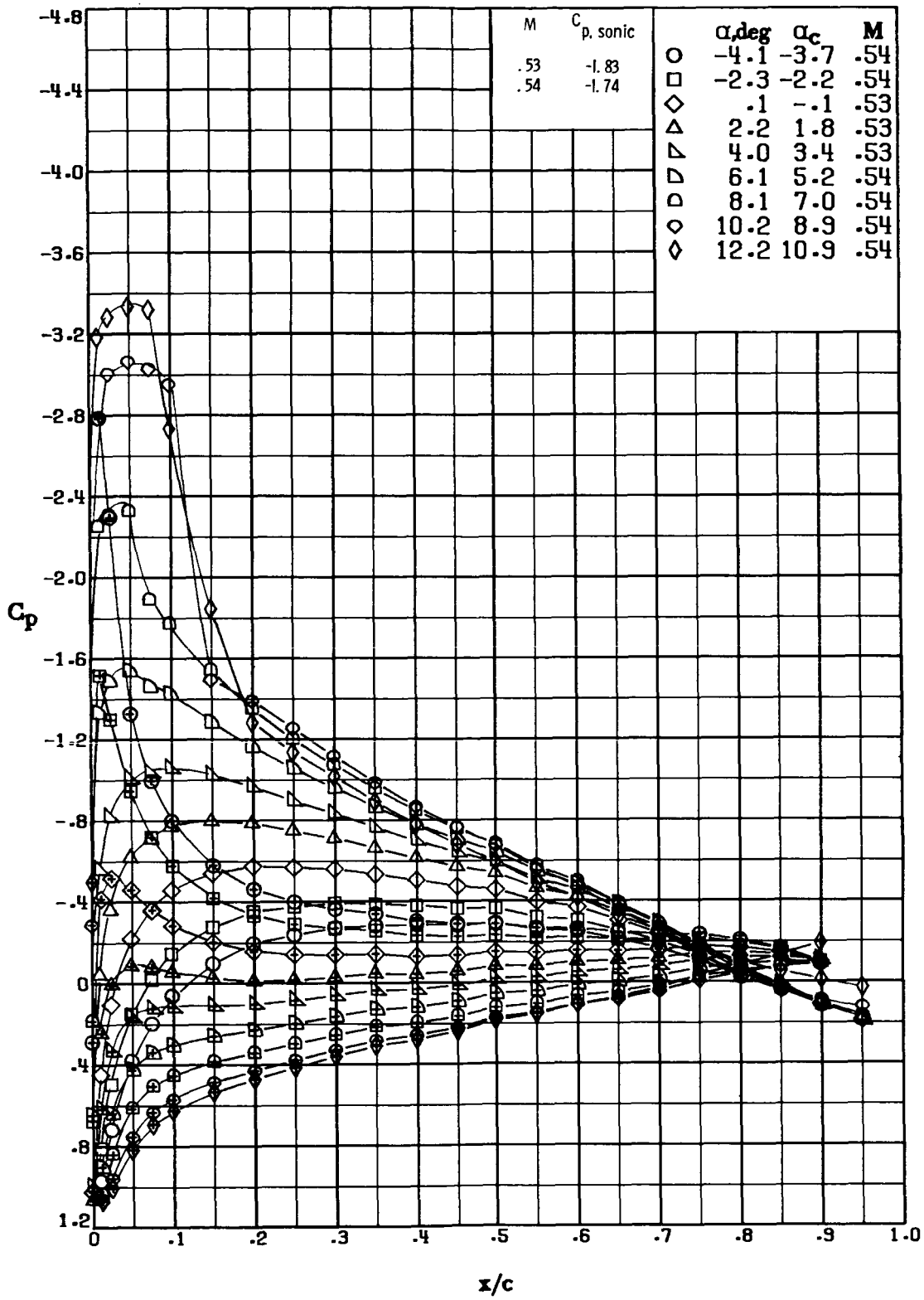

(e) $M \approx 0.54$; $R \approx 6.8 \times 10^6$.

Figure 16.- Continued.

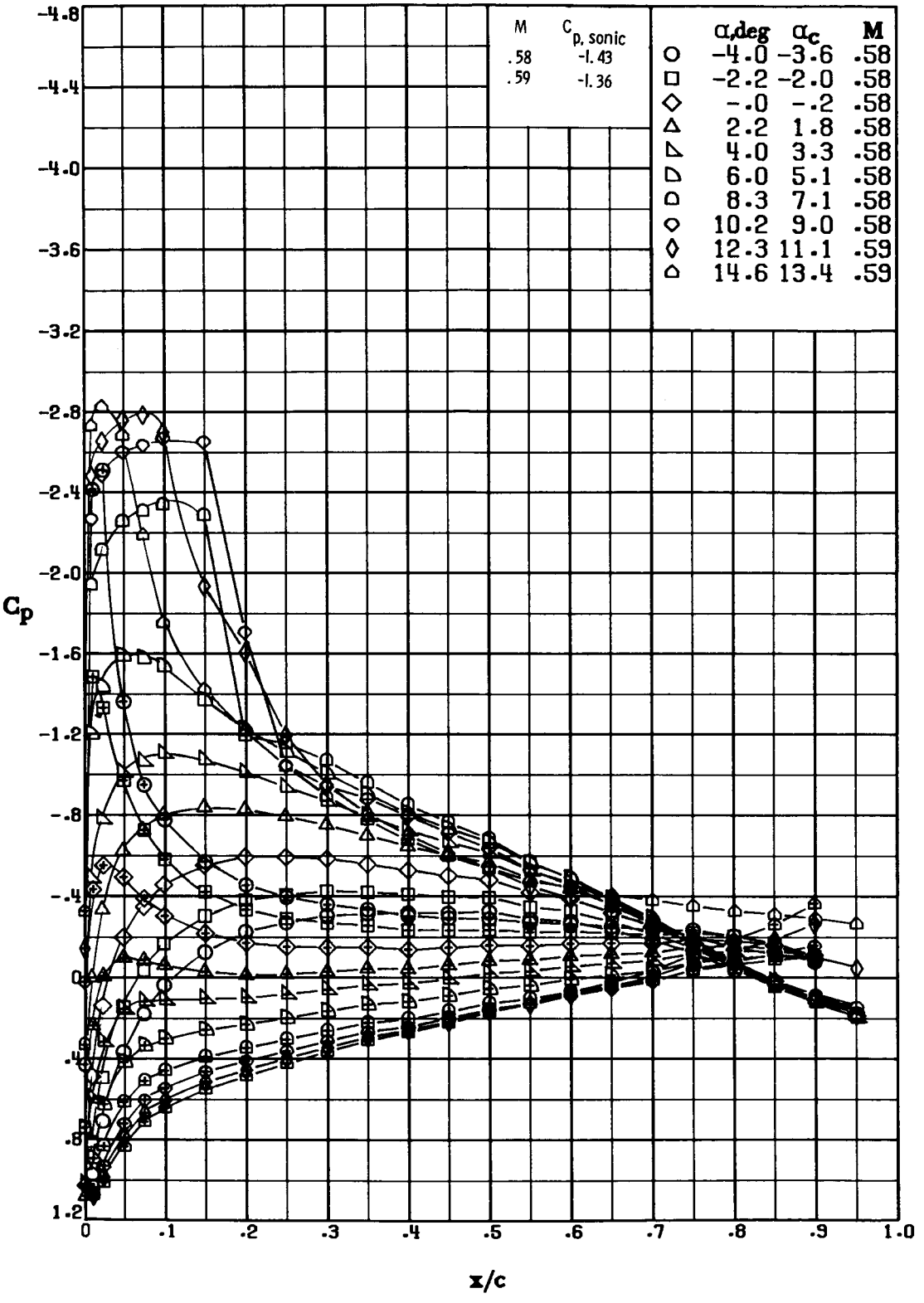

(f) $M \approx 0.58$; $R \approx 7.3 \times 10^6$.

Figure 16.- Continued.

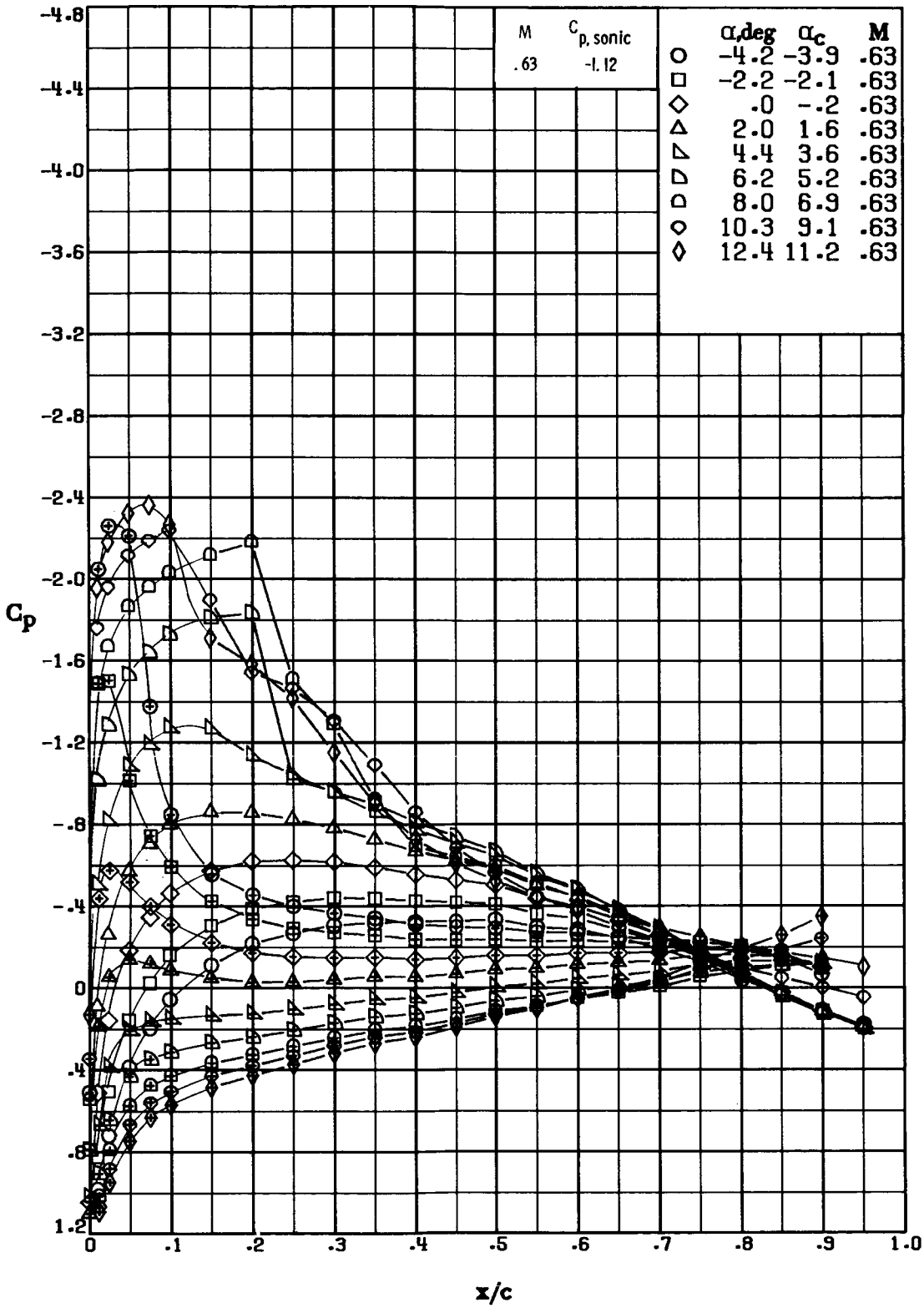

(g) M = 0.63; R ≈ 8.0 × 10^6.

Figure 16.- Continued.

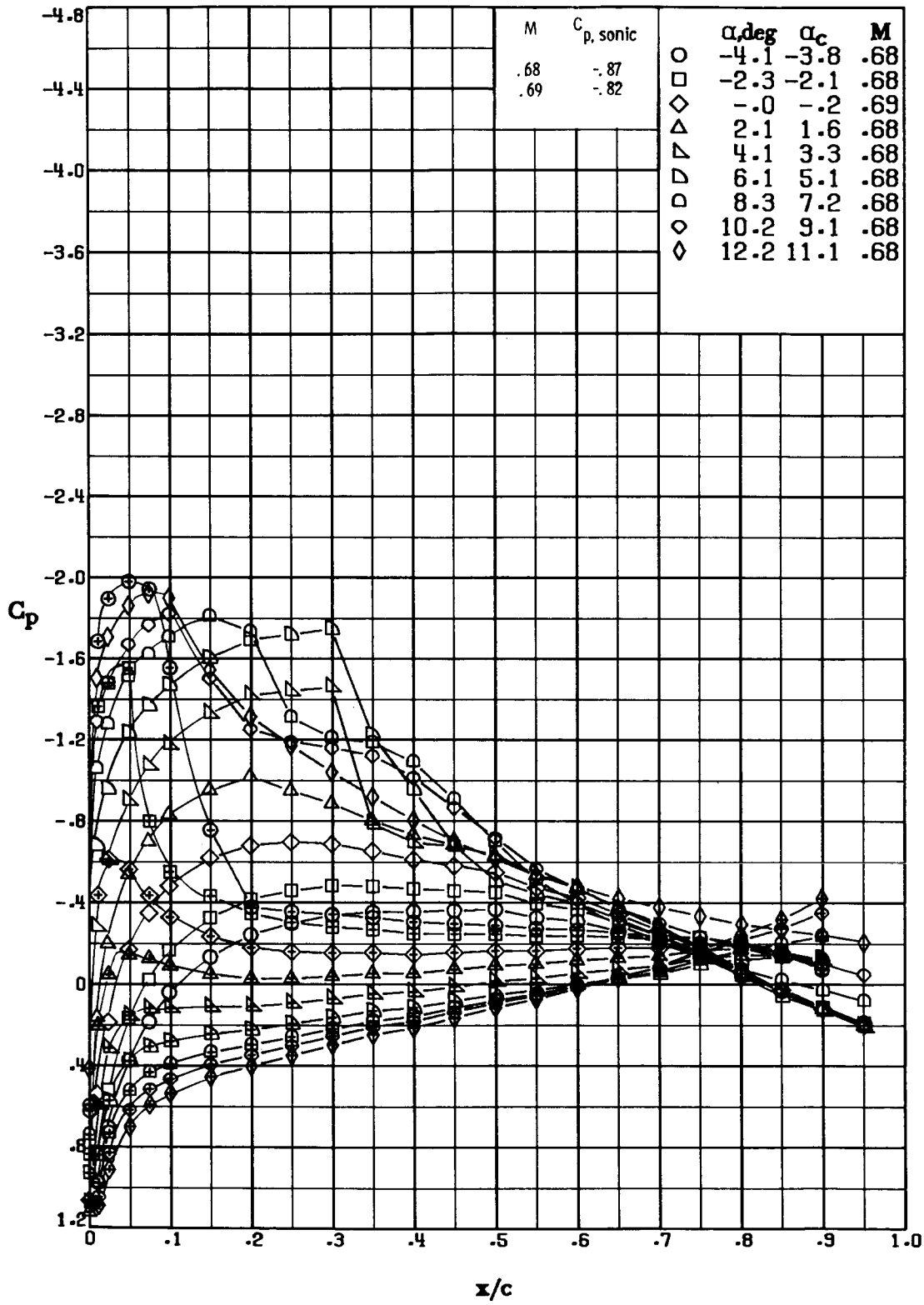

(h) M ≈ 0.68; R ≈ 8.3 × 10^6.

Figure 16.- Continued.

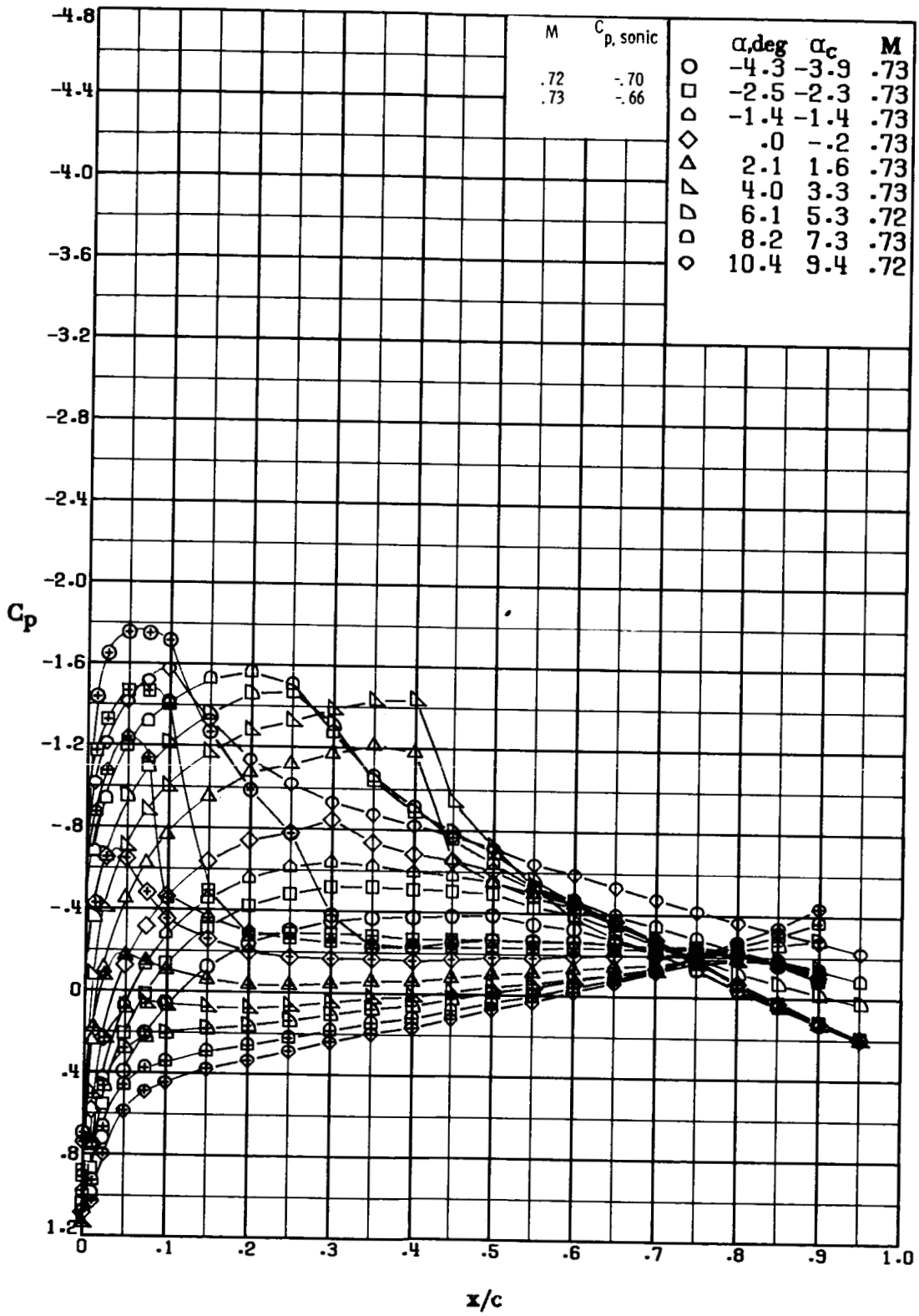

(i) $M \approx 0.73$; $R \approx 8.5 \times 10^6$.

Figure 16.- Continued.

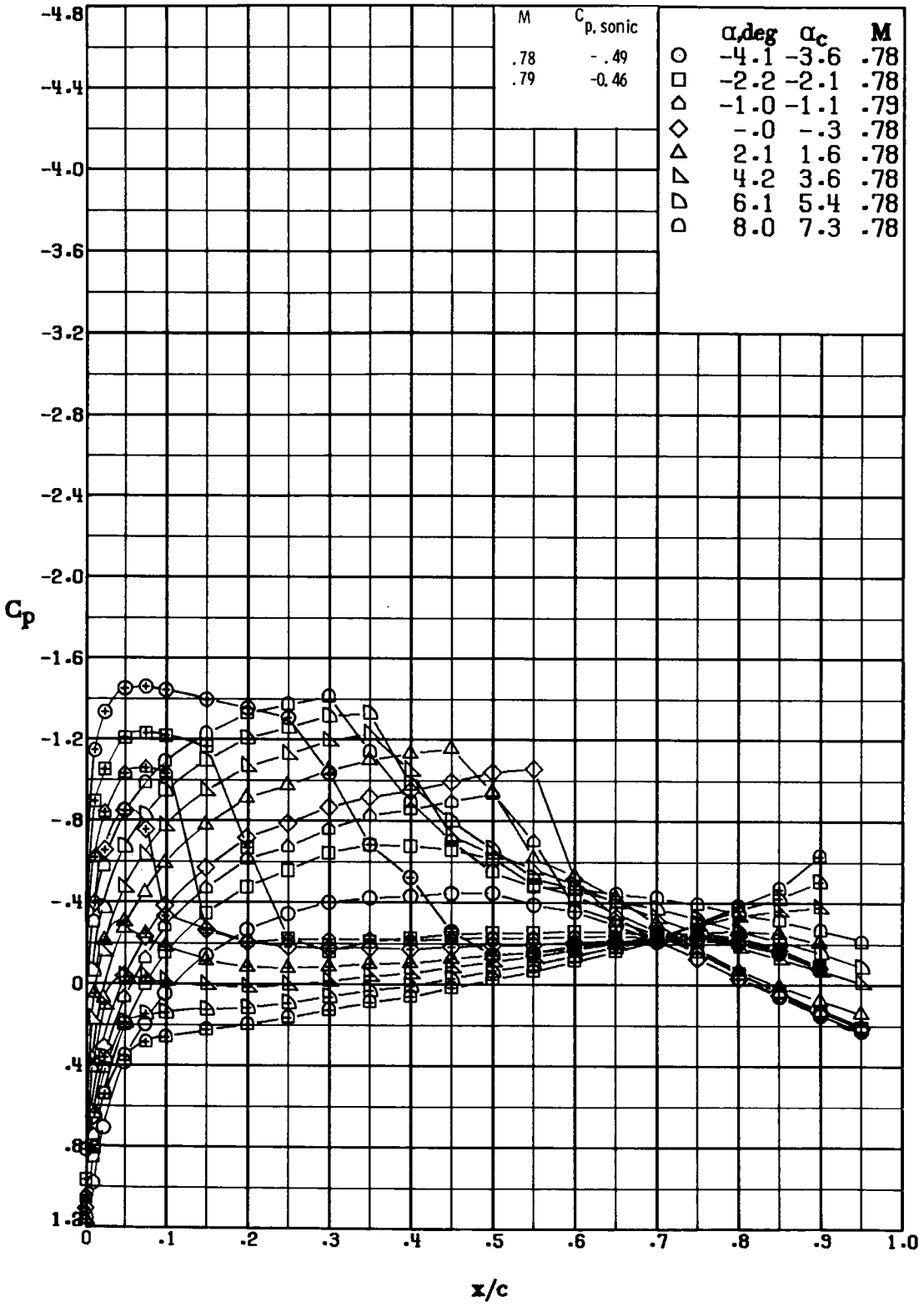

(j) $M \approx 0.78$; $R \approx 8.8 \times 10^6$.

Figure 16.- Continued.

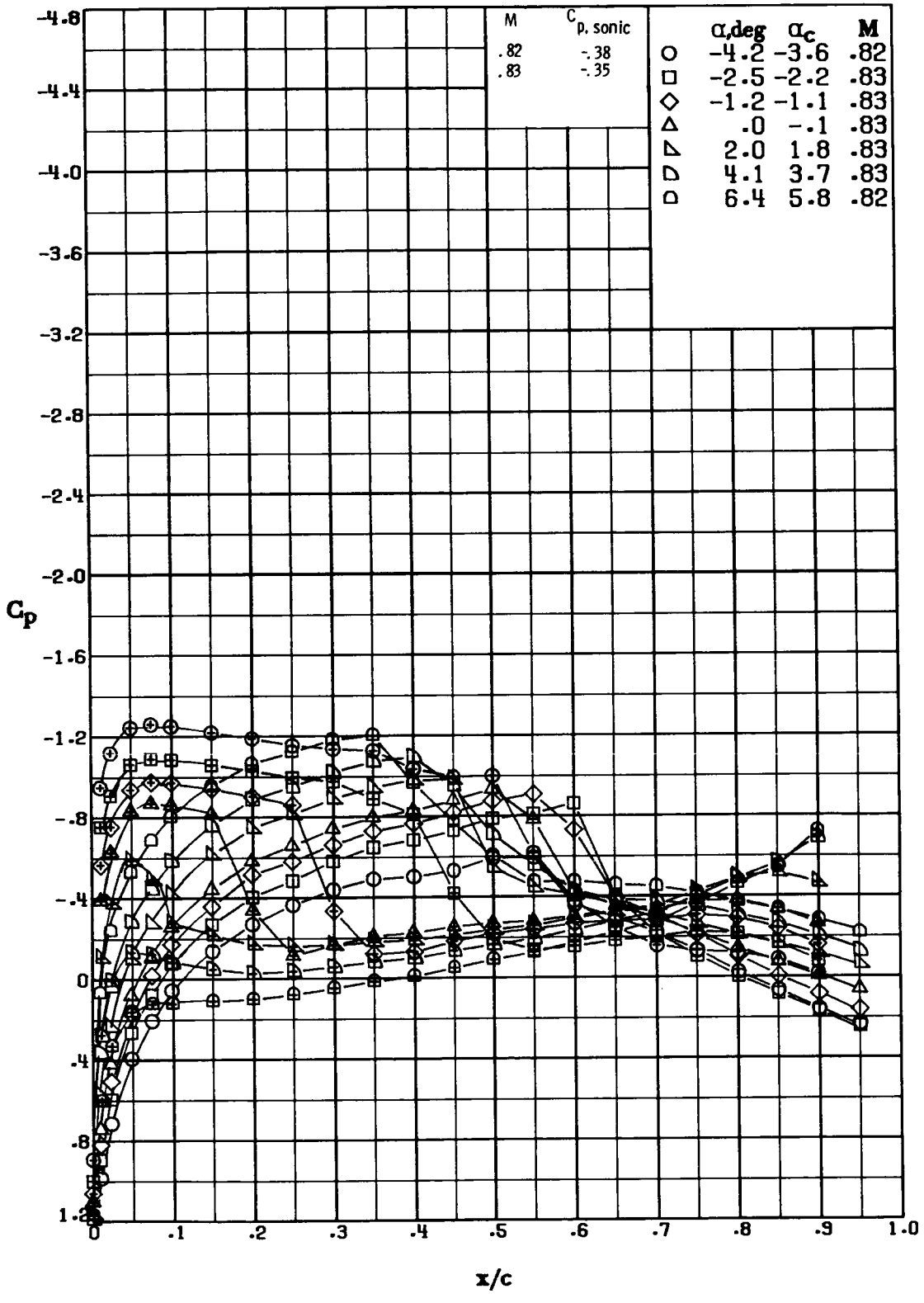

(k) $M \approx 0.83$; $R \approx 9.1 \times 10^6$.

Figure 16.- Continued.

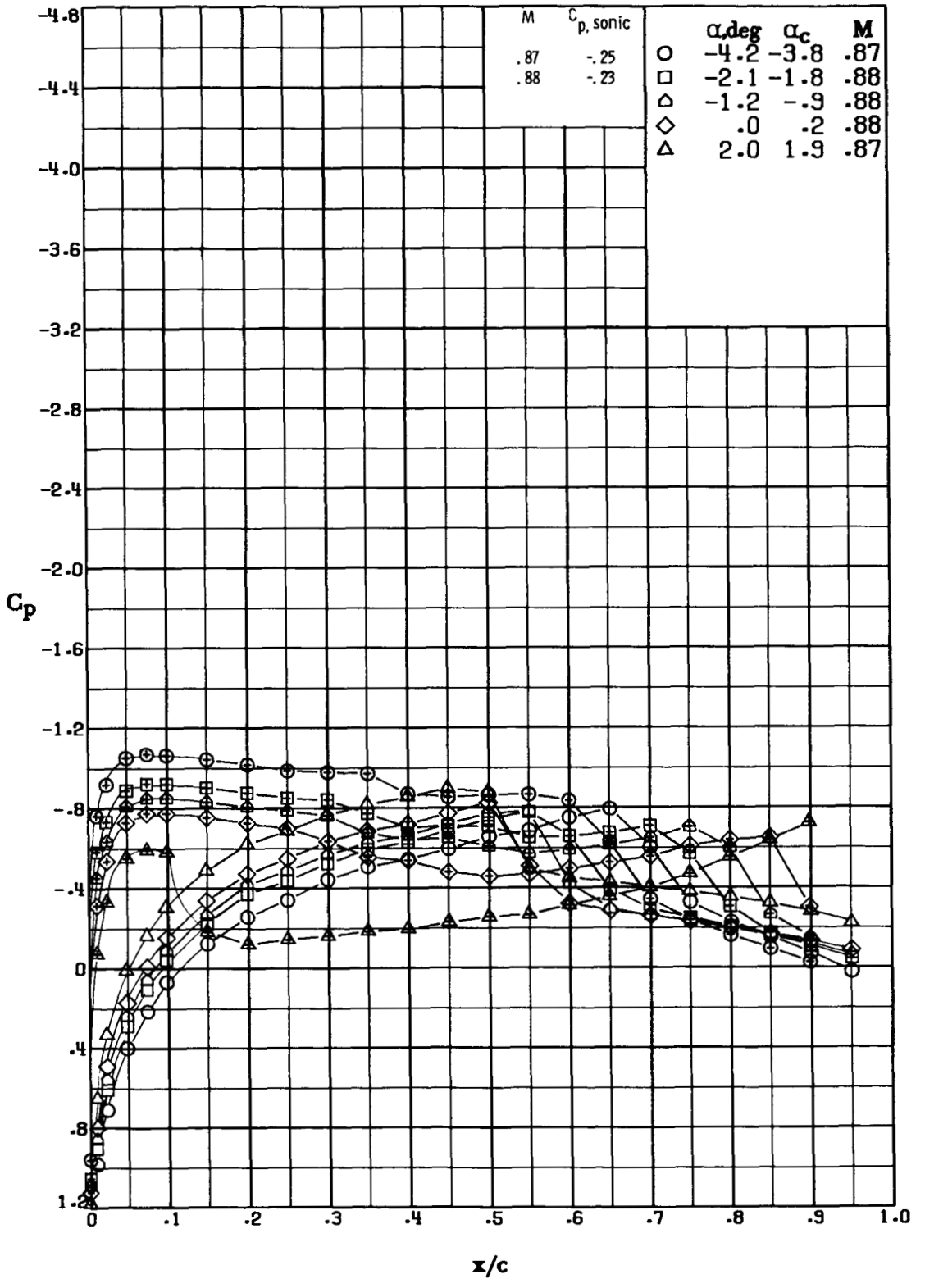

(l) M ≈ 0.88; R ≈ 9.5×10^6.

Figure 16.- Concluded.

1. Report No.	2. Government Accession No.	3. Recipient's Catalog No.
NASA TP-2000 AVRADCOM TR 82-B-2		

4. Title and Subtitle	5. Report Date
TWO-DIMENSIONAL AERODYNAMIC CHARACTERISTICS OF THREE ROTORCRAFT AIRFOILS AT MACH NUMBERS FROM 0.35 to 0.90	May 1982
	6. Performing Organization Code 505-31-33-07
7. Author(s) Gene J. Bingham and Kevin W. Noonan	8. Performing Organization Report No. L-14955
	10. Work Unit No.
9. Performing Organization Name and Address Structures Laboratory AVRADCOM Research and Technology Laboratories NASA Langley Research Center Hampton, VA 23665	11. Contract or Grant No.
	13. Type of Report and Period Covered Technical Paper
12. Sponsoring Agency Name and Address National Aeronautics and Space Administration Washington, DC 20546 and U.S. Army Aviation Research and Development Command St. Louis, MO 63166	14. Army Project No. 1L161102AH45

15. Supplementary Notes

Gene J. Bingham and Kevin W. Noonan: Structures Laboratory, AVRADCOM Research and Technology Laboratories.

16. Abstract

Three airfoils designed for helicopter rotor application have been investigated in the Langley 6- by 28-Inch Transonic Tunnel to determine the two-dimensional aerodynamic characteristics at Mach numbers from 0.34 to 0.88 and respective Reynolds numbers from about 4.4×10^6 to 9.5×10^6. The airfoils have thickness-to-chord ratios of 0.08, 0.10, and 0.12. Trailing-edge reflex was applied to minimize pitching moment. The maximum normal-force coefficient of the RC(3)-12 airfoil is from 0.1 to 0.2 higher, depending on Mach number M, than that of the NACA 0012 airfoil tested in the same facility. The maximum normal-force coefficient of the RC(3)-10 is about equal to that of the NACA 0012 at Mach numbers to 0.40 and is higher than that of the NACA 0012 at Mach numbers above 0.40. The maximum normal-force coefficient of the RC(3)-08 is about 0.19 lower than that of the NACA 0012 at a Mach number of 0.35 and about 0.05 lower at a Mach number of 0.54. The drag-divergence Mach number of the RC(3)-08 airfoil at normal-force coefficients below 0.1 was indicated to be greater than the maximum test Mach number of 0.88. At zero lift, the drag-divergence Mach numbers of the RC(3)-12 and the RC(3)-10 are about 0.77 and 0.82, respectively.

17. Key Words (Suggested by Author(s))	18. Distribution Statement
Airfoils Airfoil design Helicopter airfoils	[redacted] Subject Category 02

19. Security Classif. (of this report)	20. Security Classif. (of this page)	21. No. of Pages	22. Price
Unclassified	Unclassified	71	

[redacted]

NASA-Langley, 1982